SITE-SPECIFIC BIOMOLECULE MODIFICATION FOR DIRECTED SURFACE ATTACHMENT

Dissertation zur Erlangung des naturwissenschaftlichen Doktorgrades der

Julius-Maximilians-Universität Würzburg

vorgelegt von

Joel van Dorp

aus Zeulenroda

Würzburg 2023

Eingereicht bei der Fakultät für Chemie und Pharmazie am

_____

Gutachter der schriftlichen Arbeit

1. Gutachter: Prof. Dr. Tessa Lühmann

2. Gutachter: Prof. Dr. Ulrike Holzgrabe

Prüfer des öffentlichen Promotionskolloquiums

1. Prüfer: Prof. Dr. Tessa Lühmann

2. Prüfer: Prof. Dr. Ulrike Holzgrabe

3. Prüfer: Prof. Dr. Utz Fischer

Datum des öffentlichen Promotionskolloquiums

_____

Doktorurkunde ausgehändigt am

_____

Die vorliegende Arbeit wurde in der Zeit von

November 2012 bis März 2016 und von Dezember 2021 bis Juli 2023 am

Institut für Pharmazie und Lebensmittelchemie der

Bayerischen Julius-Maximilians-Universität Würzburg unter der Anleitung von

Frau **Prof. Dr. Tessa Lühmann** angefertigt.

Table of Contents

1 Summary

Site-directed bioorthogonal conjugation techniques have substantially advanced research in numerous areas. Their exceptional value reflects in the extent of applications, that have been realized with spacial-controlled bioorthogonal reactions. Specific labeling of surfaces, proteins, and other biomolecule allows for new generations of drug delivery, tracking, and analyzing systems. With the continuous advance and refinement of available methods, this field of research will become even more relevant in the time to come. Yet, as individual as the desired purpose is, as different can be the most suitable modification strategy. In this thesis, two different bioconjugation approaches, namely CuAAC and factor XIIIa mediated ligation, are used in distinct application fields, featuring eGFP as a model protein showcasing the advantages as well as the challenges of each technique.

The introduction of a unique accessible functionality is the most critical feature of a site-specific reaction, and the first considerable hurdle to clear. While most surfaces, peptides, or small molecules might require less expenditure to modulate, equipping large biomolecules like proteins with additional traits requires careful consideration to preserve the molecule's stability and function. Therefore, the first section of this project comprises the engineering of eGFP via rational design. Initially, wild-type eGFP was subcloned, expressed, and characterized to serve as a reference value for the designed variants. Subsequently, eGFP was mutated and expressed to display a recognition site for factor XIIIa. Additionally, a second mutant harbored a TAG-codon to enable amber codon suppression and consequently the incorporation of the alkyne bearing unnatural amino acid Plk to support a CuAAC reaction. Fluorescence spectroscopy was used to confirm that the fluorescent properties of all expressed muteins were identically equal to wild-type eGFP, which is a reliable marker for the intact barrel structure of the protein. Trypsin digestion and HPLC were deployed to confirm each protein variant's correct sequence and mass.

The second part of this work focuses on the conjugation of cargo molecules deploying the chosen approaches. Solid-phase peptide synthesis was used to create a peptide that served as a lysine donor substrate in the crosslinking mechanism of FXIIIa. Additionally, the peptide was provided with a cysteine moiety to allow for highly flexible and simple loading of desired cargo molecules via conventional thiol-Michael addition, thus establishing an adaptive labeling platform. The effective ligation was critically reviewed and confirmed by monitoring the exact mass changes by HPLC. Protocols for attaching payloads such as biotin

and PEG to the linker peptide were elaborated. While the biotin construct was successfully conjugated to the model protein, the eGFP-PEG linkage was not achieved judging by SDS-PAGE analysis. Furthermore, featuring isolated peptide sequences, the properties of the FXIIIa-mediated reaction were characterized in detail. Relative substrate turnover, saturation concentrations, by-product formation, and incubation time were comprehensively analyzed through HPLC to identify optimal reaction conditions. CuAAC was successfully used to label the Plk-eGFP mutein with Azide-biotin, demonstrated by western blot imaging.

Within the last part of this study, the application of the conjugation systems was extended to different surfaces. As regular surfaces do not allow for immediate decoration, supplementary functionalization techniques like gold-thiol interaction and silanization on metal oxides were deployed. That way gold-segmented nanowires and Janus particles were loaded with enoxaparin and DNA, respectively. Nickel and cobalt nanowires were modified with silanes that served as linker molecules for subsequent small molecule attachment or PEGylation. Finally, the eGFP muteins were bound to a particle surface in a site-specific manner. Beads displaying amino groups were utilized to demonstrate the effective use of FXIIIa in surface modification. Moreover, the bead's functional moieties were converted to azides to enable CuAAC "Click Chemistry" and direct comparison. Each modification was analyzed and confirmed through fluorescence microscopy.

2 Zusammenfassung

Techniken zur ortsspezifischen bioorthogonalen Konjugation von Biomolekülen haben die Forschung in zahlreichen Bereichen erheblich vorangebracht. Ihr außerordentlicher Wert spiegelt sich in der Vielzahl der Anwendungen wider, die mit bioorthogonalen Reaktionen realisiert werden konnten. Die kontrollierte Bestückung von Oberflächen, Proteinen und anderen Biomolekülen ermöglicht neue Generationen von Systemen zur Arzneimittelapplikation als auch zu Tracking- und Analyseverfahren. Mit der kontinuierlichen Weiterentwicklung und Verfeinerung der verfügbaren Methoden wird dieses Forschungsgebiet in Zukunft noch mehr an Bedeutung gewinnen. Doch so individuell wie der gewünschte Zweck ist, so unterschiedlich kann auch die am besten geeignete Modifikationsstrategie sein. In dieser Arbeit werden zwei verschiedene Biokonjugationsansätze, nämlich CuAAC und Faktor-XIIIa-vermittelte Ligation, in unterschiedlichen Anwendungsbereichen eingesetzt, wobei eGFP als Modellprotein dient, um sowohl die Vorteile als auch die Herausforderungen der jeweiligen Technik aufzuzeigen.

Die Einführung einer genau abgrenzbaren Funktionalität ist das wichtigste Merkmal einer ortsspezifischen Reaktion und die erste große Hürde, die es zu nehmen gilt. Während die meisten Oberflächen, Peptide oder kleinen Moleküle mit geringem Aufwand moduliert werden können, erfordert das Ausstatten von Proteinen mit zusätzlichen Merkmalen sorgfältige Überlegung und weitreichende Kenntnis, um die Stabilität und Funktion der Molekülstruktur zu erhalten. Der erste Abschnitt dieses Projekts umfasst daher das Protein-Engineering von eGFP durch rationales Design. Zunächst wurde der Wildtyp von eGFP subkloniert, exprimiert und charakterisiert, um als Referenzwert für die entworfenen Varianten zu dienen. Anschließend wurde eGFP so mutiert und exprimiert, dass es eine Erkennungsstelle für Faktor XIIIa aufweist. Zusätzlich enthielt eine zweite Mutante ein TAG-Codon, um die Unterdrückung des Amber-Codons und damit den Einbau der Alkin-tragenden unnatürlichen Aminosäure Plk zu ermöglichen, um wiederum eine CuAAC-Reaktion zu unterstützen. Mit Hilfe von Fluoreszenzspektroskopie wurde bestätigt, dass die Fluoreszenzeigenschaften aller exprimierten Muteine identisch mit denen des Wildtyps eGFP sind, was ein zuverlässiger Marker für die intakte Barrel-Struktur des Proteins ist. Trypsinverdau und HPLC wurden eingesetzt, um die korrekte Sequenz und Masse der einzelnen Proteinvarianten zu bestätigen.

Der zweite Teil dieser Arbeit konzentriert sich auf die Konjugation von „Cargo-Molekülen“ unter Verwendung der gewählten Ansätze. Mittels Festphasen-Peptidsynthese wurde ein Peptid hergestellt, das als Lysin-Donor-Substrat im Vernetzungsmechanismus von FXIIIa diente. Zusätzlich wurde das Peptid mit einem Cystein-Element versehen, um eine hochflexible und einfache Beladung mit gewünschten Frachtmolekülen durch konventionelle Thiol-Michael-Addition zu ermöglichen und so eine adaptive Koppelungsplattform zu schaffen. Die effektive Ligation wurde durch die Überwachung der genauen Massenänderungen mittels HPLC kritisch überprüft und bestätigt. Es wurden Protokolle für die Anbringung von Nutzlasten wie Biotin und PEG an das Linker-Peptid ausgearbeitet. Während das Biotin-Konstrukt erfolgreich an das Modellprotein konjugiert wurde, konnte die eGFP-PEG-Bindung nach Auswertung der SDS-PAGE-Analyse nicht erreicht werden. Darüber hinaus wurden anhand der isolierten Peptidsequenzen die Eigenschaften der FXIIIa-vermittelten Reaktion im Detail charakterisiert. Relativer Substratumsatz, Sättigungskonzentrationen, Nebenproduktbildung und Inkubationszeit wurden mittels HPLC umfassend analysiert, um optimale Reaktionsbedingungen zu ermitteln. CuAAC wurde erfolgreich zur Markierung des Plk-eGFP-Muteins mit Azid-Biotin eingesetzt, was durch Western-Blot-Darstellung nachgewiesen wurde.

Im letzten Teil dieser Arbeit wurde die Anwendung der Konjugationssysteme auf verschiedene Oberflächen übertragen. Da normale Oberflächen keine unmittelbare Dekoration erlauben, wurden zusätzliche Funktionalisierungstechniken wie Gold-Thiol-Wechselwirkung und Silanisierung auf Metalloxiden eingesetzt. Auf diese Weise wurden goldsegmentierte Nanowires und Januspartikel mit Enoxaparin bzw. DNA beladen. Nickel- und Kobalt-Nanowires wurden mit Silanen modifiziert, die als Verbindungsmoleküle für die anschließende Anlagerung kleiner Moleküle oder PEGylierung dienten. Schließlich wurden die eGFP-Muteine ortsspezifisch an eine Partikeloberfläche gebunden. Beads mit Aminogruppen wurden verwendet, um den effektiven Einsatz von FXIIIa bei der Oberflächenmodifikation zu demonstrieren. Darüber hinaus wurden die funktionellen Einheiten der Beads in Azide umgewandelt, um eine CuAAC-„Klickchemie" und somit einen direkten Vergleich zu ermöglichen. Jede Modifikation wurde mit Hilfe der Fluoreszenzmikroskopie analysiert und bestätigt.

3 Introduction

3.1 Biofunctionalization Strategies

The modification of biomolecules finds extensive usage in today's research as well as commercial applications and will continue to gain importance in the future. The reasons for this lie in the innumerable utilization possibilities that this field of research offers: Augmentation of pharmacokinetic and pharmacodynamic drug properties as well as shelf life [1], development of innovative screenings and analytical methods [2], or even creation of exciting new ways for foundational protein and proteomic research [3], are typical examples, but they do not come anywhere near to exhausting the scope of the practiced and potential options.

The most interesting area for the pharmaceutical industry is arguably the development of new biologicals in every aspect. Besides the often inherent effect-specific superiority of endogenous proteins and peptides, conjugations can influence and further improve stability, toxicity, and release profiles [4].

Novel approaches can lead to fundamental insights into the stability of proteins and biomolecules and thus provide information on optimal drug formulation. In this context, the European project MANAQA (Magnetic Nano Actuators for Quantitative Analysis), in which the binding forces in a single molecule were investigated using an atomic force microscope (AFM), was supported in this work [5]. Roughly, a typical experiment can be described as follows: A molecule with two engineered anchor points is fixated to the tip of the AFM cantilever on one side and to a manipulable carrier such as a magnetic bead or nanowire on the other side. Subsequently, the molecule is pulled apart using an electromagnet, while the forces required to overcome the inner molecular bonds are recorded via the AFM. A simplified representation of the experimental setup is shown in ***Scheme 1***. At an advanced stage, this provides unprecedented opportunities for the formulation development of medically significant biologics, for example, through stability screening with various buffer conditions such as pH value, ionic strength, or other additives. By adjusting the corresponding properties, the resulting energy changes in the biomolecule can be used to draw conclusions about the quality of the formulation, which can then be modified accordingly.

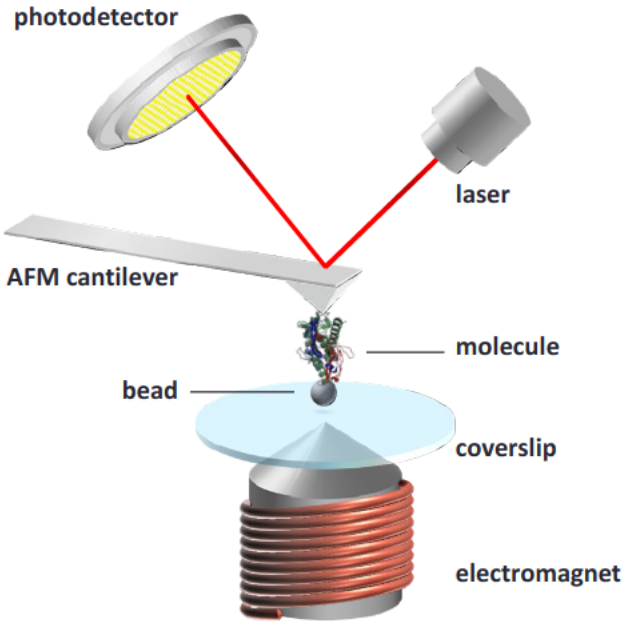

Scheme 1 **Schematic illustration of the MANAQA AFM setup.**

The accuracy of the expected statements strongly depends on the chosen anchor points at which the molecule of interest is immobilized in the experimental setup, in order to obtain a complete and reproducible energy fingerprint. For this demand, the most marginal positions of a given molecule must be chosen, naturally given by the N- and C-terminal end of a protein.

With a vast variety of modification and conjugation strategies available, the proper functionalization route must be chosen in deference to the targeted application and the biomolecule's individual properties. As a rough classification, those methods can be divided into enzyme-mediated or fusion protein reliant as well as chemically induced modifications. An overview of selected methods with a brief description can be found in ***Table 1***.

There is a remarkable range of strategies that exploit enzymatic reactions for ligation processes of all kinds [6, 7]. The most prevalent approaches however deploy sortase A (SrtA) or microbial transglutaminase (mTG) [8]. Naturally, enzyme-supported approaches take place in physiological reaction environments with fast reaction kinetics when high-affinity substrates are present, providing an outstanding option when handling sensitive functionalization candidates. Another strong asset of deploying biocatalysts is their great substrate specificity, whereby many enzymes operate exclusively on distinct amino acid motifs as recognition sites, which offers an excellent tool to achieve the desired site-

selectivity. The requisiteness for these consensus sequences, however, makes antecedent protein engineering inevitable. An often challenging procedure since the necessary insertions need to be carefully placed in order to leave the structural und functional integrity of the polypeptide of interest unaffected. Lastly, the conversion efficacy of every enzyme can suffer due to poor steric availability of its substrate location.

With exceptional substrate specificity, fusion protein modifications found their well-earned place in the spectrum of bioconjugation strategies. Yet, typical fusion proteins exhibit non-neglectable sizes, which proves to be a hindrance when a low-impact conjugation linker is vital. Their strength is often exploited in protein assays, as cellular signal reporters, or for *in vivo* imaging in general. In addition, their specific solubility and stability properties may facilitate the target protein's isolation and purification or can be used to modify their interactions and distribution.

Chemical bioconjugation techniques comprise widely differing approaches regarding their applicability and specificity. Straightforward methods exploit present carboxyl groups and primary amines of lysines for N-hydroxysuccinimide (NHS) and isothiocyanate (ITC) mediated conjugates or make use of existing thiol groups of cysteines to apply Michael-addition driven modifications. They benefit from their universal availability but suffer at the same time from their limited specificity.

To a certain extent, the aforementioned characteristics are inverted when so-called “click-chemistry” reactions are deployed. Typically, in biochemistry, techniques, that feature outstanding chemoselectivity with high yields in aqueous media and incur no or easy-to-remove byproducts, are classified as “click reactions” [9]. Their unique reactive groups grant distinct site-specificity, as they do not occur in natural peptides or proteins. At the outset, however, the integration of these groups by protein engineering is essential. The most common representative of this reaction category is certainly the Cu(I) catalyzed azide-alkyne cycloaddition (CuAAC), but the related strain-promoted pathway (SPAAC) and other mechanisms like the Diels-Alder cycloaddition and the Staudinger ligation are equally useful tools for protein functionalization.

Modification strategy	Principle of functionalization	References
Enzymatic methods		
Sortase A (SortA)	SortA recognizes an LPXTG motif and replaces the C-terminal glycine residue with an N-terminal glycine from the conjugation partner.	[10], [11]
Microbial transglutaminase (mTG)	mTG facilitates the ligation of glutamine residues with a lysine substrate resulting in a covalent isopeptide bond.	[12], [13]
Trans-splicing with split inteins	Intein fragments fuse and excise themselves in an autocatalytic process, forming a peptide bond between the fragment-containing components.	[14], [15], [16]
Subtiligase	Subtiligase ligates an ester-containing sequence to a range of primary amines (e.g. the N-termini of proteins or peptides).	[17], [18]
Butelase	Butelase cleaves after Asn or Asp in a C-terminal BHV sequence and ligates it to N-terminal amino acids.	[19], [20], [21]
Farnesyltransferase (FTase)	FTase ligates farnesyl diphosphate (or cargo-loaded analogs) solely to the cysteine residue of a C-terminal CAAX-tag.	[22]
Surfactin phosphopantetheinyl transferase (Sfp)	Sfp transfers the 4′-phosphopantetheine (PPT) moiety of coenzyme A to a serine residue in an 11 amino acid sequence. PPT exhibits a thiol group, which can be modulated beforehand or may serve as a handle.	[23]
Formylglycine-generating enzyme (FGE)	FGE converts Cys in an LCXPXR-consensus sequence into formylglycine. Subsequently, conjugates can be installed via the aldehyde functionality exploiting Hydrazino-iso-Pictet-Spengler (HIPS) ligation.	[24], [25]
Tubulin-tyrosine ligase (TTL)	TLL links tyrosine or functionalized derivates to a unique 14 amino acid motif, thus creating a site-specific handle for further attachments.	[26], [27]
Fusion proteins		
Streptavidin	After fusing Streptavidin to a protein of interest, conjugates can be formed with biotinylated payloads, via an extraordinarily strong protein – ligand connection.	[28]
SNAP- and CLIP-tags	A covalent connection emerges between the fused enzyme itself (mutants of O^6-alkylguanine-DNA alkyltransferase) and the ligands (cargo-tagged O^6-benzylguanine or O^2-benzylcytosine derivates).	[29], [30]

HaloTag	The HaloTag (a modified bacterial haloalkane dehalogenase) covalently binds chloroalkane-functionalized load.	[31]
Standard chemical methods		
EDC - NHS chemistry	Carboxyl groups can be activated via EDC and (Sulfo-)NHS to form stable amide bonds with amines.	[32]
Native chemical ligation (NCL)	The sulfhydryl group of an N-terminal cysteine residue attacks a C-terminal thioester resulting in a transthioesterification. After a spontaneous S-N acyl rearrangement, a stable peptide bond emerges.	[33]
Isothiocyanates (ITC)	The ITC functionality binds to primary amines, creating thiourea conjugations.	[34]
Thiol-Michael reaction	Thiol groups react via Michael addition with various enolate nucleophiles like maleimides, acrylates, or acrylamides.	[35]
Click chemistry reactions		
Huisgen azide-alkyne cycloaddition	Azide groups and alkyne functionalities react under mild conditions, creating a triazole conjugation either Cu(I) catalyzed (CuAAC) or strain promoted (SPAAC).	[36]
Diels-Alder cycloaddition	Electron-deficient dienophiles and electron-rich 1,3-dienes ligate in a [4+2] cycloaddition resulting in carbocycle conjugate.	[37], [38], [39]
Staudinger ligation	Azides react with ortho-phosphine terephthalic acid derivates to yield a cyclization intermediate, which is spontaneously hydrolyzed to form a stable amide bond.	[40], [41], [42]
Thiol-ene reaction	Radical induced (photochemically or metal-catalyzed), hydrothiolation of carbon-carbon double bond structures.	[43], [44]

Table 1 **Selection of bioconjugation strategies**

As biocatalysts, transglutaminases are exceptional in that they do not depend on an exact recognition pattern but are rather governed by the accessibility of the individual substrate and its circumjacent structures [45]. This characteristic along with its well-established large-scale preparation has made microbial transglutaminase (mTG) one of the most studied and extensively used enzymes today [46]. Although Ca^{2+}-dependent eukaryotic transglutaminases have fallen somewhat behind over the years due to their generally slower

reaction kinetics, studies suggest that large differences in reaction speed can be realized by minor changes in the substrate sequences [47, 48]. In addition, the different transglutaminases exhibit considerable deviations in their substrate specificities [49], so the distinct selection of the appropriate enzyme can have a major influence on product formation. Especially, when considering the approval conditions for new biologicals according to the EMA or FDA, enzymes of human origin are of particular interest, as they can more easily cope with immunogenicity and toxicity concerns. In fact, mTG and some industrial crosslinked compounds have recently been identified to be immunogenic to patients with coeliac disease [50]. Although comparable findings are also known for human tissue transglutaminase, no direct correlation has been demonstrated for other members of the enzyme family [51].

On that note, factor XIIIa (FXIIIa), another human transglutaminase, has successfully been used in different applications such as the formation of hydrogels or in the context of wound healing using tissue-engineering [52, 53].

FXIIIa is the thrombin-activated form of factor XIII, a heterotetramer composed of two a and two b subunits, whereby both b units get separated in the activated state [54]. Its intrinsic purpose is to facilitate blood coagulation by crosslinking adjoining fibrin fibers with each other and other plasma proteins to stabilize blood clots. Its catalytic triad of Cys314, His373, and Asp396 promotes an acyl-transfer between the γ-carboxamide group of a glutamine residue and the ε-amino group of a lysine residue, forming an ε-(γ-glutamyl)lysyl bond [55]. In particular, glutamine-containing substrates have been studied to gain a better understanding of FXIIIa specificity [56-58]. It is of critical importance to be aware of possible substrate structures within the targeted protein and to select high-affinity donor peptides to achieve the desired modifications in high yield.

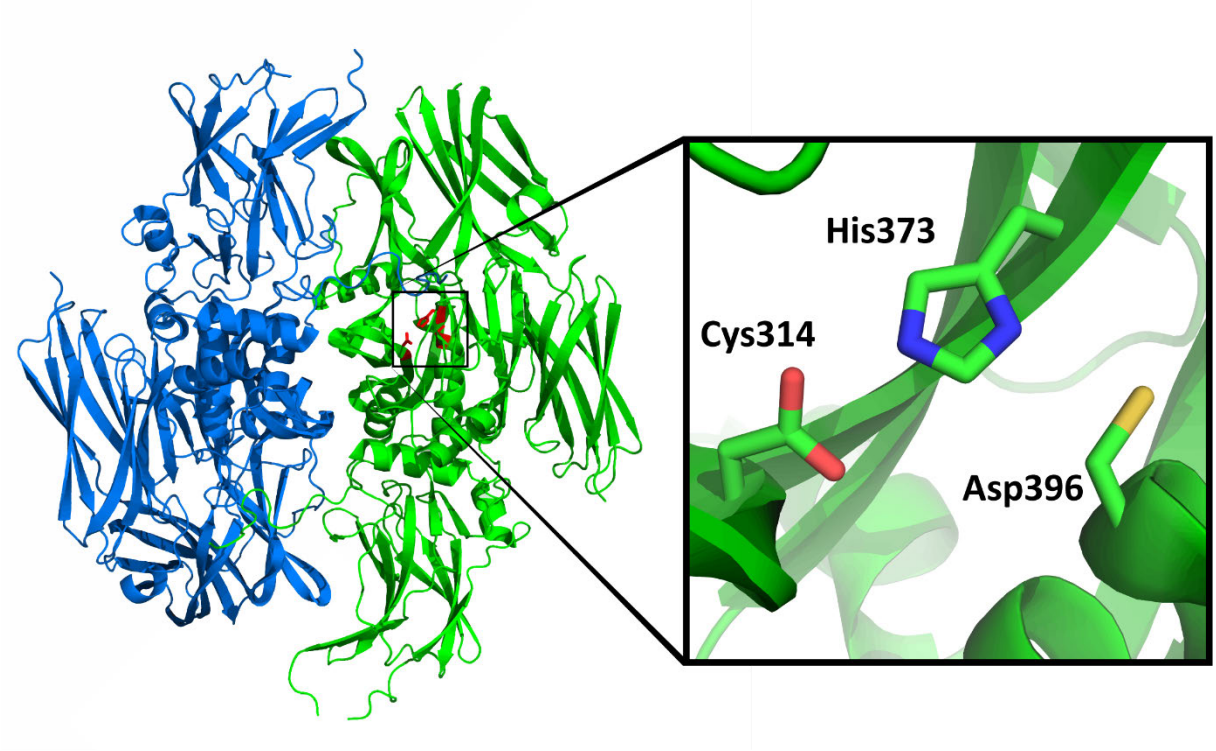

Figure 3.1.1 **X-ray crystal structure of factor XIII (PDB 1F13) with both A subunits, highlighting the catalytic triad of one chain in its inactive state.**

As arguably the most popular "click-reaction", CuAAC alias azide-alkyne Huisgen cycloaddition is excellent for use in bio-orthogonal functionalization. Although the reaction principle was already known in the late nineteenth century, it was not until Huisgen, that its potential was truly realized. For this highly regioselective formation of a 1,4-disubstituted 1,2,3-triazole, basically any azide group and terminal alkyne can be deployed [59]. The most significant constraint for this reaction is the need for a copper catalyst, which is proven to be cytotoxic and can moreover cause unspecific byproducts through the formation of reactive oxygen species (ROS) [60]. However, stabilizing copper(I) ligands such as TBTA or THPTA are routinely used as counter measurement and boost reaction kinetics at the same time. In fact, Besanceney-Webler *et al.* found a BTTAA-Cu(I) complex that shows no cellular toxicity whatsoever [61]. Alternatively, the ligation can be achieved without the use of a metal catalyst, exploiting the strain energy of cyclic alkynes via SPAAC. Albeit cycloalkynes generally boast higher reaction rates, they suffer from reduced selectivity when compared to linear alkyne analogs [62, 63]. However, SPAAC and CuAAC, are equally versatile tools. Both techniques are used continuously, even to the extent that they are deployed side by side [64].

3.2 Protein and Genetic Code Engineering

Within the scope of this work two distinctive conjugation strategies are pursued, namely an enzymatic approach with transglutaminase factor XIIIa (FXIIIa), and the CuAAC as a "click-reaction", combined with basic chemical methods to prepare and link payloads when desired. Both techniques however require specific adaptations within the protein of interest to make their application possible.

Within the relatively young discipline of protein engineering, rational design and directed evolution can be seen as the two fundamental approaches, although the manifold deriving strategies often intertwine [65]. Directed molecular evolution is a powerful tool when the structure and/or function of the protein of interest is insufficiently understood to induce targeted alterations [66]. Through random mutagenesis techniques, e.g., DNA-Shuffling or error-prone PCR, large libraries are generated, which in turn are screened for suitable candidates with the desired perks. This procedure resembles the evolutionary principle, hence the titling. Attributable to the vast possibilities of random formations, non-rational design approaches have great potential when basic properties, like general stability or affinity, of the protein are in focus [67].

However, while aiming for extremely specific, deliberate customizations, which are crucial for many biofunctionalization strategies mentioned in the previous section, a rational design approach is the logical choice. While the scale of methods includes very recent de novo protein designs with computational techniques and algorithms [68, 69], well-established procedures like site-directed mutagenesis are the perfect tool to introduce minor alterations. For whichever rational design strategy to be deployed, extensive knowledge about the protein of interest's properties is required, since any modification to the molecule may interfere with its functional or structural integrity.

For this reason, enhanced green fluorescent protein (eGFP) was chosen as a model protein in this work. It is comprehensively studied and brings unique features, which make it a perfect proof-of-concept protein for various research purposes [70, 71]. GFP's characteristic beta-barrel scaffold harbors a green fluorescence emitting chromophore, that forms autocatalytic after translation.

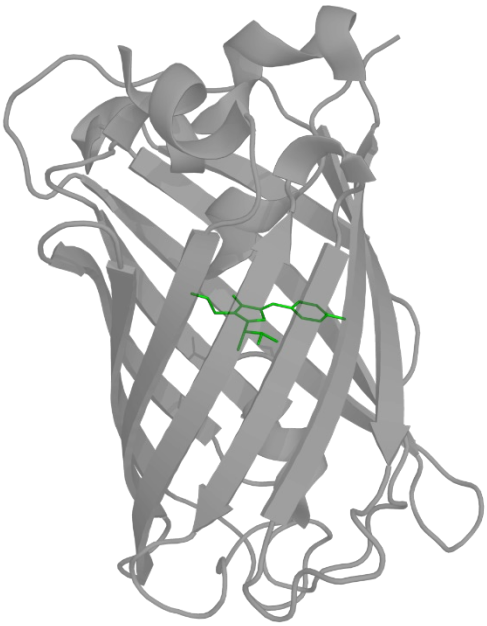

Figure 3.2.1 **Enhanced green fluorescent protein (eGFP) (PDB 2Y0G) with its chromophore highlighted in the center.**

The chromophore-mutated eGFP is significantly brighter than wild-type GFP, originating from the jellyfish Aequorea Victoria. A substantial asset of any GFP variant is, that its functional efficiency is inextricably linked with its proper folding, with the result that integrity-interfering modifications can easily be recognized since they will cause the protein to lose its fluorescence. Various data about eGFP's sequence and structure have proven that modifications can comfortably be implemented at its terminal ends [71-73].

Consequently, rational methods like overlap extension and point mutation are readily applicable. Here, the desired mutations are incorporated into the protein via PCR using synthetic DNA primers. In this way, amino acid motifs for enzymatic approaches like the mentioned FXIIIa strategy can conveniently be introduced to the protein.

Allowing for a much smaller footprint than an average amino acid motif, while maintaining exceptional specificity, the use of genetic code expansion [74] has formed into a versatile tool to incorporate unnatural amino acids (uAA) carrying exclusive functional groups, which enable "click-chemistry" techniques like CuAAC. The procedure requires the implementation of an amber (TAG) codon in the gene of interest. While this codon normally causes the translation process to stop since there is no corresponding tRNA available in standard expression hosts, the utilization of the biological machinery found in methanogenic archaebacteria makes the incorporation of non-canonical amino acids possible. In natural

surroundings, the amino acid L-pyrrolysine (Pyl) is transferred to the respective $tRNA^{Pyl}$ via pyrrolysyl-tRNA synthetase (PylRS). Due to the fact that this specific synthetase also accepts certain Pyl-analogues as ligation substrates, alkyne derivates have been successfully introduced in other proteins [75-77]. Therefore, equipping an expression strain with the respective tools creates an exceptionally flexible protein modification strategy.

3.3 Surface Functionalization

The decoration of biologics is certainly not the only discipline that benefits from site-directed biofunctionalization. In recent years, the immobilization of proteins has found countless potential use cases, e.g., for drug release systems in therapeutics [78], as biosensors and chips in diagnostics [79], or as selective bioreactors in industrial biotechnology [80, 81]. Analogously, therapeutically, and diagnostically utilized surfaces arise in an ever-growing variety of geometries and materials ranging from metallic nanoparticles, over polymeric films, and microspheres to carbon nanotubes as well as silicon or glass carriers [82, 83].

At the same time, metallic structures have rarely found direct application in medicine. Superparamagnetic particles, utilized to induce cancer cell death by tissue heating through magnetic hyperthermia [84], and iron oxide particles as imaging agents in magnetic resonance tomography, or as coated compounds in iron replacement therapy [85], are a few exceptions. Apart from this Gupta *et al.* demonstrated as early as 2004, that lactoferrin and ceruloplasmin derivatized iron particles can effectively manipulate particle distribution in the body [86, 87]. Instead, ferromagnetic structures, such as nanowires [88], are primarily deployed as untethered bio sensors in bio-devices or bioelectronics [89], and as probes in microrheology [90], or fundamental biophysical phenomena, in the manner of facilitating the investigation of inter- and intramolecular binding strengths of proteins and protein complexes in projects like MANAQA. Multisegmented structures are frequently used for these applications. For example, a magnetic segment can be used to create maneuverability, while another part made of non-magnetic metal or polymer layers with functional groups can be used for decoration.

Among metallic surfaces, gold in particular is widely used due to its ability to strongly bind thiols, which arrange in ordered self-assembled monolayers (SAM) [91]. Furthermore, carboxyl groups and siloxanes can selectively bind to transition metals such as cobalt and nickel [92]. If the corresponding substances are loaded with additional functional groups or

recognition patterns, a flexible basis for further specific decoration can be created. By means of subsequent site-directed conjugation of desired enzymes and proteins, these methods can ensure precisely modulatable and homogeneous products with maximum catalytic activity, substrate recognition, or receptor binding, respectively.

4 Aim

As the fields of application for biologics are ever-growing, so is the demand for highly selective conjugation strategies for potential biological APIs [93]. Exploring new or refining existing modification methods play a vital part in this development. Therefore, two different site-directed bioorthogonal conjugation techniques were featured within the scope of this work to parallelly undergo the complete procedure of prerequisite protein design, functionalization, and immobilization, elaborating their transferability and applicability in the process. CuAAC, as a well-established chemical method, and the transglutaminase factor XIIIa, which was rarely used for typical modification tasks by this point, were chosen. In the first step, eGFP as a model protein was engineered at its terminal ends to enable either strategy. After the muteins were expressed and characterized, small molecule conjugation studies were conducted to confirm the expected reactivity while also showcasing their potential as a flexible platform to modify the protein with any desired functionality. Subsequently, the manipulation and decoration of various surfaces were investigated. Nanowires and other particles were deployed to demonstrate preliminary modifications like self-assembled monolayers at a thiol-gold interface or silanization of nickel oxides. Finally, the ability and quality of the featured bioconjugation techniques were validated by their performance in surface decoration. Consequently, this thesis follows the logical outline depicted in ***Scheme 2***.

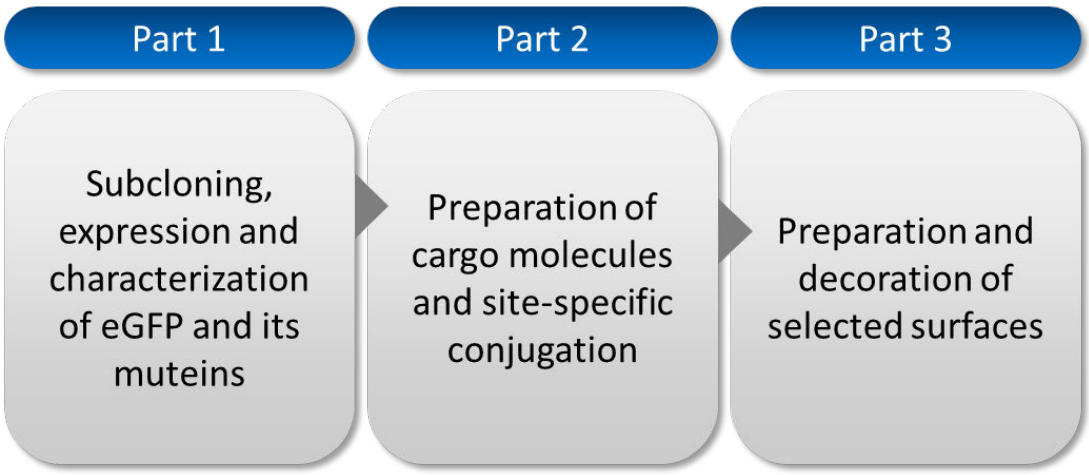

Scheme 2 **General study design**

Aim

5 Materials and Methods

5.1 Materials

5.1.1 Equipment

5.1.1.1 Preparational

Thermal cycler T-Personal	Biometra (Göttingen, DE)
Electrophoresis Power Supply 3000Xi	Bio-Rad (Hercules, CA, US)
Electrophoresis cell Mini Sub Cell GT	Bio-Rad (Hercules, CA, US)
Electrophoresis cell Mini Protean II	Bio-Rad (Hercules, CA, US)
pH Meter Phenomenal 221	VWR (Radnor, PA, US)
Incubator TH15	Edmund Bühler (Bodelshausen, DE)
Shaking incubator MIR 220	Sanyo Gallenkamp (Loughborough, GB)
Ultrasonic homogenizer SONOPULS	BANDELIN electronic (Berlin, DE)
Thermoblock Thermomixer comfort	Eppendorf (Hamburg, DE)
Vortex mixer VV3	VWR (Radnor, PA, US)
Centrifuge Varifuge 3.ORS	Heraeus (Hanau, DE)
Centrifuge Allegra®X-15R	Beckman-Coulter (Brea, CA, US)
Centrifuge 5804 R	Eppendorf (Hamburg, DE)
Ultracentrifuge L8-60M	Beckman-Coulter (Brea, CA, US)
Research pipettes Research® plus	Eppendorf (Hamburg, DE)
Dialysis membranes Spectra/Por	Spectrum Labs (Saint Paul, MN, US)
Centrifugal concentrators Vivaspin 6	Sartorius (Göttingen, DE)
Centrifugal filter Amicon® Ultra	Merck (Darmstadt, DE)
Conical base tubes	Sarstedt (Nümbrecht, DE)
Purification system ÄKTA purifier™ FPLC	GE Healthcare (Buckinghamshire, GB)
Evaporator TurboVap LV	Zymark (Hopkinton, MA, US)
Freeze dryer Alpha 1-4 LSC	Christ (Osterode am Harz, DE)

5.1.1.2 Analytical

FluorChem FC2 imaging system	Alpha Innotech (San Leandro, CA, US)
Genesys 10S UV-Vis spectrophotometer	Thermo Scientific (Waltham, MA, US)
Spectramax 250 microplate reader	Molecular Devices (Sunnyvale, CA, US)
MALDI-MS Autoflex II LRF	Bruker (Billerica, MA, US)
Axio Observer.Z1 microscope	Zeiss (Oberkochen, DE)
La ChromUltra HPLC	Hitachi (Tokyo, JP)

5.1.2 Chemicals and Consumable Supplies

Unless noted otherwise, chemicals used were at least of pharmaceutical grade and were purchased from Sigma-Aldrich (St. Louis, MO, US), Merck (Darmstadt, DE), Roth (Karlsruhe, DE), VWR (Radnor, PA, US), or the chemical supply of the Institute of Organic Chemistry at the University of Würzburg.

mPEG-Acrylamide, 10k Da	Creative PEGWorks (Chapel Hill, NC, US)

5.1.3 Enzymes

Pfu DNA-Polymerase	Thermo Scientific (Waltham, MA, US)
T4 DNA Ligase	New England Biolabs (Frankfurt a. M., DE)
Restriction enzymes	New England Biolabs (Frankfurt a. M., DE)

5.1.4 Molecular-Weight Size Markers

GeneRuler™ 1 kb Plus DNA Ladder	Thermo Scientific (Waltham, MA, US)
GeneRuler™ Low Range DNA Ladder	Thermo Scientific (Waltham, MA, US)
PageRuler™ Prestained Protein Ladder	Thermo Scientific (Waltham, MA, US)
PageRuler™ Unstained Protein Ladder	Thermo Scientific (Waltham, MA, US)

5.1.5 Solutions, Buffers and Growth Media

10x Pfu buffer	200 mM	Tris-HCl pH 8.8
	100 mM	$(NH_4)_2SO_4$
	100 mM	KCl
	1 % (v/v)	Triton X-100
	1 mg/mL	BSA
TAE buffer	40 mM	Tris
	0.11 % (v/v)	Glacial acetic acid
	2 mM	EDTA
	pH 8.5	
Tris-HCl	50 mM	Tris-base
	150 mM	NaCl
PBS	137 mM	NaCl
	2.7 mM	KCl
	10 mM	Na_2HPO_4
	2 mM	KH_2PO_4
	pH 7.4	
MES	50 mM	MES
	500 mM	NaCl
	pH 6.0	
HisTag binding buffer	500 mM	NaCl
	17 mM	Na_2HPO_4
	3 mM	NaH_2PO_4
	25 mM	Imidazole
	pH 7.5	
HisTag elution buffer	500 mM	NaCl
	17 mM	Na_2HPO_4
	3 mM	NaH_2PO_4
	500 mM	Imidazole
	pH 7.5	
Sodium bicarbonate buffer	0.1 M	$NaHCO_3$
	pH 8.2	

TBST	15 mM	Tris
	137 mM	NaCl
	1 %	Tween 20
Agar medium	1.4 %	Agar
	0.8 %	NaCl
	1 %	Tryptone
	0.5 %	Yeast extract
	0.5 %	Glucose
	pH 7.5	
Minimal medium	137 mM	NaCl
	2,7 mM	KCl
	10 mM	Na_2HPO_4
	2 mM	KH_2PO_4
	2 mM	$MgSO_4$
	0.1 mM	$CaCl_2$
	2 %	Glycerol
	pH 7.4	
SOC medium	20 g/l	Tryptone
	5 g/l	Yeast extract
	10 mM	NaCl
	2.5 mM	KCl
	10 mM	$MgCl_2$
	10 mM	$MgSO_4$
	20 mM	Glucose
LB medium	10 g/l	Tryptone
	5 g/l	Yeast extract
	86 mM	NaCl
	20 mM	$MgSO_4 \cdot 7H_2O$
	5.5 mM	Glucose
TB medium	12 g/l	Tryptone
	24 g/l	Yeast extract
	4 %	Glycerol
	17 mM	KH_2PO_4
	72 mM	K_2HPO_4

Glycerol stock solution	25 %	Glycerol
	75 %	LB medium
Sonication buffer	500 mM	NaCl
	17 mM	Na_2HPO_4
	3 mM	NaH_2PO_4
	25 mM	Imidazole
	1 mM	PMSF
	pH 7.5	
4x Separating gel buffer	1.5 M	Tris
	0.4 %	SDS
	pH 8.8	
4x Stacking gel buffer	500 mM	Tris
	0.4 %	SDS
	pH 6.8	
Acrylamide/bisacrylamide solution	30 %	Acrylamide
	0.8 %	N,N'-methylene-bisacrylamide
SDS electrophoresis buffer	25 mM	Tris
	192 mM	Glycine
	3.5 mM	SDS
6x SDS sample buffer	70 % (v/v)	4x Stacking gel buffer
	30 % (v/v)	Glycerol
	10 % (w/v)	SDS
	0.6 M	DTT
	0.12 ‰ (w/v)	Bromophenol blue
APS solution	10 % (w/v)	Ammonium persulfate
Coomassie staining solution	0.25 ‰ (w/v)	Coomassie blue G-250
	20 % (v/v)	Acetic acid
Coomassie destaining solution	10 %	Glacial acetic acid
	20 %	Methanol
WB-transfer buffer	25 mM	Tris
	192 mM	Glycine
	20 % (v/v)	Methanol

Ponceau red solution	0.1 % (w/v)	Ponceau S
	5 %	Acetic acid
CAM stain	2.5 % (w/v)	Ammonium molybdate tetrahydrate
	1 % (w/v)	Cerium ammonium sulfate dihydrate
	10 % (v/v)	H_2SO_4
Janus particle DNA buffer	20 mM	Tris pH 8.0
	1 M	NaCl
	0.01 %	Tween 20

5.1.6 Oligos

5.1.6.1 Primers for PCR

WT_eGFP_for
CCCCATATGCATCATCACCATCACCACGTGAGCAAGGGCGAGGAGC

WT_eGFP_rev
CCCGGATCCTTACTTGTACAGCTCGTCCATGCCG

TG_eGFP_for
CCCCATATGGGCGGTAACCAGGAACAGGTTTCTCCGCTGTGAGCAAGGGCGAGGAGC

TG_eGFP_rev
CCCGGATCCTTAGTGGTGATGGTGATGATGCTTGTACAGCT CGTCCATGCCG

iA_eGFP_for
CCCCATATGGGCGGTGTGAGCTAGGGCGAGGAGC

eA_eGFP_for
CCCCATATGCTGGGTGGCGGTGGTTAGGCTGCGGCTGTGAGCAAGGGCGAGGAGC

A_eGFP_rev
CCCGGATCCTTAGTGGTGATGGTGATGATGCTTGTACAGCTCGTCCATGCCG

Primers were manually designed and synthesized by Invitrogen (Carlsbad, CA, US). Detailed structural description for each primer:

Wild-type eGFP sense primer (WT_eGFP_for):

Wild-type eGFP antisense primer (WT_eGFP_rev):

Transglutaminase eGFP sense primer (TG_eGFP_for):

Transglutaminase eGFP anti-sense primer (TG_eGFP_rev):

Internal amber eGFP sense primer (iA_eGFP_for):

External amber eGFP sense primer (eA_eGFP_for):

Amber eGFP anti-sense primer (A_eGFP_rev):

5.1.6.2 Oligos for Surface Attachment

Cy3_test_strand_for	Biotin - TTGACCTCGTAGGGCAGCTCCGGA-Cy3
Cy3_test_strand_rev	Thiol - C9 Spacer - TCCGGAGCTGCCCTACGAGGTCAA
Dbl_attachment_for	Biotin - TTGACCTCGTAGGGCAGCTCCGGA - C9 Spacer - Thiol
Dbl_attachment_rev	Thiol - C9 Spacer-TCCGGAGCTGCCCTACGAGGTCAA - Biotin

Modified oligos were manually designed and synthesized by Biolegio (Nijmegen, NL).

5.1.7 Plasmids

pET11a (Novagen)

An ampicillin-resistant plasmid containing the pyrrolysine tRNA, the lipoprotein promotor lpp, and the terminator RRN b/c as described by Eger *et al.* Kindly provided by Dr. Marina Rubini. Graphical representation of essential plasmid features:

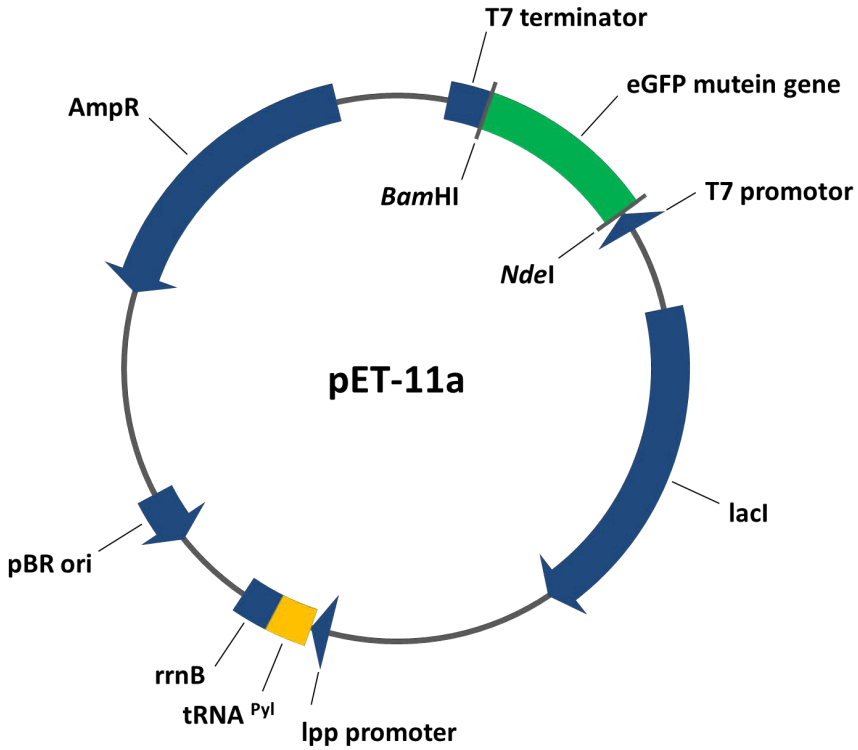

pRSF-Duet (Novagen)

A kanamycin-resistant vector containing the gene for the pyrrolysine tRNA synthetase pylS in the MCS II as described by Eger *et al.*

Kindly provided by Dr. Marina Rubini.

Graphical representation of essential plasmid features:

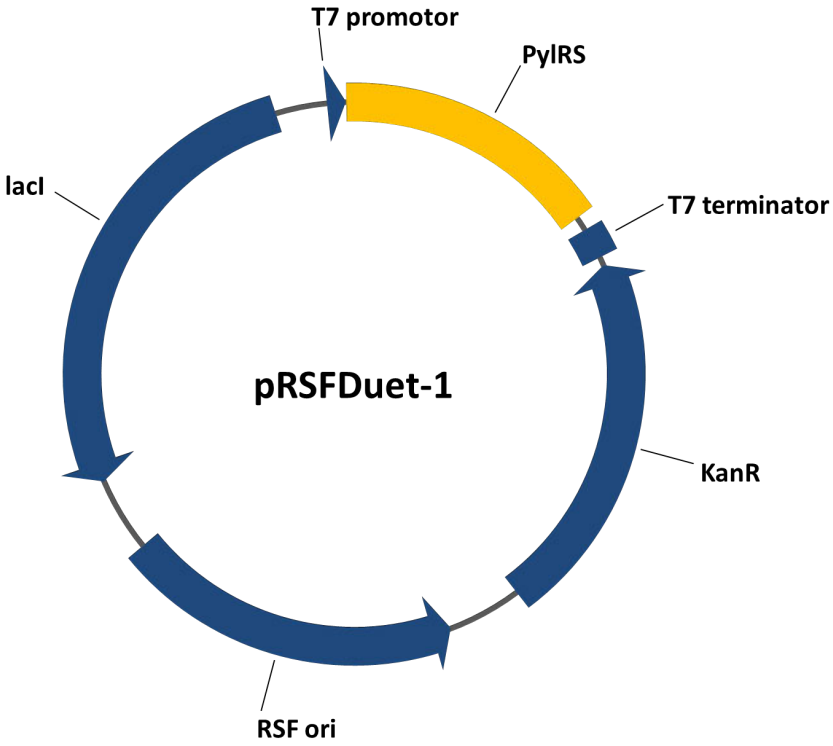

pHisTrx (Novagen)

An ampicillin-resistant plasmid containing the gene for *E. coli* thioredoxin (trxA), an N-terminal 6-His tag, a thrombin cleavage site, and a unique MCS. Kindly provided by Dr. Richard A. Kammerer.

5.1.8 *E. coli* Strains

One Shot® MAX Efficiency® DH5α™-T1^R Competent Cells

F$^-$φ80*lac*ZΔM15 Δ(*lac*ZYA-*arg*F)U169 *rec*A1 *end*A1 *hsd*R17(r_k^-, m_k^+) *pho*A *sup*E44 *thi*-1 *gyr*A96 *rel*A1 *ton*A

Purchased from Thermo Scientific (Waltham, MA, US).

DH5α

F⁻ *endA1 glnV44 thi-1 recA1 relA1 gyrA96 deoR nupG purB20* φ80d*lacZ*ΔM15 Δ(*lacZYA-argF*)U169, hsdR17($r_K^- m_K^+$), λ⁻

Kindly provided by Prof. Dr. Sven Panke.

BL21(DE3)

B F⁻ *ompT gal dcm lon* $hsdS_B(r_B^- m_B^-)$ λ(DE3 [*lacI lacUV5-T7p07 ind1 sam7 nin5*]) $[malB^+]_{K\text{-}12}(\lambda^S)$

Kindly provided by Prof. Dr. Sven Panke.

5.1.9 Surface Materials

Nanowires of variable compositions	Kindly provided by Bumjin Jang
Ti/Ni/Au composed Janus-particles	Kindly provided by Dr. Carlos Alcantara
PEG-NH_2 modified micromer®-M particles	micromod Partikeltechnologie (Rostock, DE)

5.2 Methods

5.2.1 Subcloning and Protein Preparation

5.2.1.1 DNA Amplification via Polymerase Chain Reaction (PCR)

Primers were designed to meet the required alterations and ordered accordingly from Invitrogen by Life Technologies (Carlsbad, CA, US). To introduce any desired modification (a hexa histidine-tag for purification, a recognition sequence for FXIIIa, or a TAG-codon for Plk incorporation) into wild-type eGFP, overlap extension- and point mutation-primers were used. Typically, the following reactants and concentrations were prepared:

Reagent	Volume [µL]
Pfu DNA 10x buffer	5
dNTPs 10 mM	0.15 each
$MgSO_4$ 50 mM	1
upstream primer 10 µM	1.5
downstream primer 10 µM	1.5
eGFP-N1 DNA 2.8	1
Pfu DNA Polymerase 2.5	0.4
nuclease-free water	ad 50

Using a preheated Biometra T-Personal cycler, the PCR program steps were set up as follows:

1. initial denaturation 95 °C 2 min
2. denaturation 95 °C 45 sec
3. annealing 60 - 69 °C 30 sec
4. extension 72 °C 4.75 min
5. final extension 72 °C 5 min
6. hold 4°C ∞

Steps 2 – 4 were repeated in 30 cycles. To determine the annealing temperature for each pair of primers individually, OligoCalc was used [94].

5.2.1.2 Agarose Gel Electrophoresis, DNA Extraction, and Concentration Determination

Gels with 2 % agarose in TAE buffer were cast to isolate the amplified DNA from the PCR reaction mixture. To visualize the DNA, Midori Green Advanced DNA Stain (Nippon Genetics Europe) was added during the gel casting. Samples were loaded into the gel with 6x Mass Ruler DNA Loading Dye and separated deploying a BIORAD electrophoresis model 3000 Xi combined with a Mini Sub Cell GT. An electrical current was applied for about 45 min at 100 V. Appropriate DNA ladders were applied for assessing the size of the resulting DNA fragments. The detection and documentation were accomplished through a GelVue Transilluminator model GVM 20 at 302 nm combined with a Gene Flash Gel documentation system (Syngene, Europe). To release the DNA from excised gel slices, the GeneJET™ Gel Extraction Kit (Fermentas) and the associated protocol were used.

The concentration of purified DNA samples was estimated by using a Genesis 10 S spectrophotometer (Thermo Scientific) with a TrayCell cuvette (Hellma Analytics) by following the equation:

$$\text{dsDNA [ng/µL]} = OD_{260} \cdot 50 \cdot 10 \text{ (cuvette cap factor)}$$

5.2.1.3 Digestion of DNA with Restriction Endonucleases

One µL of each restriction enzyme (20,000 units/mL) was added to a total volume of 50 µL containing the appropriate NEB buffer with BSA and 3-4 µg of host-vector or insert DNA, respectively. Samples were carefully mixed by pipetting them up and down, before they were incubated in an Eppendorf Thermomixer at 37 °C for 3-5 h, depending on the enzyme combination. In case double digestion was not suitable, a serial digestion was performed and the Purelink® PCR Purification Kit was used to remove waste products in between. Subsequently, the DNA was purified and processed as described in Chapter 5.2.1.2, however, not before the vector DNA was dephosphorylated (see Chapter 5.2.1.4).

5.2.1.4 Vector Dephosphorylation

To prevent self-ligation of the linearized plasmid, a DNA dephosphorylation was performed in situ right after the restriction digest. Therefor 2 µL Antarctic phosphatase (5,000 units/mL) were added after the solution was adjusted with 10x Antarctic phosphatase

reaction buffer (NEB). The reaction was incubated at 37 °C for 30 min and stopped through enzyme inactivation at 65 °C for 5 min.

5.2.1.5 Ligation of DNA Fragments

The optimal amounts of vector- and insert-DNA for an efficient ligation were calculated using the following equations [95]:

$$(1)\quad V_V = \frac{T}{\left(\frac{V_C \cdot I_L \cdot R}{I_C \cdot V_L}\right) + 1} \qquad (2)\quad I_V = T - V_V$$

Where V_V and I_V are the required amounts of (V) vector- and (I) insert-DNA in µL. T is the total volume reserved for both reactants and was generally set to 17 µL since 1 µL T4 DNA ligase and 2 µL 10x ligase reaction buffer (NEB) had still to be added. R is the targeted insert-/vector-DNA ratio and it was varied from 1 to 4 but set to 2 in most cases. Variables containing subscripted Cs are the given DNA concentrations in ng/µL, whereas I_L and V_L involve the DNA fragment lengths in base pairs.

Prior to the addition of ligase and the related buffer, DNA fragments were mixed, heated up to 45 °C for 5 min to carefully melt eventually cohesive ends, and cooled down again on ice for 30 sec. The combined ligation mixture was incubated for 3-5 h at room temperature. The ligase has not been inactivated afterward.

5.2.1.6 Heat-Shock Transformation of Competent *E. coli* Cells

Competent cells were thawed on ice. Not more than 100 ng or 5 µL of ice-cooled plasmid DNA were added to 50 µL cells and mixed by carefully flicking the tube. The combined suspension was incubated for 20 min on ice. Subsequently, the tube was put in a water bath at 42 °C for 45 s and placed back on ice for at least 2 min immediately after. 250 µL prewarmed SOC medium was added and the diluted suspension was allowed to outgrow in a TH15 orbital incubation shaker (Edmund Bühler, Hechingen) at 37 °C and 225 rpm for 1 h. Finally, 200 µL of bacterial culture were streaked on prewarmed agar plates, containing appropriate antibiotics, and single colonies were selected after overnight incubation at 37 °C. Competent DH5α bacteria were used after initial insert/vector ligations, whereas BL21(DE3) cells were deployed for isolated plasmids intended for expression. In cases were

the pRSF-Duet vector was cotransformed, it was used in threefold molar excess to its partner plasmid.

5.2.1.7 Plasmid Preparation

For small-scale preparations, selected colonies of a transformation were incubated overnight in 6 mL LB medium with appropriate antibiotics at 37 °C in 15 mL tubes at 250 rpm, using a MIR 220 shaking incubator (Sanyo Gallenkamp, Loughborough, UK). Samples were gradually transferred into a 2 mL tube, accumulating a pellet via centrifugation at 11,000 g for 30 s, while discarding the supernatant after each step. Subsequently, the DNA isolation and purification were run following the NucleoSpin® Plasmid kit (Macherey-Nagel, Oensingen, Switzerland) instructions.

NucleoBond® Xtra Maxi kit (Macherey-Nagel, Oensingen, Switzerland) was used for large-scale preparations. The initial incubation volume was set to 200 mL.

5.2.1.8 Diagnostic Digest and DNA Sequencing

To verify completed insert integration, new plasmid constructs were digested with two restriction endonucleases, of which at least one differed from the enzymes used for the initial installation (Chapter 5.2.1.3), and analyzed via agarose gel electrophoresis (Chapter 5.2.1.2). Samples showing the right fragment lengths were sent off for T7 terminator-based sequencing (Eurofins Genomics, Ebersberg). Correctly build constructs were transformed into BL21(DE3) bacteria as described in Chapter 5.2.1.6.

5.2.1.9 Preparation of Competent Bacteria Cells

To generate competent *E. coli* cells a simplified calcium chloride method was deployed. A single colony of a given bacteria strain was inoculated with 10 mL LB medium in a 50 mL falcon tube and incubated overnight at 37 °C and 180 rpm. Subsequently, 0.5 mL of that culture was used to inoculate 100 mL fresh LB medium in a 500 mL flask, applying the same growing conditions. At an OD_{600} of 0.6, cells were put on ice for at least 10 minutes and kept cold for the remaining procedure. For handling reasons, the bacteria culture volume was split in half, but each portion was treated equally. Cells were collected by centrifugation at 5000 rpm, 4 °C for 10 min. After decanting the supernatant, the pellets were carefully resuspended in 45 mL of modified $CaCl_2$ solution and incubated on ice for 30 minutes, before they were

centrifuged once more. Once the supernatant was discarded, pellets were gently resuspended in 2 mL modified $CaCl_2$ solution and quickly dispensed to precooled Eppendorf tubes in 50 µL aliquots. Competent cells were stored at -80 °C.

5.2.1.10 Expression of Wild-Type eGFP

All protein genes were carried by pET11a vectors and transformed into *E. coli* strain BL21(DE3). In a 200 mL flask, starter cultures, consisting of 50 mL LB medium with 2 % glucose and the appropriate antibiotic (100 µg/mL carbenicillin), were inoculated with very little bacterial suspension taken from a glycerol stock. Precultures were incubated at 33 °C and 220 rpm overnight. TB medium supplemented with 2 % glycerol, 2 mM $MgSO_4$, and the required antibiotic (identical to starter cultures) was prepared for expression cultures and inoculated with 1 % starter culture. In most cases 500 mL medium was used in 2 L baffled flasks, whereby traces of PPG were added to prevent excessive foaming. In general, the culture volume never exceeded 25 % of the flask's total volume. At 37 °C and 190 rpm, bacteria were allowed to grow up to an optical density of 0.6 -0.7 at 600 nm before they were induced with 0.3 mM IPTG for 6 - 7 h. Next, bacteria were spun down by centrifugation (4 °C, 4000 rpm, 20 min) and washed with cold His-Tag binding buffer at least once. Subsequently, the resulting pellets were either resuspended or frozen at -80 °C for later purification.

5.2.1.11 Expression of TG-eGFP

TG-eGFP expression was identical to the preparation of wild-type eGFP (Chapter 5.2.1.10) up to the point of induction. Before 1 mM IPTG was added to the culture, the temperature was decreased to 20 °C and the incubation was continued for 24 h. Further processing was unaltered.

5.2.1.12 Expression of Plk-eGFP Mutants

The expression procedure of Plk-eGFP mutants was based on the one detailed in Chapter 5.2.1.10. Due to the cotransformed pRSF-Duet vector, kanamycin was added to the media. The starter culture contained 50 µg/mL of the additional antibiotic, ensuring enhanced selective pressure, whereas the expression culture was provided with a reduced

concentration of 30 µg/mL kanamycin to reduce metabolic stress. As a second adjustment, unnatural amino acids were added at an OD_{600} of 0.3 before bacteria were induced with 1 mM IPTG at an OD_{600} of approximately 0.75.

The incubation temperature was adjusted to 33 °C upon induction and the expression was terminated after 8 h. Post-treatment was unaltered.

5.2.1.13 Protein Purification

Pellets harvested from 500 mL culture medium were resuspended in 20 mL cold His-Tag binding buffer and transferred into a 50 mL conical base tube, precooled in an ice bath. 1 mM PMSF was added before cells were lysed by sonication (Sonoplus, Bandelin, Berlin) using 1-sec pulses with an amplitude of 70 % and 0.8 s pause intervals, in six cycles each lasting 30 s with a 2 min pause in between. The lysate was separated from the unsolvable cell material by two steps of centrifugation (1^{st}: 4 °C, 30 min, 5000 rpm and 2^{nd}: 4 °C, 60 min, 100,000 g ultracentrifugation). The centrifugate was filtered (0.22 µM) and loaded onto an ÄKTApurifier™ chromatography system deploying a HisTrap™ FF crude Ni-column (GE Healthcare, Freiburg). After equilibrating the column and washing the loaded sample, the protein was eluted with His-Tag elution buffer. The eluate was apportioned through absorbance detection at 280 nm. Fractions assigned to the target protein were pooled and dialyzed against PBS overnight using a Spectra/Por® 4 dialyze hose with a 12,000 – 14,000 Da cut-off membrane. The dialysate amounted to at least 200 times the volume of the sample and was replaced after 3 - 4 h to enhance the dialysis efficacy.

At this state, the purified proteins were either stored at 4 °C for immediate use or dialyzed again, gradually reducing salt concentration down to pure water. Subsequent freeze drying was performed for long time storage and a convenient reconstitution.

5.2.1.14 Sodium Dodecyl Sulfate-Polyacrylamide Gel Electrophoresis (SDS-PAGE)

SDS-PAGE analysis was carried out following the commonly used Laemmli protocol [96]. After assembling the casting stands, the separating gel was prepared with 12 % acrylamide using 6.0 mL acrylamide/bisacrylamide solution, 3.75 mL separating gel buffer, and 5.25 mL Millipore water. The mixed solution was degassed for 20 min, before 50 µL of a fresh APS aliquot and 10 µL TEMED were added. The activated solution was immediately cast

into the provided gap and covered with 70 % isopropanol during polymerization to ensure an even surface. After 45 min, the solvent was washed off and the stacking gel was prepared, consisting of 0.65 mL acrylamide/bisacrylamide solution, 3.75 mL stacking gel buffer, and 3.05 mL Millipore water. Polymerization was started with 25 µL APS solution and 5 µL TEMED after the mixture was degassed as well. Teflon combs were inserted, once the still fluent stacking gel was pipetted onto the separating gel. The gels were ready to use after approximately 45 min, but in most cases left overnight in a moist environment at 4 °C to allow for a thorough and uniform polymerization.

Samples, mixed with 6x SDS sample buffer and heated at 95 °C for 5 min, and a molecular weight marker were loaded into the pockets. Sample separation was performed in SDS electrophoresis buffer deploying a BIORAD electrophoresis model 3000 Xi in conjunction with a Mini Protean II. The electric potential was set to 80 V until the samples fully transitioned into the separating gel. At this point, the voltage was increased to 120 V and separation was continued until the marker indicated sufficient distribution.

Following this, the gel was either analyzed by WB analysis or Coomassie blue staining.

5.2.1.15 Matrix-Assisted Laser Desorption Ionization-Mass Spectroscopy (MALDI-MS)

Each sample, containing roughly 20 µg protein in 50 µL buffer, was acidified with 0.1 % TFA and desalted deploying Zip Tip® pipette tips (C18 resin, Millipore, Billerica, MA) following the manufacturer's instructions. Two µL of the eluate was embedded in the same amount of matrix, consisting of equal parts of ACN/water with 0.1 % TFA (1:2, v/v) and HCCA for peptides or Sinapinic acid for proteins, respectively. An Autoflex II LRF instrument (Bruker Daltonics Inc., Billerica, MA) fitted with a 337 nm wavelength nitrogen laser was used to acquire the respective mass spectra in linear positive mode. Protein standard I, containing insulin, ubiquitin, myoglobin, and cytochrome C, or Peptide standard II, containing bradykinin 1-7, angiotensin I and II, substance P, bombesin, ACTH clips 1 – 17 and 18 – 39 as well as somatostatin 28 (both standards: Bruker Daltonics Inc., Billerica, MA), for protein or peptide samples, respectively, were applied for external calibration. Theoretical masses of peptides and proteins were calculated (http://web.expasy.org/peptide_mass) and adjusted manually in case non-canonical amino acids were present.

5.2.1.16 Electrospray Ionization Mass Spectrometry Analysis (ESI-MS) of peptides derived from tryptic in-gel digestion of proteins.

ESI-MS was performed by Werner Schmitz (University of Würzburg) using an APEX-II FT-ICR (Bruker Daltonic GmbH, Bremen, Germany) equipped with a 7.4 T magnet and an Apollo ESI ion source in positive mode. For the generation of peptide mass fingerprints, proteins were separated by SDS-PAGE and stained with colloidal Coomassie. The bands containing the proteins of interest were cut out and treated with trypsin as described by Neuhoff *et al.* [97]. The resulting peptide mixture was desalted using the Zip Tip® C18 resin according to the instructions of the manufacturer (Millipore, Billerica, MA). The desalted sample was continuously injected using a Hamilton syringe at a speed of 2 µL/min with a capillary voltage of 160 V. The detection range was typically set to 300 m/z − 2100 m/z. For each measurement, 128 scans were accumulated at a resolution of 256 K. For evaluation, the mass spectra were deconvolved to the single protonated ion mode using the Bruker Xmas software. The monoisotopic signals were selected for mass determination.

5.2.1.17 Protein Concentration Determination

Bradford assay was used to determine the total protein amount in each sample. A BSA standard was prepared in six dilutions ranging from 50 to 1000 µg/mL protein concentration. Samples were diluted to varying concentrations and analyzed in duplicates. Five µL of each sample was mixed with 145 µL 1x Bradford dye solution (Quick Start™ Bradford protein Assay, Bio-Rad, München) and incubated for 10 min. Blank values were analyzed in water and protein buffer. The absorbance was measured in a Spectromax 250 microplate reader (Molecular Devices, Sunnyvale, CA) at 595 nm, using the dedicated SoftMax Pro software.

To analyze the folded (active) portion of eGFP proteins UV-Vis spectroscopy was used. Samples were diluted to range between 0.1 and 0.3 in absorbance at 488 nm to minimize the self-quenching effects of active eGFP molecules, while the extinction at 280 nm was also monitored to acquire total protein concentration. Taking the respective molecular weights into account, the concentration was calculated using Beer Lambert's law. The extinction coefficient for total eGFP concentration (at 280 nm) was set to 21,890 $M^{-1}cm^{-1}$, whereas the active eGFP specific value (at 488 nm) was calculated with 56,000 $M^{-1}cm^{-1}$ [98].

5.2.1.18 Fluorescence Spectroscopy

The concentration of protein solutions was adjusted to approximately 30 µg/mL before fluorescence spectra were acquired on an LS 50B Fluorescence Spectrometer (PerkinElmer, Waltham, MA). A quartz cuvette was used as measuring cell and all scans were recorded ranging from 200 nm to 800 nm with a scan speed of 150 nm/min. Following the reported values [98], the excitation wavelength was set to 488 nm for emission spectra, and the emission wavelength was set to 510 nm for excitation spectra. All recordings were made with a slit width of 4.7 nm for emission and 9.7 nm for excitation.

5.2.1.19 Active eGFP Concentration Estimation of Live Samples

To rapidly assess the amount of active eGFP generated in a running expression and therefore omit the need to fully express and purify the protein samples at hand, the following method was applied. Relative to the batch size either 2 mL or 10 mL of expression culture were spun down in a 2 mL Eppendorf tube or 50 mL conical base tube, respectively, and washed with HisTag binding buffer three times. Thereafter the samples were resuspended in half the initial volume and supplemented with 1 mM PMSF. With ice-cooling, samples were subsequently lysed by sonication using an appropriate probe diameter. After five cycles of 30 seconds intervals applying 1-sec pulses (with an amplitude ranging from 40 % when using small Eppendorf tubes to 70 % for larger vessels) and 0.8 s pause, with 2 min rest for temperature leveling in between sets, samples were centrifugated at maximum speed for 10 min to remove the majority of cell debris. The resulting supernatant was used for analysis via fluorescence spectroscopy described in Chapter 5.2.1.18.

5.2.1.20 Lyophilization

Protein and peptide samples were cooled down to 4 °C before they were frozen at -80 °C. The condenser of the instrument (Alpha 1-4, Martin Christ Gefriertrocknungsanlagen, Osterode am Harz) was operated at -65 °C. The pre-frozen samples were dried in separately attachable round-bottom flasks above the condenser camber for 48 h at a constant vacuum level of 0.16 mbar. Lyophilized samples were stored at -20 °C.

5.2.2 Site-specific Biomolecule Coupling

5.2.2.1 Propargyl-protected Lysine Derivate (Plk) Preparation

Plk was prepared as previously described [75]. 6.2 g BOC-L-Lys-OH were dissolved in 60 mL 1 M NaOH and 60 mL THF before the solution was cooled to 0 °C in an ice bath. Subsequently, a burette was used to carefully add 1.96 mL propargyl chloroformate dropwise. The mixture was stirred at room temperature for 18 h before it was cooled down again, and the aqueous phase was washed with 300 mL ice-cold Et_2O. 300 mL 1 M HCl was added, and the acidified solution was extracted twice with 300 mL ice-cold EtOAc. The pooled organic phases were dried over approximately 50 g $MgSO_4$ for at least 10 min before the salt was filtered off again. A rotary evaporator was deployed to remove the solvent and obtain a highly viscous residue, which was dissolved in 52 mL dry DCM before 52 mL TFA was added dropwise under stirring. After 1 h, the solvent was evaporated again, and the product was precipitated with 400 mL Et2O as TFA-salt. The white slurry was collected and dried employing consecutive cycles with an applied vacuum and grinding the product to a fine powder in between. H-NMR analysis, performed by Johannes Wiest (University of Würzburg), was deployed for purity and structural integrity evaluation.

5.2.2.2 Solid Phase Peptide Synthesis (SPPS)

SPPS was conducted with a Rink amide resin (Chem-Impex Wood, Dale, IL, US) on a 100 µmol-scale per reaction vessel. The resin was weighed into a syringe and covered with DMF for at least 30 min to allow swelling. The reaction was agitated with 320 rpm on a KS 130 basic shaker (IKA, Staufen) during each incubation time. Fmoc-protection group cleavage was performed in two steps: 3 min exposure with 3 mL freshly prepared 40 % piperidine in DMF and another 12 min with a second solution containing only 20 % piperidine. Subsequently, the resin was washed thoroughly with DMF at least 6 times. For each coupling step, 500 µmol of the respective Fmoc-protected amino acid (Novabiochem Merck-Millipore, Darmstadt) was dissolved in 2 mL DMF containing 0.5 M HOBt. 80 µL DIC was added, and the mixture was incubated for 10 min before it was transferred into the resin hosting vessel. After ten more minutes, 90 µL DIPEA was added, and the reaction was shaken for at least 6 h under the exclusion of light. The resin was washed again with DMF, and the procedure was repeated for the remaining amino acids. The N-terminal amino acid of each peptide was acetylated by treating the resin with a solution of 50 µL acetic anhydride

and 90 µL DIPEA in 2 mL DMF for 20 min. Finally, the resin was washed 6 times with DMF and DCM, respectively and air dried overnight. To cleave the completed peptide from the resin and remove protective side chain groups, a solution composed of TFA/thioanisole/EDT/anisole (90:5:3:2, v/v/v/v) was prepared. 2 mL of the solution was added to the resin and blanketed with N_2, while the reaction was still protected from light. An additional milliliter of the cleavage reagent was added after 1 h and the reaction was continued for another 60 min. The peptide was precipitated by transferring the solution dropwise into a 50 mL Flacon tube filled with 40 mL diethyl ether cooled to -20 °C. The tube was placed into a freezer for 30 min. By centrifugation at 1620 g for 5 min and resuspension of the sediment in replaced diethyl ether, the peptide was washed three times. The pellet was dried under an exhaustion hood overnight prior to its purification.

5.2.2.3 Peptide Purification

Peptide purification was performed on the same preparative chromatography system as used for proteins (Chapter 5.2.1.13). The deployed column was a Jupiter 15 µm C18 300 Å (Phenomenex, Torrance, CA, US). Equilibration and baseline screening were conducted with 2 column volumes of 5 % ACN in water with 0.1 % TFA and a blank run. Samples were loaded at 95 % solvent A (water, 0.1 % TFA) and 5 % solvent B (ACN, 0.1 % TFA). The composition of the eluent was changed in a linear gradient over 5 column volumes to a concentration of 60 % ACN at a flow rate of 8 mL/min. Eluted peptides were detected at 214 nm. After the organic solvent in each fraction was evaporated, the samples were frozen and lyophilized (see Chapter 5.2.1.20). To neutralize the embedded TFA, the pH of reconstituted peptides was adjusted with NaOH.

5.2.2.4 Transglutaminase (TG) Factor XIII (FXIII) Activation

The activation procedure was oriented towards a previously described protocol [52]. At first, lyophilized thrombin powder was dissolved in TBS pH 7.6 to obtain a 1 U/µL solution. Redundant thrombin was aliquoted and stored at -80 °C. FXIII was dissolved in sterile filtered Milli-Q® water to yield a solution of 200 U/mL. Reconstituted thrombin, additional TBS pH 7.6, and 1 M $CaCl_2$ solution were combined (2:95.5:2.5, v/v/v) and sterile filtered to prepare the activation buffer, which was then mixed with the transglutaminase in a ratio

of 1 to 10, by gently flicking the tube. The mixture was incubated in a water bath at 37 °C for 30 min before the activated FXIII (FXIIIa) was aliquoted and stored at -80 °C.

5.2.2.5 Reverse Phase-High Pressure Liquid Chromatography (RP-HPLC)

Protein and peptide purity, as well as TG-reaction specific kinetics, were assessed via RP-HPLC analysis, using a LaChromUltra system (Hitachi, Tokyo, Japan) combined with a diode array detector and EZChrom Elite version 3.3.2 (Agilent, Pleasanton, CA) as analytical software. Purity studies were performed on a Zorbax Eclipse XDB-C18 column (4.6 x 150 mm, 5 µm, Agilent, Pleasanton, CA) equilibrated with a solvent composition of 5 % ACN and 95 % water, both containing 0.1 % TFA as an ion-pair reagent. Elution was induced with a linear gradient ramping up from 5 % to 60 % ACN over 30 min with a 0.7 mL/min flow rate. Injection volume was maintained at 30 µL while the sample concentration was typically around 0.5 – 3 mg/mL. The temperature of the column chamber was constantly held at 40 °C and detection was provided by absorbance measurements at 214 nm and 280 nm.

For kinetic studies, a Synergi™ 2.5 µm Hyrdo-RP 100 Å column (Phenomenex, Aschaffenburg) with 4.6 x 50 mm was used. Solvents, equilibration routine, and gradient range were unaltered, using a steady injection volume of 20 µL. The running time was compressed, and the flow rate was adjusted to 1 mL/min during the separation phase. Sample preparation was standardized and is described in Chapter 5.2.2.9.

5.2.2.6 Peptide Biotinylation

A two-fold molar excess of Biotin-maleimide (Biotin-MI) in proportion to the thiol-containing peptide was dissolved in acetic acid. The combined reagents were incubated at room temperature for at least 5 d, due to pH-reduced reaction kinetic. The reaction was stopped with SpinOut™ GT-100 columns (G-Biosciences, St. Louis, MO), removing unreacted educts through the molecule cut-off. The process was conducted via the manufacturer's instructions. Reaction progression and product purity were assessed by RP-HPLC.

5.2.2.7 Peptide PEGylation

PEG acrylamide (ACRPEG) was dissolved in TBS pH 8.8 providing a 1.5 molar excess over the thiol-containing peptide. The reaction was incubated for 72 h at room temperature. At regular intervals (24 h and 48 h) dithiothreitol (DTT) was added to the solution to reduce oxidized peptide species. The amount of DTT, that was given to the mixture, was limited to 50 % of the initial molar peptide concentration for the first step and 25 % for the second addition, to prevent an excessive competitive reaction with the acrylamide species. HPLC was used to track the reaction progress. The product was purified and characterized by MALDI-MS.

5.2.2.8 Detection of Amino Acids and Aliphatic Amines via Folin's Reagent

The reagent solution was freshly prepared from 100 mg 1,2-naphthoquinon-4-sulphonate dissolved in 50 mL 10 % (w/v) aqueous sodium bicarbonate solution. Analytes with a concentration of approximately 1 mg/mL were applied on a TLC plate. After sample solvents were evaporated, the plate was briefly immersed into the reagent solution and analyzed immediately.

5.2.2.9 Transglutaminase Coupling

The acyl donor peptide (LDP) was given to a solution of an acyl group acceptor counterpart (TG-eGFP, GDP), containing 5 mM $CaCl_2$ and 10 U/mL activated factor XIII in varying concentrations. Buffer (TBS pH 7.6) was used to compensate for missing volumes if needed. The mixture was incubated at different temperatures for a period ranging from a few minutes to 24 hours and stopped by adding TFA to achieve a 0.2 % final solution. Samples were analyzed by RP-HPLC and/or SDS-PAGE. Subsequent western blotting and streptavidin-HRP chemiluminescence signaling were conducted when biotinylated peptides were coupled.

Sample preparation for Factor XIIIa kinetic studies was standardized by using a Transferpette® S-12 0.5 – 10 µL pipette (Brand, Wertheim) to perform multiple reactions at the same time. The reaction volume was set to 20 µL and was stopped with 5 µL diluted TFA solution. To determine the product formation rate, reactions were stopped at 1.5 min and 3 min and the slope was calculated from their respective product AUC.

5.2.2.10 Copper(I)-catalyzed Azide Alkyne Cycloaddition (CuAAC)

1 mM THPTA, 200 µM $CuSO_4$, and 2.5 mM NaAsc (the combination is hereafter stated as click complex) were mixed in that particular order and incubated for approximately 10 min. The mixture was added to a solution containing varying concentrations of the reactive substances. The reaction was incubated for 2 h at most and stopped with EDTA solution in excess to complex free copper ions.

5.2.2.11 Western Blotting (WB) with Streptavidin-Horseradish peroxidase (HRP) Chemoluminescence Signaling

After completing SDS-PAGE, the gel of interest was rinsed with water and WB-transfer buffer, before it was covered with a nitrocellulose blotting membrane and enclosed from both sides with a soaked filter paper and a sponge pad, respectively, ensuring that no air was trapped between any layer. The construct was fixated with a support grid and put in the transfer tank. Blotting was achieved by applying a constant voltage of 80 V for 90 min.

Using a Ponceau red solution, the successful protein transfer was verified before it was washed trice with TBST for 15 min, which removed the staining.

Unspecific bindings were prevented by blocking the membrane with a solution of 5 % BSA in TBST for 1 h. The washing procedure was repeated and streptavidin-HRP treatment with subsequent chemiluminescence activation was performed in accordance with the manufacturer's instructions, using SuperSignal® West Pico Chemiluminescent Substrate (Thermo Scientific, Rockford, IL) reagents. The signals were documented using a FluorChem FC2 encasement with dedicated imaging software and a mounted CCD camera.

5.2.3 Micro- and Nano-Surfaces

5.2.3.1 Nanowire Fabrication-Template Removal and General Handling

Nanowires were generated through electrochemical deposition and kindly supplied by Bumjin Jang (ETH Zurich) [99, 100]. In case nanowire material was not received in suspension, the following protocol was used to remove the template. The aluminum oxide scaffold was dissolved by adding the template into 5 M sodium hydroxide solution at 50 °C for about 5 minutes. The material was held in place with a magnet while DI water was used

to rinse the alkaline solution off. Subsequently, Copper Etchant 49-1 ($Fe(Cl)_3$-based solution provided by ETH Zurich) was applied to remove an additional copper segment. The etching process was not allowed to exceed 5 minutes to prevent performance-impairing nanowire oxidation. Finally, the loose nanowires were transferred to Eppendorf tubes and washed five times with DI water and ethanol. Each cleaning procedure step was facilitated by deploying low-power tip sonication. The obtained nanowire suspension was stored in ethanol until further use.

Approximately 150 µg nanowires were used in each subsequent experiment, which was conducted in 1.5 mL Eppendorf tubes. Before and in between any following dispersion or washing step low power sonication pulses were utilized. During reaction and incubation times the nanowires were agitated in an Eppendorf shaker at 1200 rpm to avoid sedimentation. These conditions were always met unless stated otherwise.

5.2.3.2 General Bead and Particle Handling

NH_2-PEG beads and Janus gold/nickel particles were stored in water and ethanol, respectively. The shaker speed to hold the material in suspension was set to 800 rpm, whereas all other conditions matched those mentioned for nanowires for surface modification (Chapter 5.2.3.1).

5.2.3.3 Nanowire Passivation and Functionalization

The passivation and functionalization process was adapted after a previously described method [92]. In the most basic setup, APTES was added to achieve a concentration of 18 mM in 500 µL ethanol and the nanowires were maintained in suspension for 24 h. The nanowires were washed with ethanol three times followed by another two times with 0.1 M sodium bicarbonate. 0.1 mg MethoxyPEG-NHS, dissolved in 500 µL of the carbonate buffer solution, was added and the nanowire suspension was agitated for 2 h. Finally, the wires were washed several times in PBS.

Different protocols were implemented to examine the effect on the silanization step, including varying concentrations of APTES (6 – 30 mM) and supplementary BTESE (one-tenth of APTES concentration), the addition of either 5 % aqueous acetic acid or concentrated ammonium hydroxide and curing the nanowires in vacuo for 24 h at 30 °C or

15 min at 115 °C [101]. Commonly, 6 mM APTES and 0.6 mM BTESE in 1.5 mL EtOH with 5% concentrated NH_4OH were allowed to hydrolyze for 5 min. Approx. 0.1 - 0.2 mg nanowires were added and incubated for 10 min with 1-sec sonication pulses every 12 seconds. Afterward, the nanowires were washed twice with ethanol. To allow for further functionalization, untreated or passivated nanowires were suspended in 500 µL of 5 mM ethanolic AUT solution for at least 18 h. Wires were then washed in an appropriate solvent dependent on the desired cargo substrate. Silanization and functionalization priming quality was monitored by FITC staining and subsequent fluorescence imaging.

5.2.3.4 FITC Staining

Nanowires were washed with DMF before 0.2 mg FITC dissolved in 700 µL DMF was added to them. After suspending the wires, 0.5 µL DIPEA was supplemented, and the reaction was allowed to proceed for 2 h. The nanowires were then washed twice with DMF and three times with ethanol. All steps were executed to the exclusion of light as much as possible.

5.2.3.5 Fluorescence Imaging

The volume of the nanowire or bead suspension was reduced to 300 µL. Following this, 7 µL of the resuspended material was placed on a microscope slide and covered with a cover glass, which was fixated by using nail polish. For evaluation, Zen 2 blue edition imaging software was used in conjunction with an Axio Observer.Z1 inverted microscope holding insertable high-efficiency GFP and Cy3 filters (Carl Zeiss, Oberkochen).

5.2.3.6 Functionalization with DNA

Double-stranded DNA was generated using a simplified PCR cycle. One nmol of corresponding single-strand DNA (Biolegio, Nijmegen, Netherlands) was mixed and heated up to 95 °C for 2 minutes, annealed for 30 seconds at 65 °C, and left until it reached room temperature. Ten µL containing 0.5 nmol of the resulting dsDNA were added to untreated gold-surface-providing material, which was previously washed and present in 500 µL modified Tris buffer. The suspended material was incubated for at least 18 h. If the DNA

was provided with a fluorescent marker, the sample was evaluated with fluorescence imaging afterward.

5.2.3.7 Functionalization with Enoxaparin

To attach enoxaparin to AUT-primed nanowires or NH_2-PEG beads a two-step EDC/Sulfo-NHS reaction was deployed. 1 mg enoxaparin (freeze-dried Clexane®, Sanofi-Aventis, Frankfurt) was dissolved in 240 µL MES buffer pH 6.0 containing 80 mM Sulfo-NHS and 8 mM EDC, which equals roughly a 10-fold molar excess over carboxyl groups present in the given enoxaparin amount. The mixture was vortexed and incubated for 15 min on a tube roller to activate a portion of the free carboxyl functional groups. Immediately after this, the solution was transferred into another Eppendorf tube containing either pretreated nanowires or amino-functionalized beads in 60 µL of 0.25 mM sodium phosphate buffer. The pH value of the resulting solution was adjusted to pH 7.2 – 7.5 After resuspension, the material was incubated for another 2 h. Finally, PBS with increased ionic strength (0.5 mM NaCl) was used to wash all samples at least five times.

5.2.3.8 Synthesis of $ImSO_2N_3$ as Azido Transfer Reagent

To allow for an amine-azide conversion and subsequent CuAAC, $ImSO_2N_3$ was synthesized following a previously described protocol [102]. In short 16.1 mL sulfuryl chloride was added dropwise to an ice-cooled suspension of 13.0 g NaN_3 in 200 mL AcN and stirred for 16 h at room temperature. While stirring, the mixture was cooled down again in an ice bath before 25.9 g of imidazole was added in small portions. After 3 h the cloudy suspension was diluted with 400 mL EtOAc before it was washed twice with 400 mL DI water and 400 mL saturated aqueous $NaHCO_3$ and finally filtered with the help of a Buchner funnel once it was dried over $MgSO_4$. Under continuous stirring, 75 mL acidified ethanol, prepared by carefully adding 21.3 mL acetyl chloride to ice-cooled dry ethanol of the given volume, was transferred dropwise to the filtrate. The resulting suspension was cooled down again and subsequently filtered using a Buchner funnel. The retentate was washed with 100 mL EtOAc three times before it was dried under vacuum to obtain $ImSO_2N_3$ as HCl salt. The product was verified by ESI-MS and NMR and stored in the freezer at -20 °C.

5.2.3.9 Amine-Azide Conversion

The deployed conversion method was derived from previously described procedures [102]. Surface material exposing amine functional groups was washed with methanol at least three times. 1.05 mg $ImSO_2N_3$, 3.4 µg $ZnCl_2$, and 3.5 µL Et_3N were dissolved in a total amount of 500 µL methanol and added to the nanowires or beads, respectively. The reaction mixture was resuspended and incubated for at least 16 h before the material was washed twice with methanol and three times with an appropriate solvent for the following experiment.

5.2.3.10 Thin-layer Chromatography

Species and reactions of interest were applied onto aluminum oxide matrices on aluminum support foils (Merck, Darmstadt) in a dotted line via a capillary. Chloroform/methanol/20 % acetic acid (65:25:5, v/v/v) was used as solvent system for primarily polar compounds, whereas hexane/EtOAc (4:1, v/v) was deployed as eluent for substances with more ambivalent characteristics. After a short incubation allowing for a sufficient compound separation, the plates were developed using CAM stain and rigorous heating.

5.2.3.11 Surfaces Functionalization via CuAAC

The CuAAC protocol for surfaces was adapted from Chapter 5.2.2.10. The general process and concentrations for all reactants were maintained, whereas the reaction volume and composition were consistently set to 250 µL of PBS with 0.01 % Tween 20. In case 5-FAM-azide was used as azide donor, 2.25 µL of a 1 mg/mL dye solution was added to the mixture. When Plk-modified eGFP was deployed, 225 µL of a 0.5 mg/mL protein solution was used in PBS buffer.

5.2.3.12 Surfaces Functionalization via FXIIIa

The procedure for transglutaminase-mediated conjugation onto surfaces was adapted from Section 5.2.2.9. The concentrations for $CaCl_2$ and FXIIIa were unaltered. The reaction volume was consistently set to 250 µL at what TG-eGFP was deployed as 225 µL of a 1 mg/mL protein solution in TBS buffer. 2 µL of magnetic NH_2-PEG polystyrene-matrix particles at the manufacturer-provided concentration were used. The reaction was stopped after 16 h at room temperature by collecting and washing the beads 5 times with TBS buffer.

6 Results

6.1 Subcloning and Protein Preparation

The following section describes the creation and characterization of the eGFP muteins, which were generated in the course of this work. EGFP served as a model protein in order to establish a reference point for subsequent conjugation reactions. A structural outline of all variants is illustrated in ***Figure 6.1.1***.

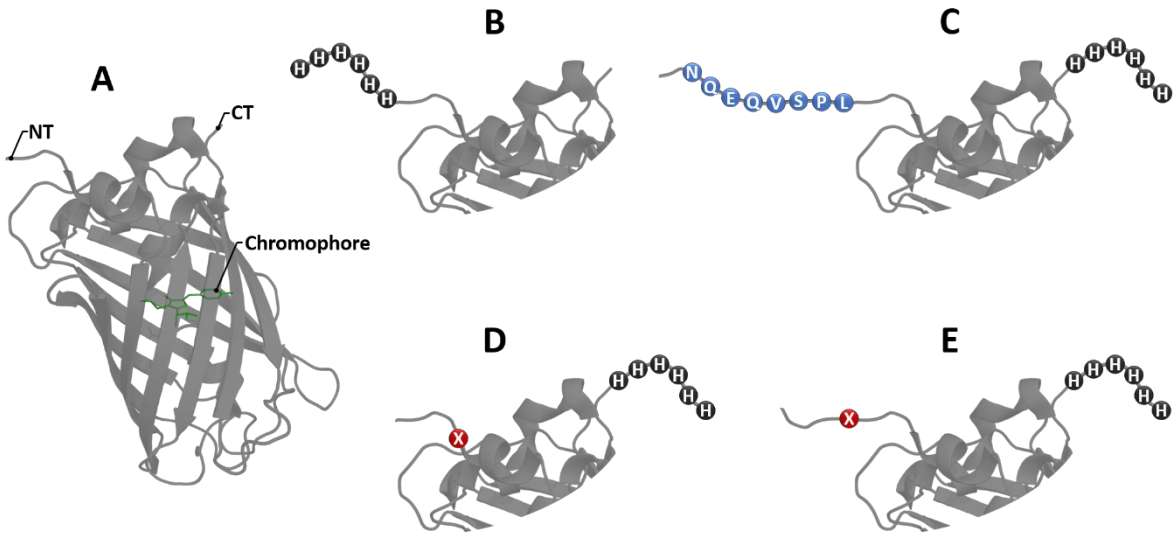

Figure 6.1.1 **Overview of eGFP mutein structures.** (**A**) Native eGFP adapted from PDB file 2Y0G highlighting N-terminus (NT) and C-terminus (CT) as well as the position of the fluorescent chromophore. (**B**) Wild-type eGFP with an N-terminal 6xHis-tag. (**C**) Transglutaminase eGFP presents an α2PI sequence on the N-terminus as well as a 6xHis-tag on the C-Terminus. (**D**) and (**E**) Propargyl-L-lysine eGFPs with an unnatural amino acid either (D) integrated into the existing sequence or (E) introduced by a preceding external sequence, also provided with an N-terminal 6xHis-tag.

6.1.1 Wild-Type eGFP (WT-eGFP)

As a reference, wild-type eGFP was produced. The amino acid sequence governed by the generated cDNA can be found in ***Figure 6.1.2***.

```
  1 MHHHHHHVSKGEELFT  GVVPILVELD  GDVNGHKFSV
 31        SGEGEGDATY  GKLTLKFICT  TGKLPVPWPT
 61        LVTTLTYGVQ  CFSRYPDHMK  QHDFFKSAMP
 91        EGYVQERTIF  FKDDGNYKTR  AEVKFEGDTL
121        VNRIELKGID  FKEDGNILGH  KLEYNYNSHN
151        VYIMADKQKN  GIKVNFKIRH  NIEDGSVQLA
181        DHYQQNTPIG  DGPVLLPDNH  YLSTQSALSK
211        DPNEKRDHMV  LLEFVTAAGI  TLGMDELYK
```

p.M1_V2insHHHHHH

Figure 6.1.2 **Amino acid sequence of WT-eGFP.** The protein was complemented with an N-terminal 6xHis-tag. The structural addition is highlighted by bold letters and underlining. A standardized description of the variation on the protein level is given in the box [103].

6.1.1.1 PCR Amplification of WT-eGFP DNA

The cDNA-fragment EGFP of the plasmid pEGFP-N1 with a length of 720 bp, served as genetic material for all eGFP subcloning procedures. To introduce site-specific terminal modifications, overlapping primers with respective mutations were deployed to alter the target DNA. A detailed picture of the oligonucleotides used to create the necessary restriction sites and to introduce a hexahistidine tag for purification can be found in the material section. The targeted DNA was amplified in a PCR process resulting in a linear DNA fragment of 752 bp (***Figure 6.1.3***).

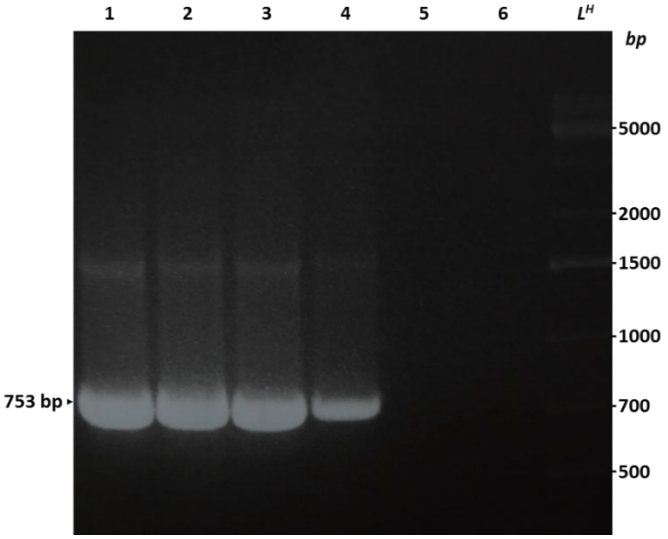

Figure 6.1.3 **Agarose gel electrophoresis for PCR product verification.** Lanes **1-4**: amplified wild-type eGFP PCR product; lanes **5-6**: negative controls omitting (5) primers or (6) polymerase; $\boldsymbol{L^H}$ displaying a high range DNA ladder.

6.1.1.2 Subcloning (Restriction and Ligation) of WT-eGFP DNA into pET-11a and Transformation into BL21(DE3) Expression Strain

A combined *Bam*HI and *Nde*I digestion reaction was used to generate sticky ends at the target vector pET-11a as well as the PCR amplicon, after its isolation. In addition, the plasmid was dephosphorylated to prevent self-ligation. For easy purification, the completed reactions were again separated by agarose gel electrophoresis (***Figure 6.1.4***).

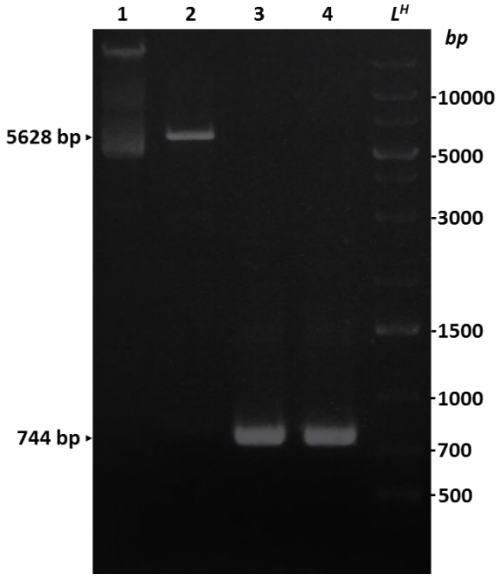

Figure 6.1.4 **Processed agarose gel after vector and insert restriction.** Lane **1**: undigested vector control, showing a broad distribution due to the different amount of coiling in the still circular plasmid; lane **2**: digested and dephosphorylated pET-11a plasmid; lanes **3-4**: restricted wild-type eGFP insert; $\boldsymbol{L^H}$ high range DNA ladder.

By deploying T4 DNA ligase, the overlapping ends of the insert and vector were fused in the ligation process, before the circular product was transformed into DH5α *E. coli* cells. The obtained plasmid was amplified and isolated again, using a commercial plasmid preparation kit. Subsequently, diagnostic digestion was conducted with *Nde*I and *Hin*dIII (***Figure 6.1.5***). Since the deployed pET-11a vector harbored another construct of similar size compared to the desired insert, the result of the digestion was diagnostically less conclusive. Consequently, the procedure was neglected as a diagnostic tool, and future eGFP constructs were directly validated by DNA sequencing data analysis.

Certain plasmids were chosen and further analyzed by DNA sequencing, which confirmed the correct nucleotide sequence of the given samples throughout the entire insert, and thus a successful subcloning of WT-eGFP into the bacterial expression vector pET11a. Verified plasmid constructs were transformed into the BL21(DE3) strain resulting in the completed expression system WT-eGFP/pET-11a/BL21(DE3).

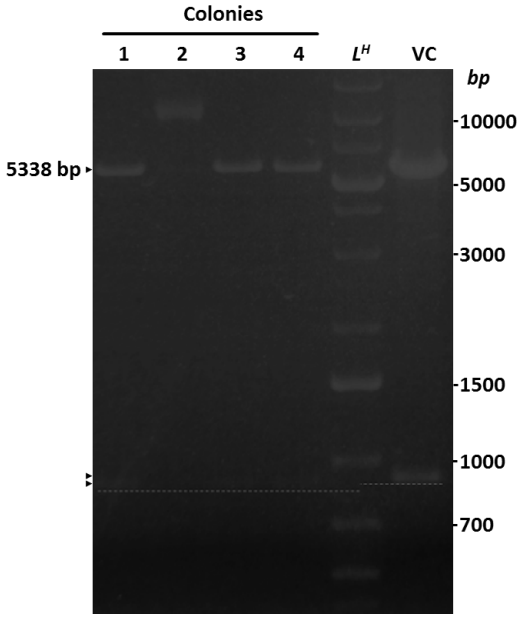

Figure 6.1.5 **Agarose gel separation of diagnostic digestion with *Nde*I and *Hin*dIII.** Lanes **1-4**: a selection of digested plasmids, originated from different colonies during plasmid preparation, where lanes 1, 3, and 4 illustrate a presumably successive ligation and transformation process with a large fragment of 5347 bp and a smaller one around 900 bp, while lane 2 showed no viable product; $\boldsymbol{L^H}$ high range DNA ladder; **VC**: source pET-11a vector, exhibiting an elevated lower fragment than the compared subcloned plasmids due to a former insert of larger size. The height difference is emphasized by an underlying dashed line and the triangular markers.

6.1.1.3 Expression and Purification of WT-eGFP

After successful subcloning, the obtained expression system WT-eGFP/pET-11a/BL21(DE3) was used to produce the desired WT-eGFP. The lacI-controlled T7 system was induced by IPTG for about 6-7 hours before the bacteria were harvested and further processed. In this way, approximately 30 mg WT-eGFP per liter expression media were obtained. ***Figure 6.1.6*** summarizes the complete expression and purification process. Due to the high sample load of the purified protein, minor impurities were visible in the lower

molecular weight area. A more distinct signal was observed at 55 kDa, which correlates to eGFP dimer formation (theoretical size at 55.4 kDa). The tendency of GFP to dimerize especially in non-reducing SDS-PAGE was described previously [104, 105].

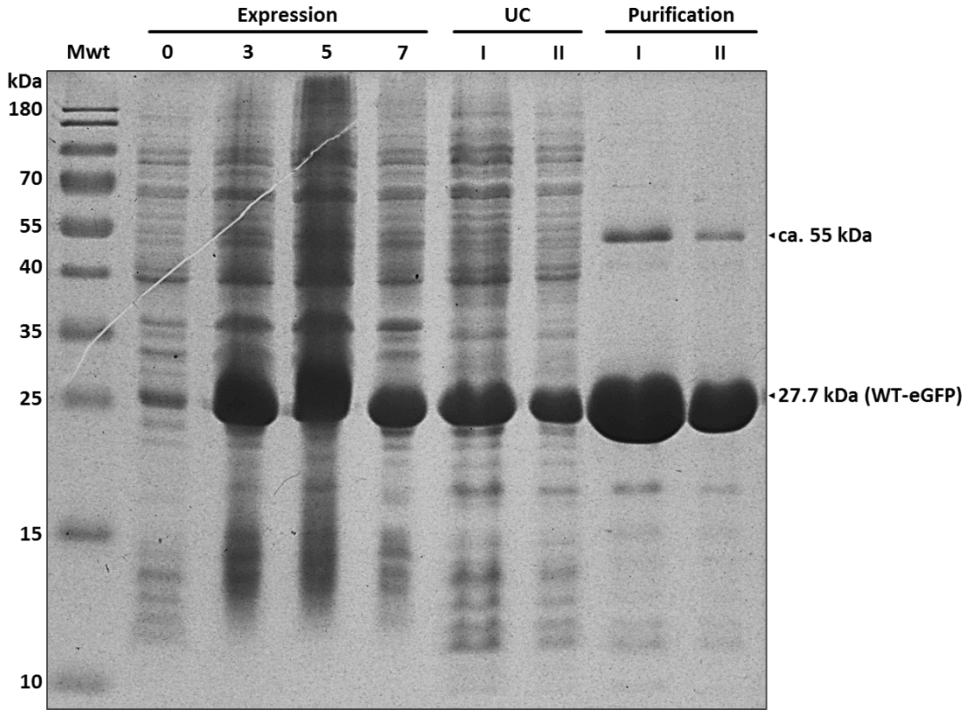

Figure 6.1.6 **Coomassie stained non-reducing SDS-PAGE analysis of WT-eGFP expression and purification. Mwt**: protein ladder with distinct molecular weights; **Expression** segment: samples taken at specific points in time (**0**, **3**, **5,** and **7** h) after induction with IPTG, illustrating the overexpression of WT-eGFP; **UC** segment: supernatant after ultracentrifugation, validating the solubility of the protein, where (**I**) is twice the loaded amount of (**II**); **Purification** segment: purified and dialyzed WT-eGFP with the same loading properties for (**I**) and (**II**) as before.

6.1.1.4 Characterization of WT-eGFP

In order to verify the protein's integrity and to establish a standard for further eGFP variations, WT-eGFP was analyzed for its mass and fluorescence properties. Mass spectrometry analysis confirmed that the protein was expressed with the expected molecular weight (***Figure 6.1.7 A***). Since eGFP's fluorescence activity is strictly related to its intact barrel structure [98], fluorometry was used as a tool for structural validation and bioactivity screening at the same time. When excited at 488 nm, WT-eGFP revealed a maximal emission at 510 nm (***Figure 6.1.7 C***), which is in good agreement with previous studies [98]. In

addition to that, WT-eGFP samples of known concentration were diluted and measured to generate a fluorescence intensity calibration curve (***Figure 6.1.7 B***), thus rendering them available for the determination of active protein content in the early stages of future expressions.

WT-eGFP exhibited all characteristic properties and was hence used as a reference material for all produced eGFP muteins, respectively.

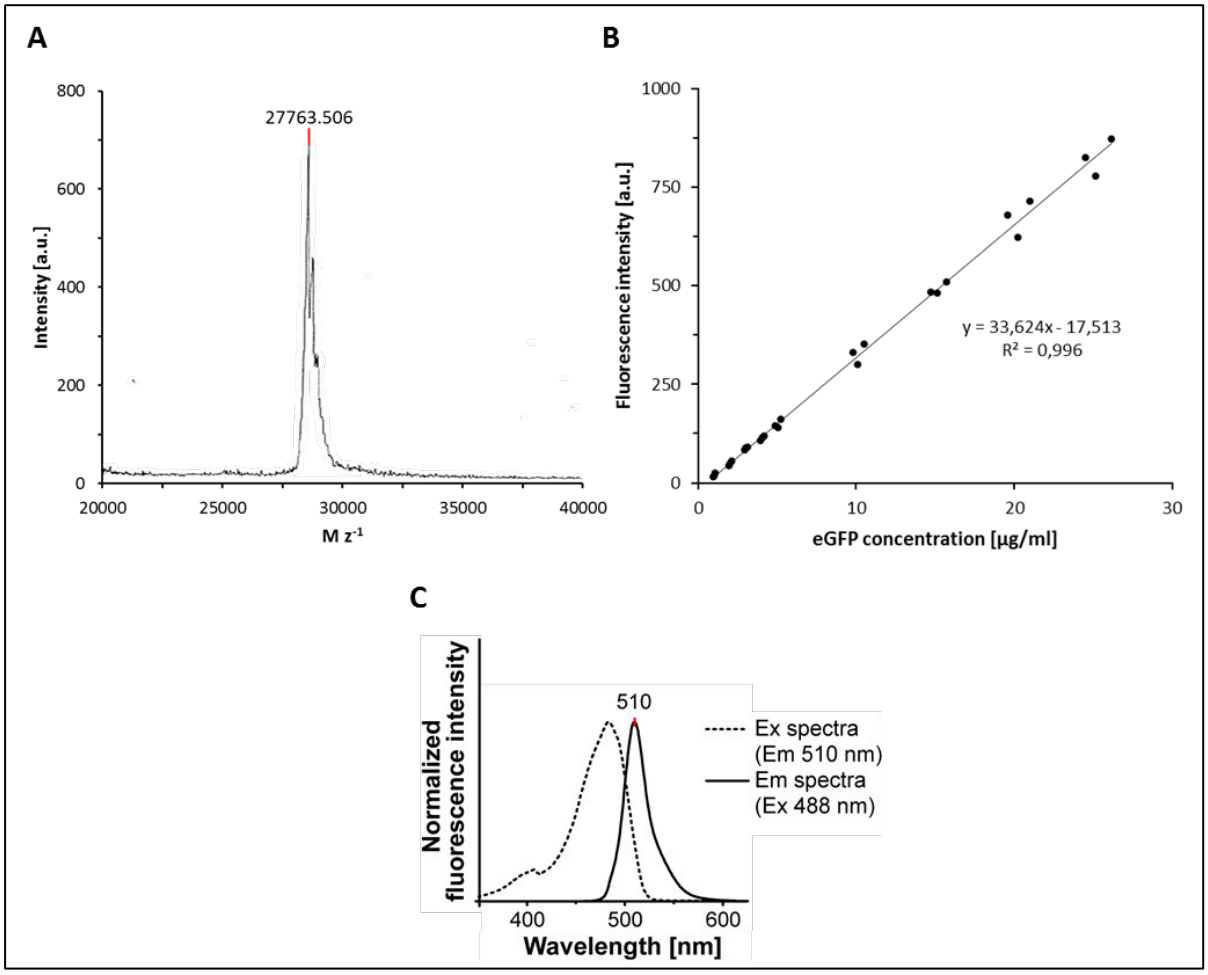

Figure 6.1.7 **Characterization of WT-eGFP.** (**A**) MALDI-MS analysis of WT-eGFP (obs. average mass 27763.503 Da, calc. average mass 27764.33 Da). (**B**) Fluorescence intensity calibration curve of three independently diluted WT-eGFP samples. (**C**) Normalized fluorescence spectra of WT-eGFP.

6.1.2 Transglutaminase eGFP (TG-eGFP)

TG-eGFP was prepared to allow for enzyme-controlled conjugation. Its amino acid sequence is shown in ***Figure 6.1.8***. The inserted segment was adapted from α_2-plasmin inhibitor (α2PI) since it represents a natural target for factor XIIIa (FXIIIa) during the blood

coagulation process and thus supports the endogenous characteristics of the physiological crosslinking reaction. It also provides a good affinity to the activated transglutaminase [58].

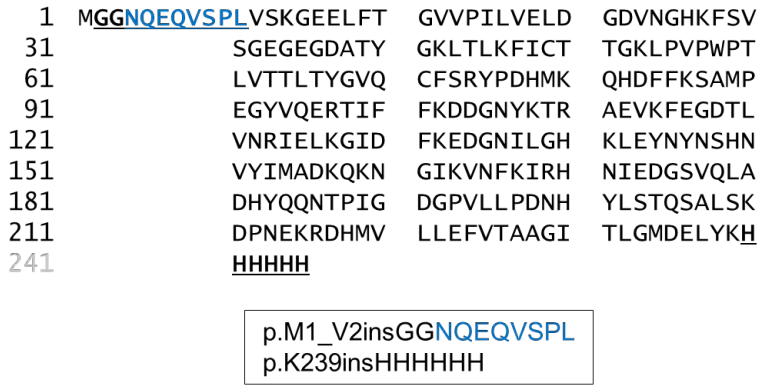

Figure 6.1.8 **Amino acid sequence of TG-eGFP.** Structural deviations from the source sequence are displayed and emphasized by underlined bold letters. The transglutaminase factor XIIIa recognition sequence adopted from α_2-plasmin inhibitor is marked in blue.

6.1.2.1 PCR Amplification of TG-eGFP DNA

To receive a transglutaminase-responsive eGFP mutein, an N-terminal primer coding for the required human transglutaminase factor XIIIa (TG) recognition region, derived from α2PI, was designed. The eGFP cDNA fragment (720 bp) of the pEGFP-N1 was used as source cDNA. The primers were constructed including sites for TG recognition, a hexa-histidine-tag for purification, and restriction sites for subcloning into the expression plasmid pET11a. Furthermore, two glycine residues were added to promote the posttranslational elimination of methionine as starting amino acid, which could otherwise have crucial effects on the protein's function and potentially affect the enzymatic recognition or accessibility [106, 107]. The assembly of the prepared oligonucleotides is depicted in the materials section.

The resulting PCR amplicon is shown in ***Figure 6.1.9*** with the calculated length of 782 bp.

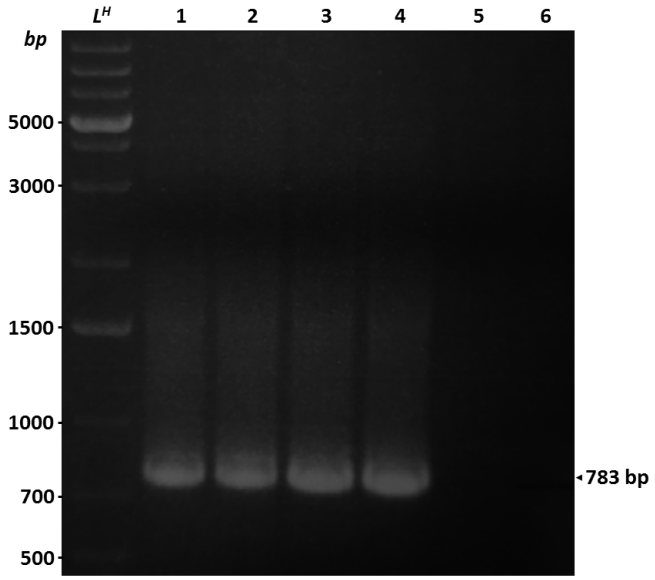

Figure 6.1.9 **Agarose gel as proof for the TG-eGFP PCR product.** L^H showing a high-range DNA ladder; lanes **1-4**: amplified transglutaminase eGFP DNA; lanes **5-6**: negative controls excluding (5) oligonucleotides or (6) DNA polymerase.

6.1.2.2 Subcloning (Restriction and Ligation) of TG-eGFP DNA into pET-11a and Transformation into BL21(DE3) Expression Strain

After extracting the amplified DNA from the agarose matrix, the restriction enzymes *Nde*I and *Bam*HI were used to digest the insert's as well as the vector's DNA. The linearized pET-11a was dephosphorylated before all DNA samples were purified by agarose gel electrophoresis (***Figure 6.1.10***) with subsequent kit extraction once again.

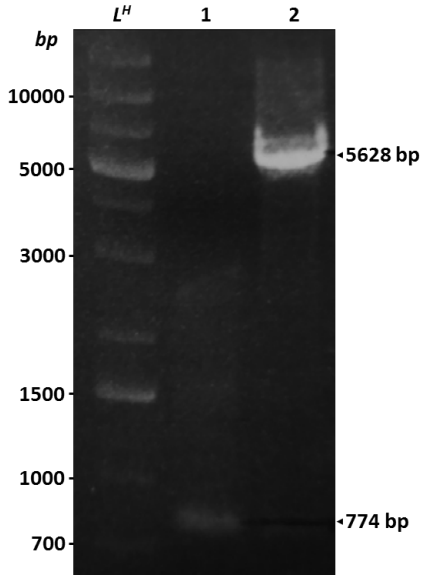

Figure 6.1.10 **Agarose gel electrophoresis of insert and vector after *Nde*I/*Bam*HI restriction.** L^H high range DNA ladder; lane **1**: digested transglutaminase eGFP DNA; lane **2**: restricted and dephosphorylated pET-11a plasmid.

Corresponding unpaired nucleotides of insert and vector, induced by the restriction digest, were merged through T4 DNA ligase, and the finalized TG-eGFP coding plasmid was transformed into DH5α *E. coli* cells. Subsequent DNA sequencing affirmed the proper nucleobase order in the TG-eGFP gene. With the transformation of a validated plasmid construct into the T7 expression host BL21(DE3), the TG-eGFP expression system was completed: TG-eGFP/pET-11a/BL21(DE3).

6.1.2.3 Expression and Purification of TG-eGFP

Initial attempts to express TG-eGFP with WT-eGFP expression conditions (37 °C, 1 mM IPTG, 6 h) failed. Therefore various expression conditions were screened. Temperature reduction to 20 °C upon IPTG induction resulted in a strong and visible band of TG-eGFP deploying SDS-PAGE analysis compared to expression at 37°C (***Figure 6.1.11***).

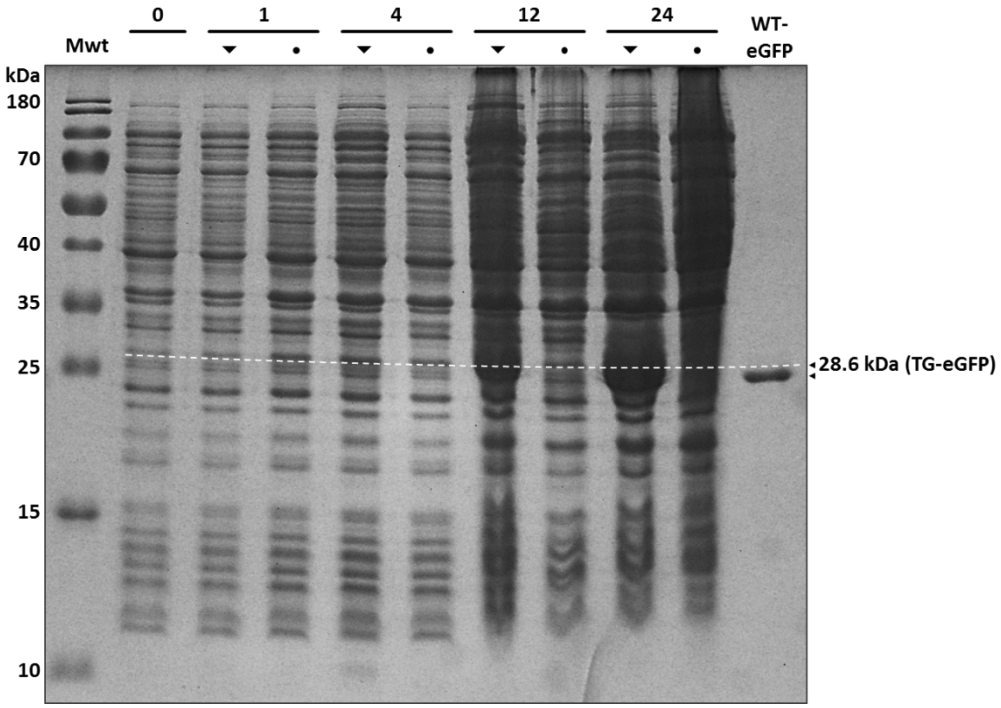

Figure 6.1.11 **SDS-PAGE of a small-scale TG-eGFP test expression. Mwt**: protein standard with defined molecular weights; bracket **0**: uninduced culture at OD_{600} = 0.6; brackets **1**, **4**, **12,** and **24**: hours after induction with IPTG, where lanes with a downward pointing triangle (▾) display samples from a batch with a reduced expression temperature (20 °C), while lanes tagged with a dot (●) reflect samples taken from a batch with unaltered temperature (37 °C); **WT-eGFP**: wild-type eGFP (27.7 kDa) as a reference for expected size. The height difference is emphasized by a dashed line and the triangular markers.

Bacteria were harvested and lysed following WT-eGFP purification procedures. The TG-eGFP-containing supernatant was purified from other soluble proteins by FPLC. Subsequent protein concentration determination resulted in approximately 30 mg TG-eGFP per liter TB medium. Several stages throughout the complete procedure are depicted in ***Figure 6.1.12***.

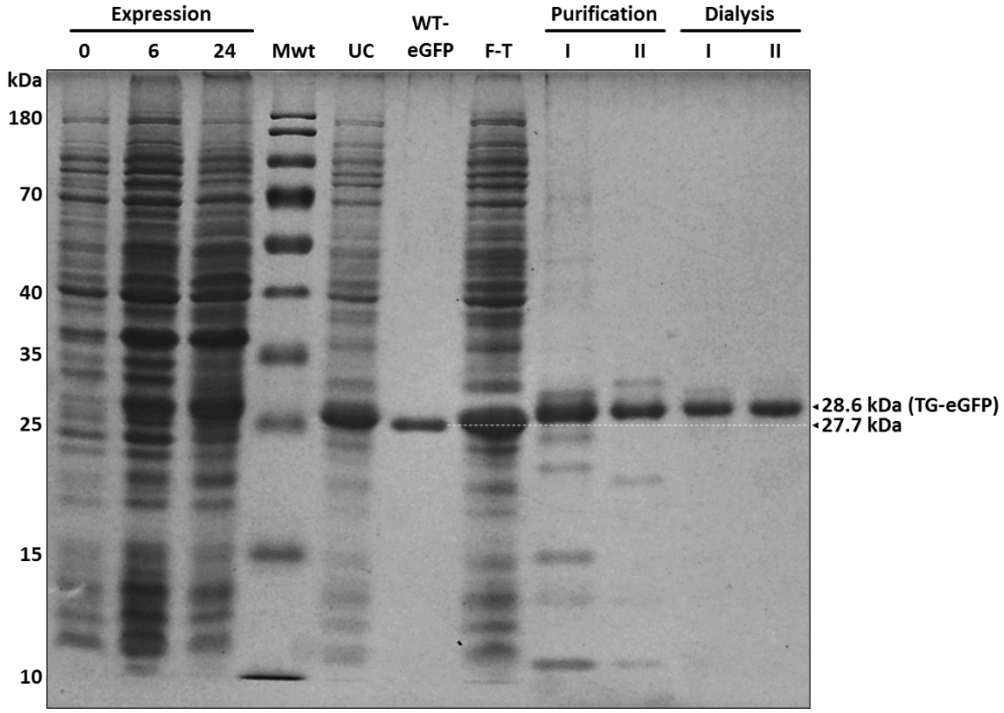

Figure 6.1.12 **Coomassie-stained SDS-PAGE analysis of TG-eGFP expression and purification process. Expression** bracket: expression samples taken **0**, **6,** and **24** hours after IPTG induction; **Mwt**: protein ladder with defined molecular weights; **UC**: centrifugate after ultracentrifugation; **WT-eGFP**: wild-type eGFP (27.7 kDa) as size reference; **F-T**: flow-through section, that did not bind to the Ni-NTA column, also containing TG-eGFP due to limited capacity; **Purification** bracket: FPLC purified TG-eGFP divided in two fractions (**I** and **II**); **Dialysis** bracket: fractions **I** and **II** after dialysis.

6.1.2.4 Characterization of TG-eGFP

The molecular weight of TG-eGFP was analyzed by MALDI MS, which confirmed the calculated mass of 28642.48 Da (Mw found = 28643.21 Da) (***Figure 6.1.13 A***). The found mass confirms the elimination of the initiating methionine residue, as discussed in Chapter 6.1.2.1. TG-eGFP was analyzed by fluorescence spectroscopy, which revealed identical characteristics (emission maximum at 510 nm, with 488 nm excitation wavelength; ***Figure 6.1.13 B***) as WT-eGFP (Chapter 6.1.1.4). Hence, the structural integrity and activity of TG-eGFP were intact and not impaired by the added α2PI recognition sequence at the N-terminal site.

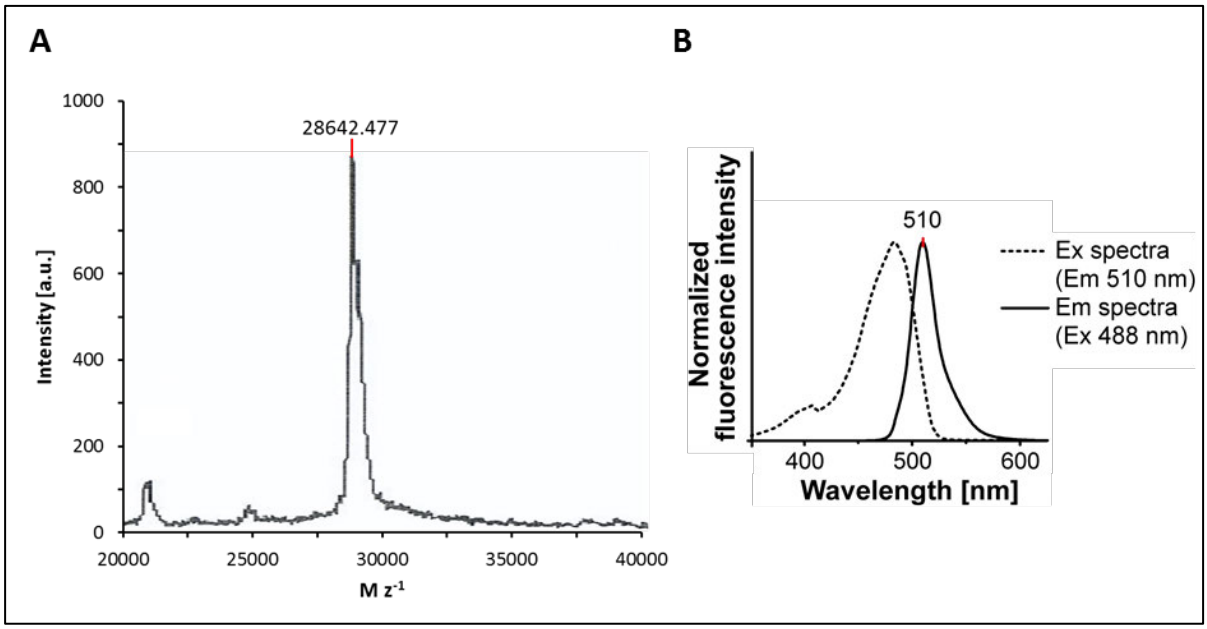

Figure 6.1.13 **Characterization of TG-eGFP.** (**A**) MALDI-MS analysis of TG-eGFP (obs. average mass 28642.477 Da, calc. average mass 28643.21 Da). (**B**) Normalized fluorescence spectra of TG-eGFP.

6.1.3 Propargyl-L-lysine eGFP (Plk-eGFP) via Amber eGFP (A-eGFP)

Two different expression variants for Plk-eGFP were designed, resulting in the amino acid sequences shown in ***Figure 6.1.14***.

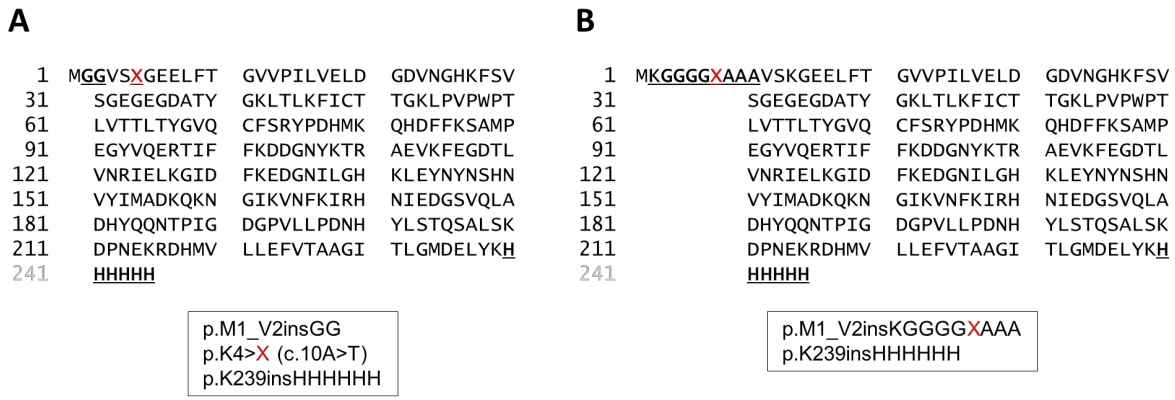

Figure 6.1.14 **Amino acids sequences of (A) internal and (B) external Amber eGFP.** Modifications introduced by subcloning are signalized through bold, underlined letters and framed standardized descriptions. Due to unavailable single-letter codes for amino acid derivates like Plk, the implemented unnatural amino acid positions are marked with a red X.

6.1.3.1 PCR Amplification of Internal (iA-eGFP) and External Amber eGFP (eA-eGFP) DNA

The PylRS/tRNA$^{Pyl}_{CUA}$ pair is a powerful tool to introduce unnatural amino acids based on pyrrolysine into a defined site of the protein structure through the translational process [77, 108-111]. The tRNA$^{Pyl}_{CUA}$ depends on the UAG nucleotide triplet (amber codon, TAG in DNA) as a counterpart to interact with the mRNA of the target gene. To provide the eGFP cDNA fragment (720 bp) of pEGFP-N1 with a TAG codon, two different strategies were perused. Internal amber eGFP was designed with minimal modifications to the cDNA. Lysine #4 was exchanged through a single point mutation to create the TAG codon and the sequence was prolonged by two glycine residues at the N-terminus (see Chapter 6.1.2.1). The external amber eGFP was planned as a second option since the possibility of a potential negative impact on the protein's structural integrity caused by the internal modification could not be ruled out. Therefore, the amber stop codon was introduced by a prefixed linker-like sequence (GGGAAA) [112]. Additionally, the flanking sites were modified with *Nde*I/*Bam*HI restriction sites and a C-terminal polyhistidine tag. For detailed primer descriptions see the materials section.

Figure 6.1.15 shows the resulting linear DNA fragments of external amber eGFP DNA (780 bp) and internal amber eGFP DNA (759 bp) after PCR processing.

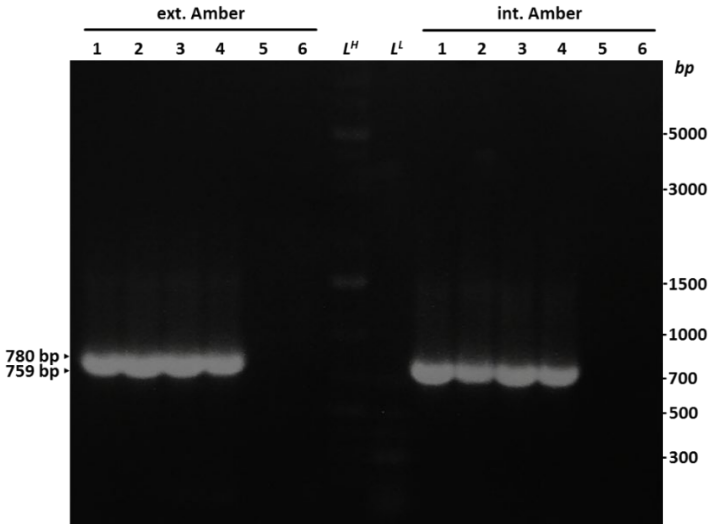

Figure 6.1.15 **Processed agarose gel for PCR product verification.** Bracket **ext. Amber** lanes **1-6**: (1-4) amplified eA-eGFP DNA, (5-6) negative control without addition of (5) primers or (6) DNA polymerase; $\boldsymbol{L^H}$ high range DNA ladder; $\boldsymbol{L^L}$ low range DNA ladder; bracket **int. Amber** lanes **1-6**: (1-4) amplified iA-eGFP DNA, (5-6) negative control missing out (5) oligonucleotides, or (6) *Pfu* polymerase.

6.1.3.2 Subcloning (Restriction and Ligation) of iA- and eA-eGFP DNA into pET-11a and Transformation into BL21(DE3) Expression Strain

Linear DNA amplicons were extracted from the agarose gel and digested with *Nde*I and *Bam*HI to generate cohesive ends. ***Figure 6.1.16*** depicts the alternative inserts (iA-eGFP DNA 750 bp; eA-eGFP DNA 771 bp) and the linearized and dephosphorylated pET-11a vector, after another separation employing agarose gel electrophoresis.

Ligation reactions of each A-eGFP DNA insert with the pET-11a vector were transformed into competent DH5α cells and manifolded by plasmid preparation. DNA sequencing confirmed the correct nucleotide configuration in the iA-eGFP DNA as well as the eA-eGFP DNA. Both plasmid constructs were transformed into a BL21(DE3) expression host, which finalized the generation of two new expression systems: iA-eGFP/pET-11a/BL21(DE3) and eA-eGFP/pET-11a/BL21(DE3).

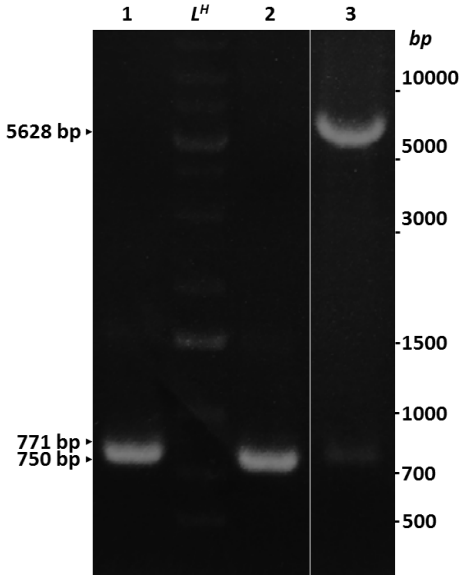

Figure 6.1.16 **Agarose gel electrophoresis after restriction digest.** Lane **1**: digested external amber eGFP DNA (771 bp); $\boldsymbol{L^H}$ high range DNA ladder; lane **2**: digested internal amber eGFP DNA (750 bp); lane **3**: digested and dephosphorylated pET-11a vector.

6.1.3.3 Expression and Purification of Plk-eGFP

The incorporation of Plk into eGFP presupposes amino acid-specific translational tools which were taken from the archaeon *Methanosarcina barkeri*. The gene for the required

$tRNA^{Pyl}$ was embedded into pET-11a and continually transcripted by the *E. coli* host's inherent RNA polymerase, whereas the tRNA synthetase (PylRS) gene was harbored by the cotransformed pRSFDuet-1 plasmid and its expression was induced by IPTG and promoted by the T7 RNA polymerase. Simplified graphical depictions of the plasmids and their features can be found in the material section.

Preliminary experiments revealed no considerable differences between (1) iA-eGFP/pET-11a/BL21(DE3) and (2) eA-eGFP/pET-11a/BL21(DE3) regarding the structural integrity yet a slightly higher expectable protein yield in favor for (1). Since no advantage accrued from the eA-eGFP construct expression, it was no longer necessary to pursue both variants. Hence, all expressions and further experiments were conducted with Plk-eGFP derived from the iA-eGFP expression plasmid. For the sake of completion, ***Figure 6.1.17*** displays a Maldi-MS analysis of the Plk-eGFP variation originating from the eA-eGFP construct.

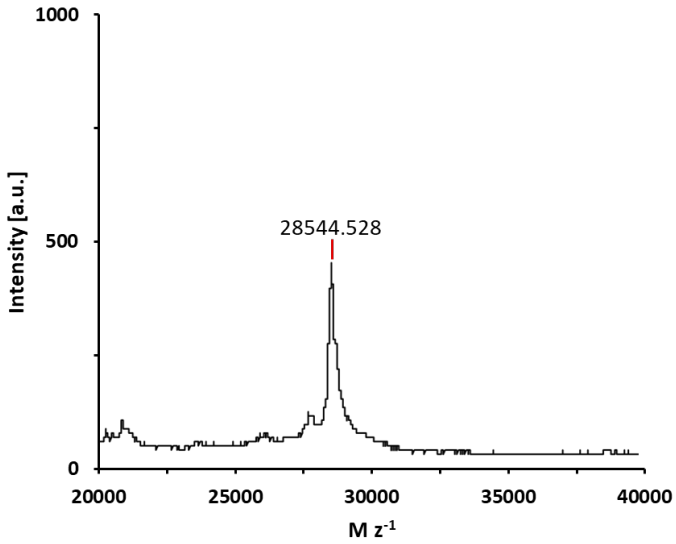

Figure 6.1.17 **Maldi-MS of a Plk-eGFP variation originated from the eA-eGFP plasmid construct.** The observed mass was 28544.528 Da, calculated mass was 28543.95 Da.

Optimization of expression parameters was challenging, as the expression levels of both Plk-variants were too low to be monitored via SDS-PAGE analysis. In contrast to pyrrolysyl-tRNA synthetase (PylRS 51 kDa), the overexpression of Plk-eGFP (27.8 kDa) resulted in an order of magnitude that was not detectable by Coomassie staining (***Figure 6.1.18 B***).

Consequently, fluorescence intensities were monitored to evaluate the best Plk-eGFP expression conditions in the supernatant of consecutive expression samples, which were lysed and centrifuged (***Figure 6.1.18 A***). Growth at 33 °C and induction with 1 mM IPTG for 8 h revealed the highest Plk-eGFP concentration.

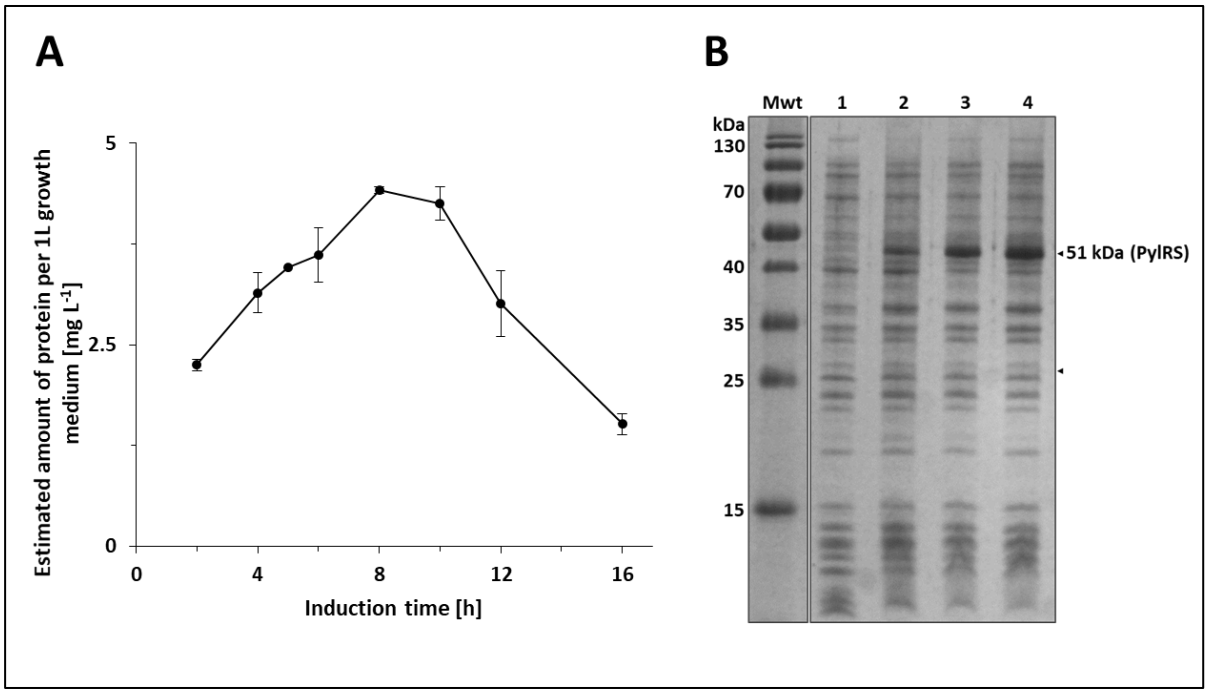

Figure 6.1.18 **Plk-eGFP expression optimization.** (**A**) An approximate estimate of expectable protein yields derived from fluorescence intensities measured in lysed bacteria samples. (**B**) SDS-PAGE of bacteria samples drawn during Plk-eGFP expression. **Mwt**: protein ladder with defined molecular weights; lane **1**: uninduced bacteria culture; lanes **2-4**: progress of induction after (**2**) 4, (**3**) 8, and (**4**) 16 hours.

Bacteria were collected and processed as WT- and TG-eGFP before. The 6xHis-tagged Plk-eGFP was obtained with an approximate yield of 2.5 mg protein per liter growth medium. ***Figure 6.1.19*** shows the purified Plk-eGFP in comparison to WT-eGFP.

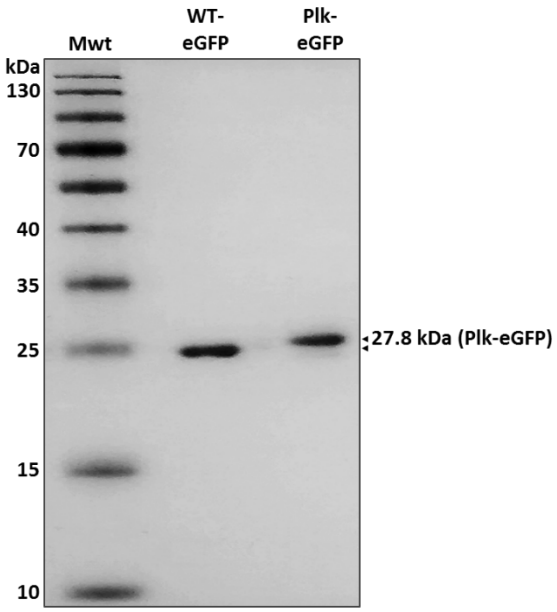

Figure 6.1.19 **SDS-PAGE after Plk-eGFP purification and dialysis. Mwt**: protein standard with different molecular weights; **WT-eGFP**: wild-type eGFP as a reference (27.7 kDa); **Plk-eGFP**: purified Plk-eGFP (27.8 kDa).

An independent optimization experiment setup gave detailed insight into induction parameter adjustment and was conducted in cooperation with Georg Wandrey (AVT, Biochemical Engineering, RWTH Aachen University, Aachen, Germany), who was responsible for online measurements and corresponding evaluation, which are described hereafter. He also contributed ***Figure 6.1.22*** and ***Figure 6.1.23*** to this work. For the purpose of this study, Alk was included as a second pyrrolysine derivate, in addition to Plk (***Figure 6.1.20***).

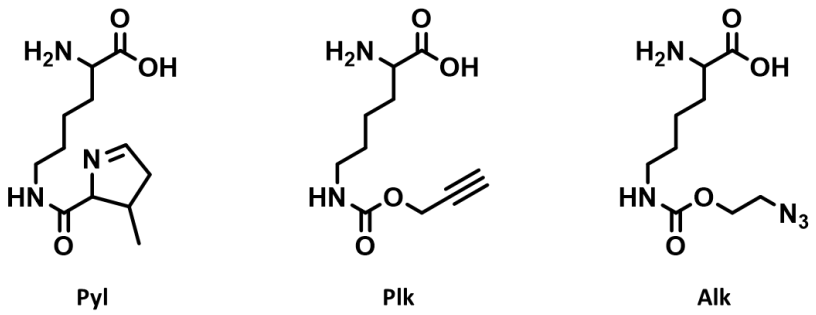

Figure 6.1.20 **Structural formula of pyrrolysine and the deployed derivates. Pyl**: L-pyrrolysin, **Plk**: propargyl-L-lysine, **Alk**: (S)-2-amino-6-((2-azidoethoxy) carbonylamino) hexanoic acid.

Bacteria were cultured in microtiter plate wells and eGFP formation was monitored through online fluorescence spectrometry, allowing for a great number of concurrent experiments. Process parameters, particularly the time and concentration of the addition of IPTG and the unnatural amino acid, respectively, were freely adjusted to allow for a comprehensive screening (***Figure 6.1.21***). Results from online measurements (***Figure 6.1.22***, ***Figure 6.1.23***) were also verified by a series of expressions, which were additionally processed conventionally and analyzed via ELISA (***Figure 6.1.24***).

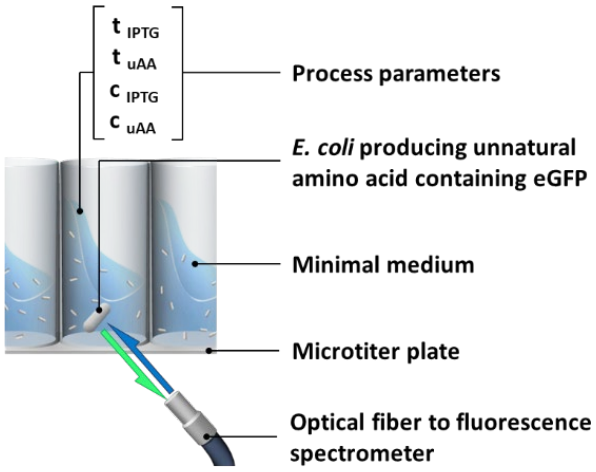

Figure 6.1.21 **Online monitoring of unnatural amino acid-containing eGFP formation in *E. coli* cultures**. Experiments were conducted in rotating microtiter plate wells using minimal medium. The influence of time of IPTG addition (t_{IPTG}), time of unnatural amino acid addition (t_{uAA}) as well as IPTG concentration (c_{IPTG}) and unnatural amino acid concentration (c_{uAA}) was studied.

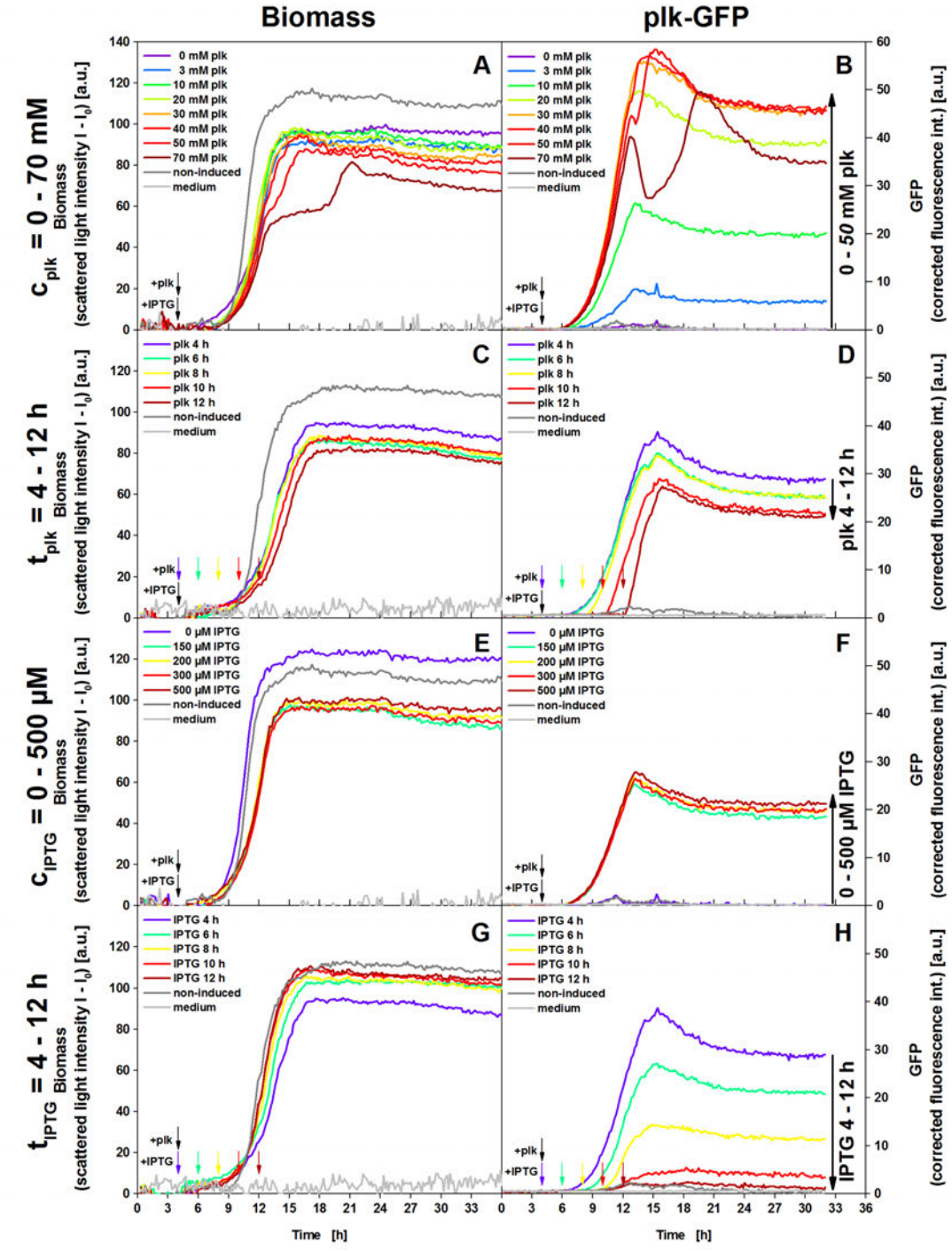

Figure 6.1.22 **Online measurement of biomass and Plk-eGFP formation.** Scattered light intensity as a measure for biomass (first column) and eGFP fluorescence intensity (second column) over time of culture of E. coli BL21 DE3 uAA-eGFP cultures. Four process parameters were varied individually: (**A**, **B**) Plk concentration c_{plk} = 0 – 70 mM; (**C**, **D**) time of Plk addition t_{plk} = 4 – 12 h (**E**, **F**) IPTG concentration c_{IPTG} = 0 – 500 µM (**G**, **H**) and time of IPTG addition t_{IPTG} = 4 – 12 h. If not varied, parameters were fixed at c_{Plk} = 10 mM, t_{Plk} = 4 h, c_{IPTG} = 200 µM, and t_{IPTG} = 4 h respectively. No Plk and no IPTG were added to cultures designated as 'non-induced' (dark grey). Small down-pointing arrows indicate the time of Plk and IPTG supplementation and large vertical arrows indicate trends in eGFP fluorescence after 32 h.

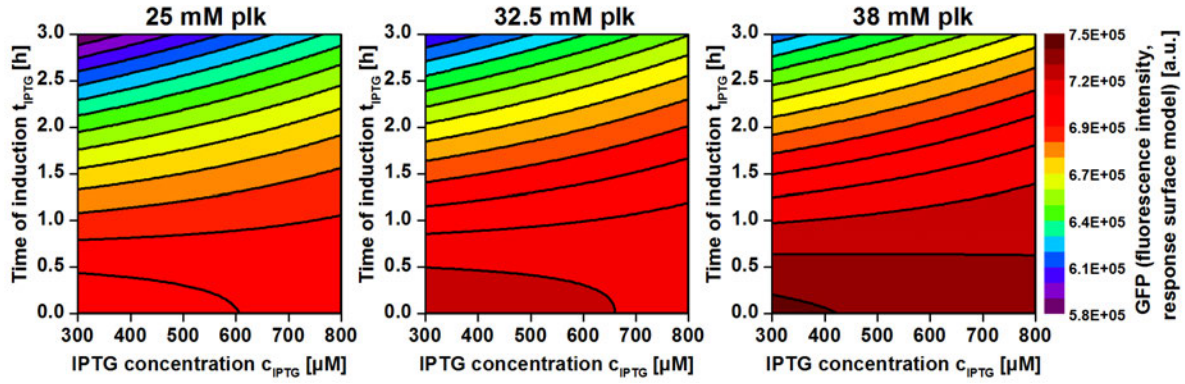

Figure 6.1.23 **Response surface model for Plk-eGFP production.** eGFP fluorescence of E. coli BL21DE3 uAA-eGFP cultures after 24 h as predicted by the response surface model as a function of Plk concentration, IPTG concentration, and time of IPTG addition (t_{plk} = 0 h). Dark red colors indicate operating conditions which lead to high Plk-eGFP fluorescence.

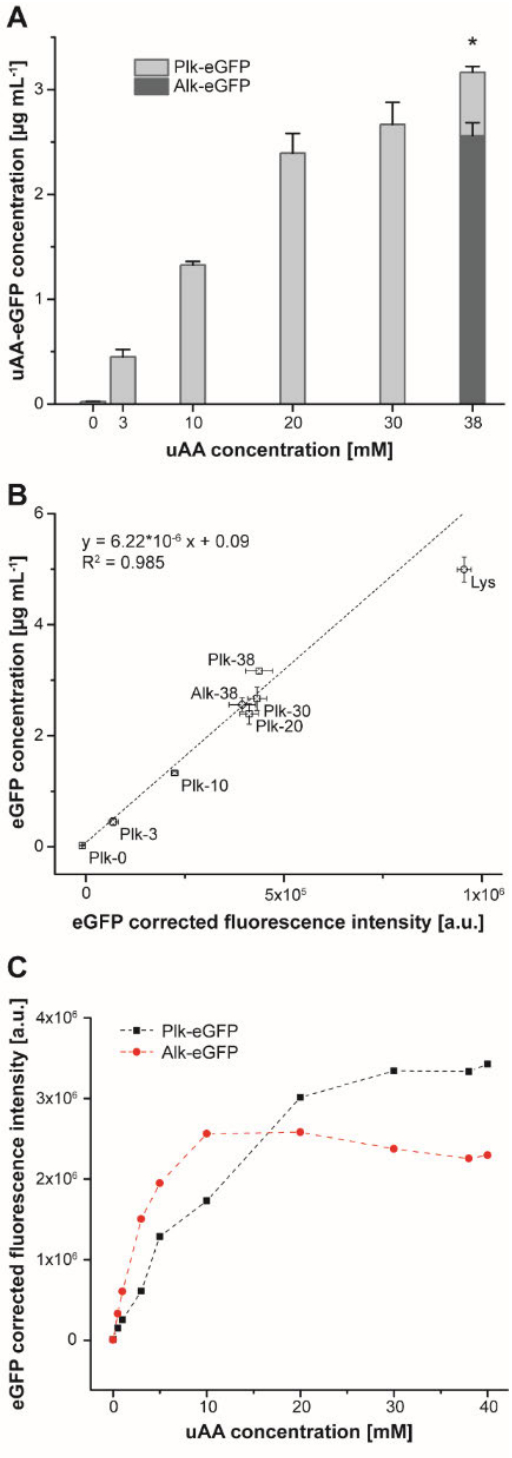

Figure 6.1.24 (**A**) Concentration of uAA-eGFP after 24 h in culture as a function of uAA concentration. Each column represents the mean + SD of four independent experiments ($p < 0.001$). (**B**) Comparison between protein concentrations of eGFP analogs as determined by ELISA and online measured fluorescence intensities of eGFP analogs. Data points illustrated as squares and labeled with Plk represent Plk-eGFP samples, whereas diamonds and circles display Alk-eGFP and Lys-eGFP, respectively. Tags indicate the uAA concentration in mM. All results are given as mean ± SD (n = 4). (**C**) Online measured fluorescence intensities of eGFP analogs relative to deployed uAA concentration. uAA and IPTG (433 µM) were added at the start of the cultivation.

The experiments revealed that under the given conditions an immediate addition of 38 mM Plk and 300 mM IPTG to a freshly inoculated culture yields the best results in terms of expectable eGFP fluorescence intensity.

6.1.3.4 Characterization of Plk-eGFP

MALDI-MS was deployed to analyze the molecular weight of Plk-eGFP, which was in good agreement with the theoretical value (27827.24 Da) (***Figure 6.1.25 A***).

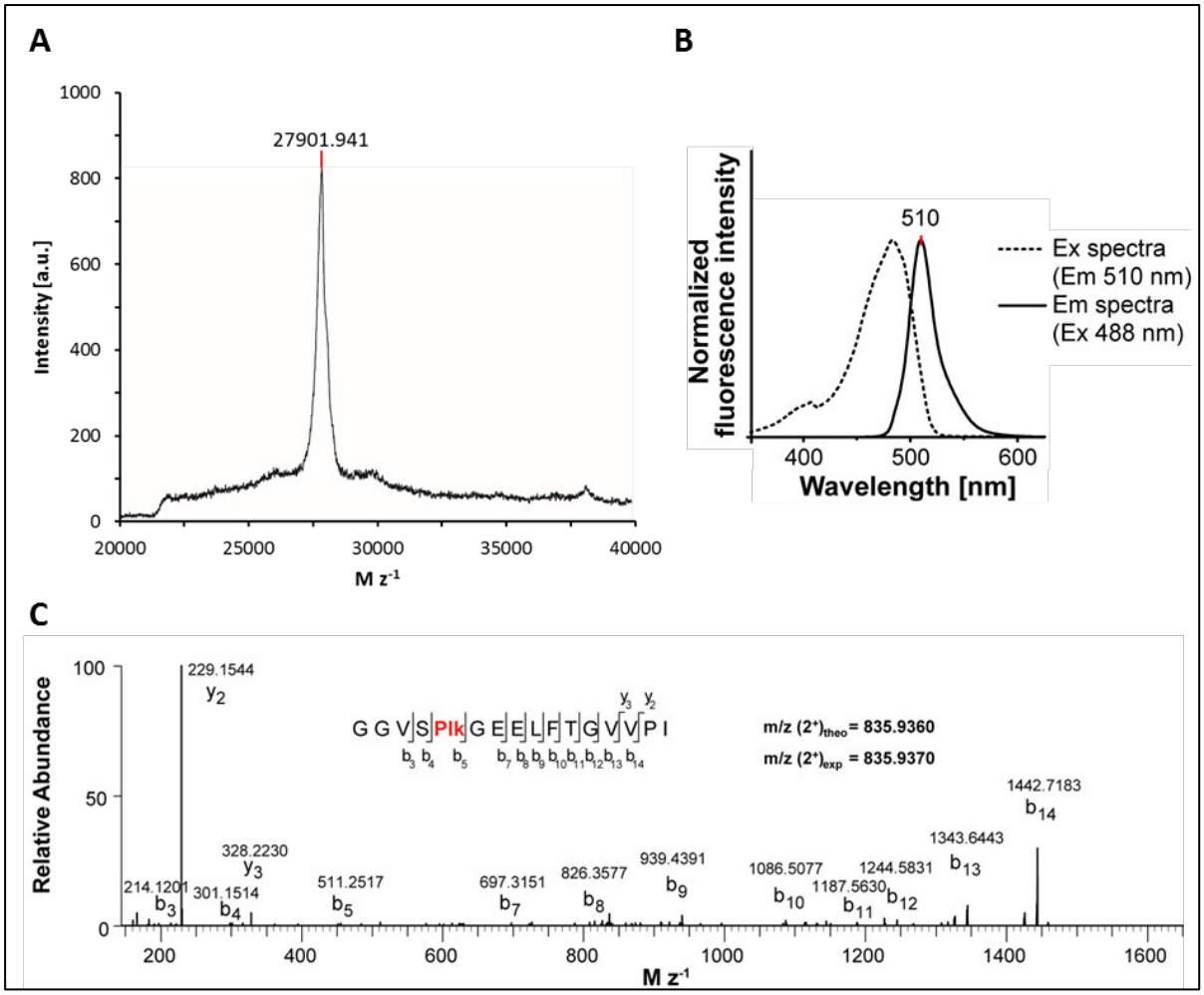

Figure 6.1.25 **Characterization of Plk-eGFP.** (**A**) MALDI-MS analysis of Plk-eGFP (obs. average mass 27901.941 Da, calc. average mass 27827.24 Da). (**B**) Normalized fluorescence spectra of Plk-eGFP. (**C**) ESI-MS spectrum of elastase digested Plk-eGFP displaying the recovered fragments of the uAA-eGFP amino acid sequence.

Furthermore, an elastase digestion reaction was performed to examine the resulting fragments by ESI-MS to assure the correct integration of the unnatural amino acid Plk into the protein sequence (***Figure 6.1.25 C***). To determine the correct folding of Plk-eGFP, fluorescence spectroscopy was used to verify eGFP-specific absorption and emission characteristics. Typical eGFP spectra were obtained (***Figure 6.1.25 B***), confirming that the amino acid substitution did not affect the structural integrity and the chromophore's activity.

6.2 Bioorthogonal Conjugation Reactions

Site-directed bioorthogonal conjugation is a most preeminent tool when precise modification of biologicals with unparalleled spatial control and homogenous product outcome is deciding. Crucially it can contribute to increased selectivity, enhanced effectiveness, and less undesirable side effects. In this work, two different approaches, namely copper(I)-catalyzed azide-alkyne cycloaddition (CuAAC) “click chemistry” and factor XIIIa (FXIIIa) mediated crosslinking, were chosen to demonstrate the viability and benefits of bio-selective conjugations including general preparation, applicability, and reproducibility. Naturally, their specific limitations were also identified. Generally, enhanced green fluorescent protein (eGFP) and other substrates were used to monitor the rate and extent of modification.

6.2.1 Conjugation via Factor XIIIa Mediated Acyl Transfer

Transglutaminases and other enzymes are known to be potent modification tools when it comes to generating highly site-specific and homogenous conjugates in a physiological environment [113]. Initially, the eGFP mutant (TG-eGFP) and a peptide counterpart, each providing the necessary feature to be recognized as substrates by the human transglutaminase, were used to demonstrate the general working principle. To further review the capabilities of factor XIIIa and validate basic reaction conditions, a reference system was built comprising a slightly modified lysine-donor peptide better suitable for UV detection and the isolated peptide sequence of α-2-plasmin inhibitor used in TG-eGFP.

A graphical abstract of the reaction promoted by FXIIIa is presented in ***Scheme 3***.

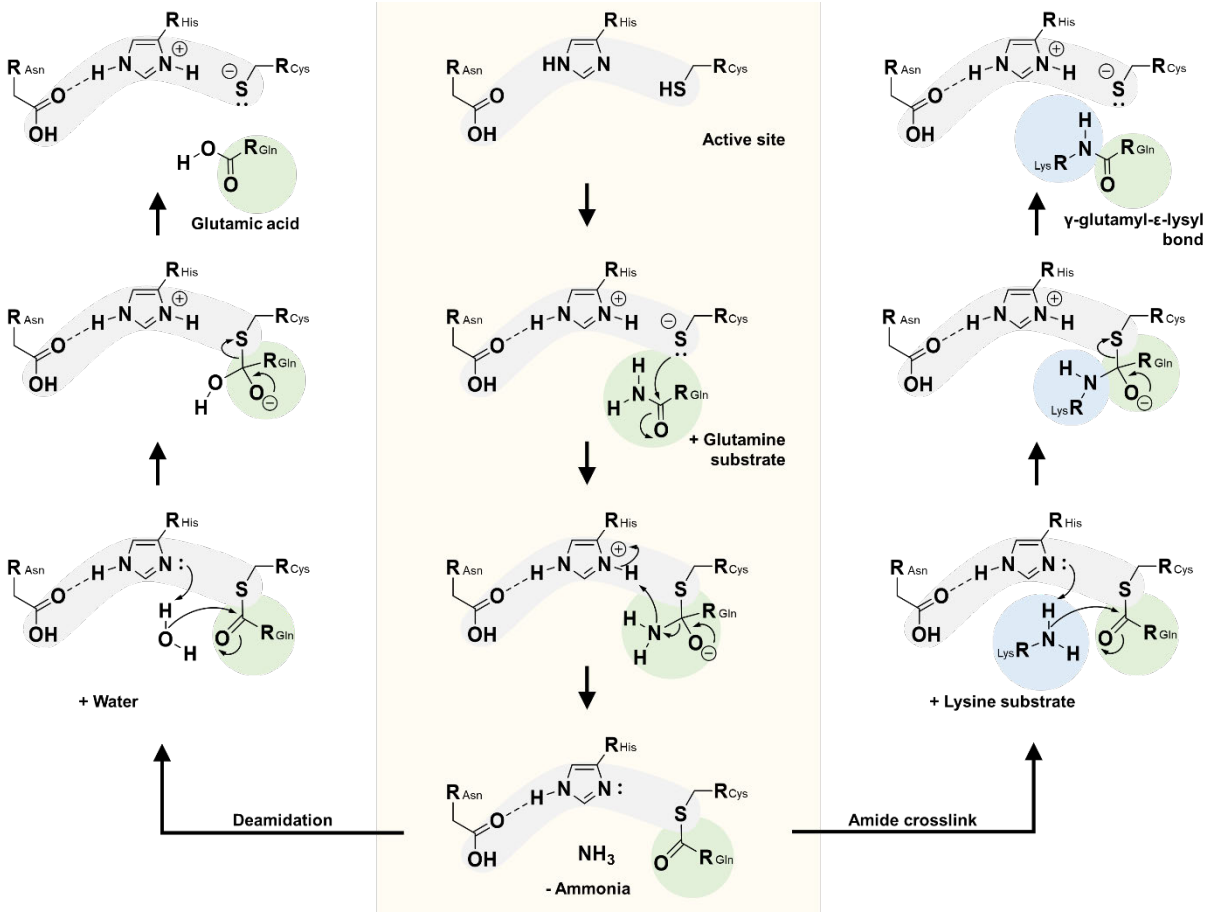

Scheme 3 **Mechanism of the reactions catalyzed by FXIIIa.**

6.2.1.1 The Lysine-Donor Peptide (LDP)

In the first step, a suitable substrate sequence for a lysine-donating peptide needed to be chosen, since FXIIIa was identified to have varying substrate affinities [114]. Although literature suggested the availability of higher affinity substrates [47], the short amino acids sequence FKGG was deployed, due to reported successful incorporation and presumably low undesired interaction potential, based on previous work of Ehrbar *et al*. [53]. As the basic idea of this approach was to preserve the freedom of interchangeable decoration, the peptide was designed to present a cysteine, providing a simple way of adding desired cargo molecules via a thiol-Michael addition "click" reaction [35, 115]. Additionally, a PEG-spacer was integrated to create enough clearance between any loaded molecule and the lysine sequence to prevent interference with the active site of FXIIIa. In order to mimic a native protein substrate, charges at both peptide termini were neutralized by N-terminal acetylation and C-terminal amidation, respectively, where the latter was inherently provided by the deployed Rink amide resin [116, 117]. The successful synthesis of the resulting Ac-FKGG-

PEG6-C-NH_2 sequence of the LDP with high purity was analyzed via MALDI-MS and HPLC (***Figure 6.2.1***). Since further peptide purification did not improve the purity but instead seemed to amplify oxidative stress to sensitive structures, which in return resulted in a worsened quality of HPLC analyses (data not shown), additional processing was omitted.

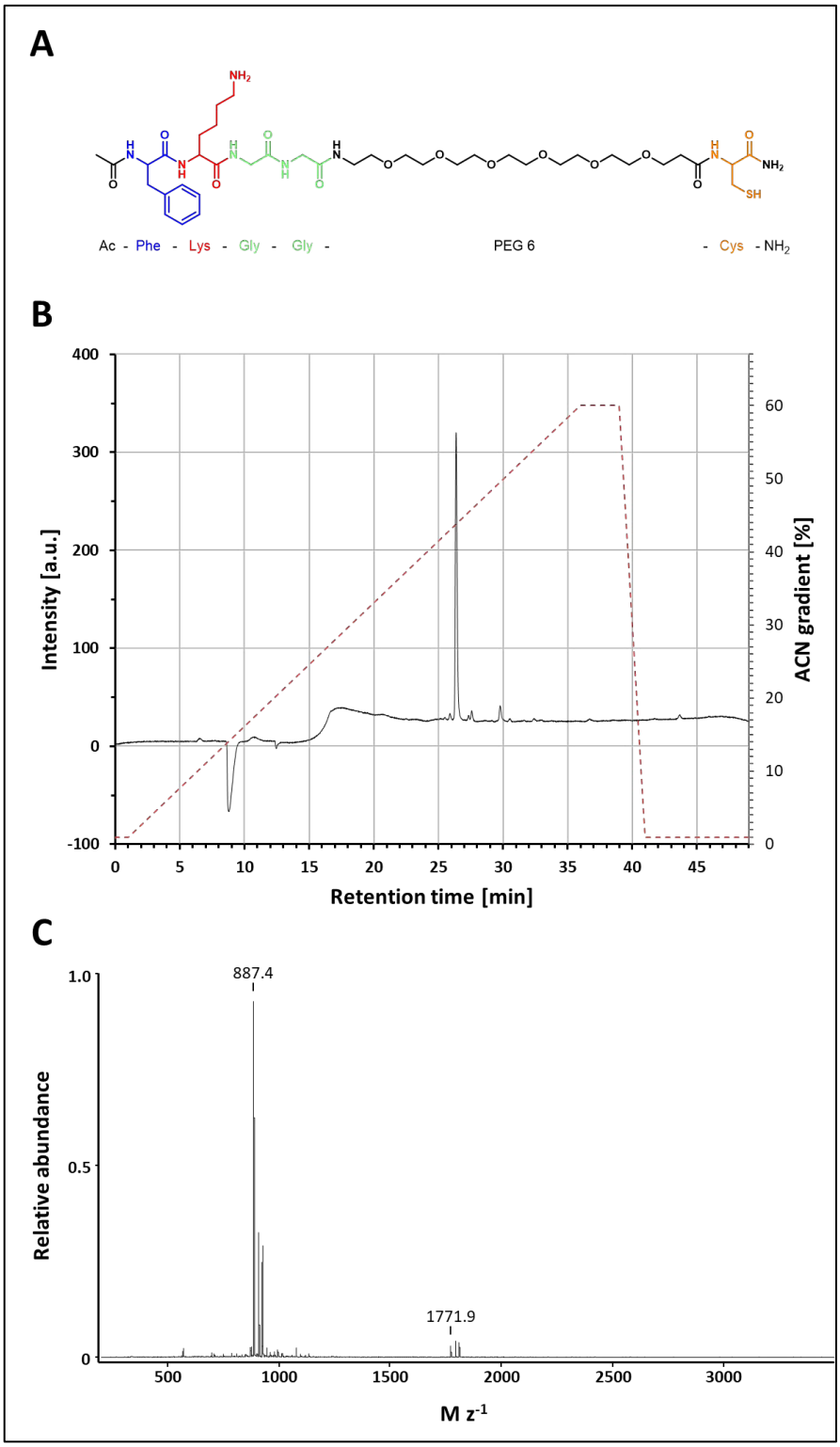

Figure 6.2.1 **Characterization of Ac-FKGG-PEG6-C-NH_2 as lysine-donor-peptide (LDP).** (**A**) Chemical structure of the Ac-FKGG-PEG6-C-NH_2 peptide outlining the amino acid sequence as well as front and end modifications. (**B**) HPLC chromatogram without further purification. (**C**) MALDI-MS spectrum of the peptide without additional purification. The three dominant peaks represent the non-oxidized peptide (theoretical signal: 887.05 Da, found: 887.4 Da) along with its sodium and potassium salt. The smaller triplet on the right displays the disulfide compound (1772.1 Da expected, 1771.9 Da observed) and the respective salts.

6.2.1.2 TG-eGFP and LDP crosslinking

To ensure that all components involved in the crosslinking process, i.e., FXIIIa, TG-eGFP, and the LDP, react in the foreseen manner a preliminary experiment setup, including various controls, was used to allow for a comprehensive assessment. Analyses of each protein by itself and mixtures precluding single reaction participants, as well as all included reactions, were conducted after 24 h of incubation under standard reaction conditions (5 mM $CaCl_2$ in TBS). This experimental series revealed that (1) the combination of enzyme, peptide, and protein did result in the desired shift of about 900 Da, which indicates the successful addition of the LDP to TG-eGFP (***Figure 6.2.2 V and VI***) and (2) FXIIIa does not accept albumin, which is stabilizing the stock solution, as lysine or glutamine substrate (**Figure 6.2.2** ***III and IV***).

While MALDI mass spectroscopy indicated a conclusive result, the quality of the obtained signals varied significantly, which prevented an adequate statement about the reaction-specific characteristics. To gain further insights into the reaction process, a positive ion mode ESI MS analysis was conducted. Therefore, TG-eGFP samples after various reaction conditions were prepared by SDS-PAGE and in-gel trypsin digestion. Since initial ESI data gave inconclusive signals for cysteine-containing fragments (data not shown), samples were treated with iodoacetamide, before gel separation, to homogenously alkylate cysteines to carboxyamidomethylcysteine (Cam-C), which resulted in a monoisotopic mass change of 57.02146 Da. As a reference point, TG-eGFP's sequence was examined, revealing the unmodified N-terminal fragment containing the NQEQVSPL sequence with 1342.7 Da (***Figure 6.2.3 I***). When only TG-eGFP underwent incubation in the presence of FXIIIa the N-terminal fragment's mass was increased by exactly 1 Da (***Figure 6.2.3 II***). This finding corresponds well to a known mechanism: In the absence of a suitable lysine donor the glutamine substrate gets hydrolyzed to glutamic acid in order to clear the active site of FXIIIa, which is demonstrated in the left array of ***Scheme 3*** [118]. When the lysine-donor peptide was added in high molar excess (1000-fold in a standard experiment), the initial N-terminal signal vanished completely, whereas a new peak emerged at 2269.1, which perfectly reflects the conjugation of the source N-terminal fragment with the carboxyamidomethylcysteine-modified LDP (***Figure 6.2.3***).

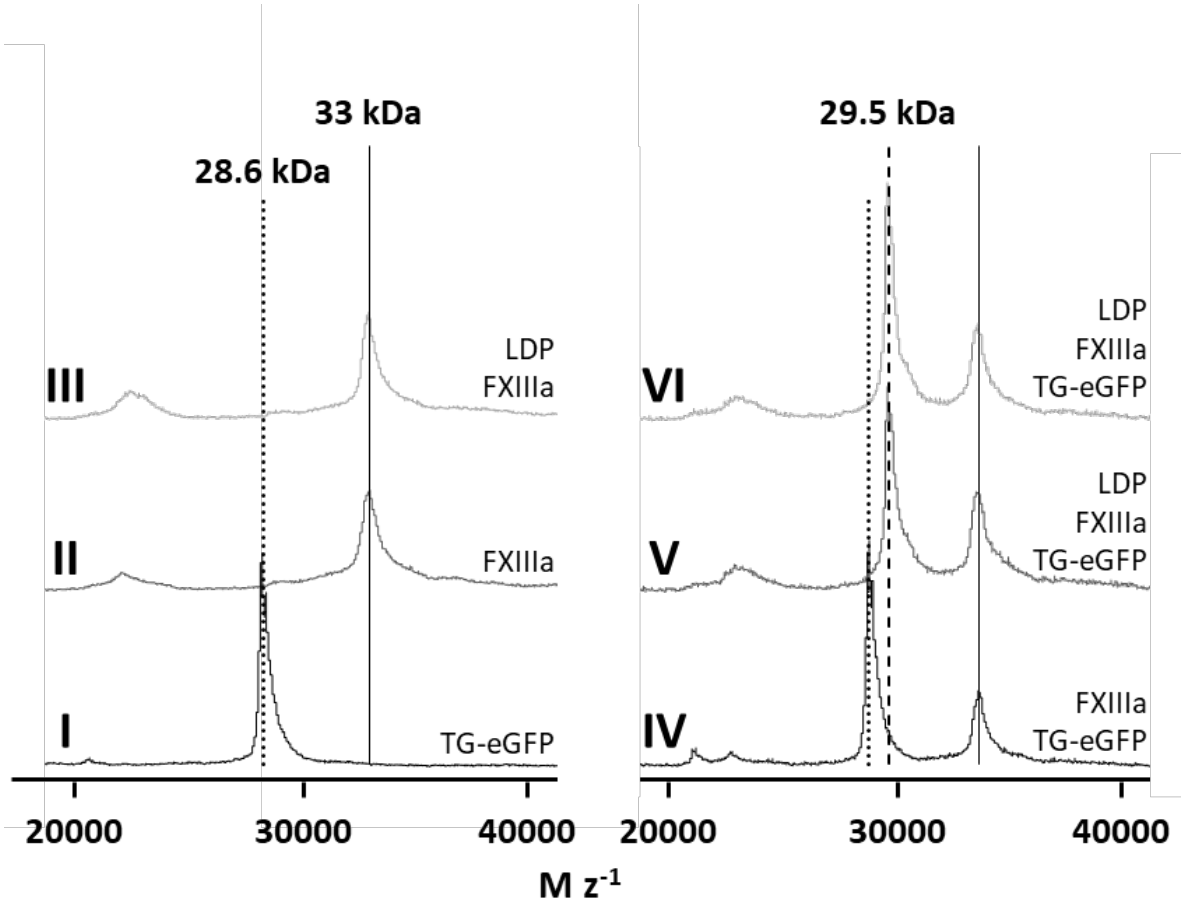

Figure 6.2.2 **MALDI-MS data of FXIIIa evaluation experiments.** (**I**) Unmodified TG-eGFP sample at about 28.6 kDA (expected mass: 28643.2 Da), marked by a dotted line for easy comparison. (**II**) Factor XIIIa control revealed a clear peak for double-charged albumin at 33 kDa, which is emphasized by a solid line. (**III**) A mixture of the lysine donor peptide and factor XIIIa excluding TG-eGFP under otherwise complete reaction conditions. (**IV**) A mixture of TG-eGFP and factor XIIIa excluding the lysine donor peptide under otherwise complete reaction conditions. (**V**) Result of a reaction with all necessary components and 5 mM $CaCl_2$ showing the desired product at about 29.5 kDa (expected: 29513.2 Da, found: 29450.6 Da), distinguishable from all other reaction components by a dashed line. (**VI**) The setup was identical to (V) but $CaCl_2$ was added to reach a final concentration of 50 mM.

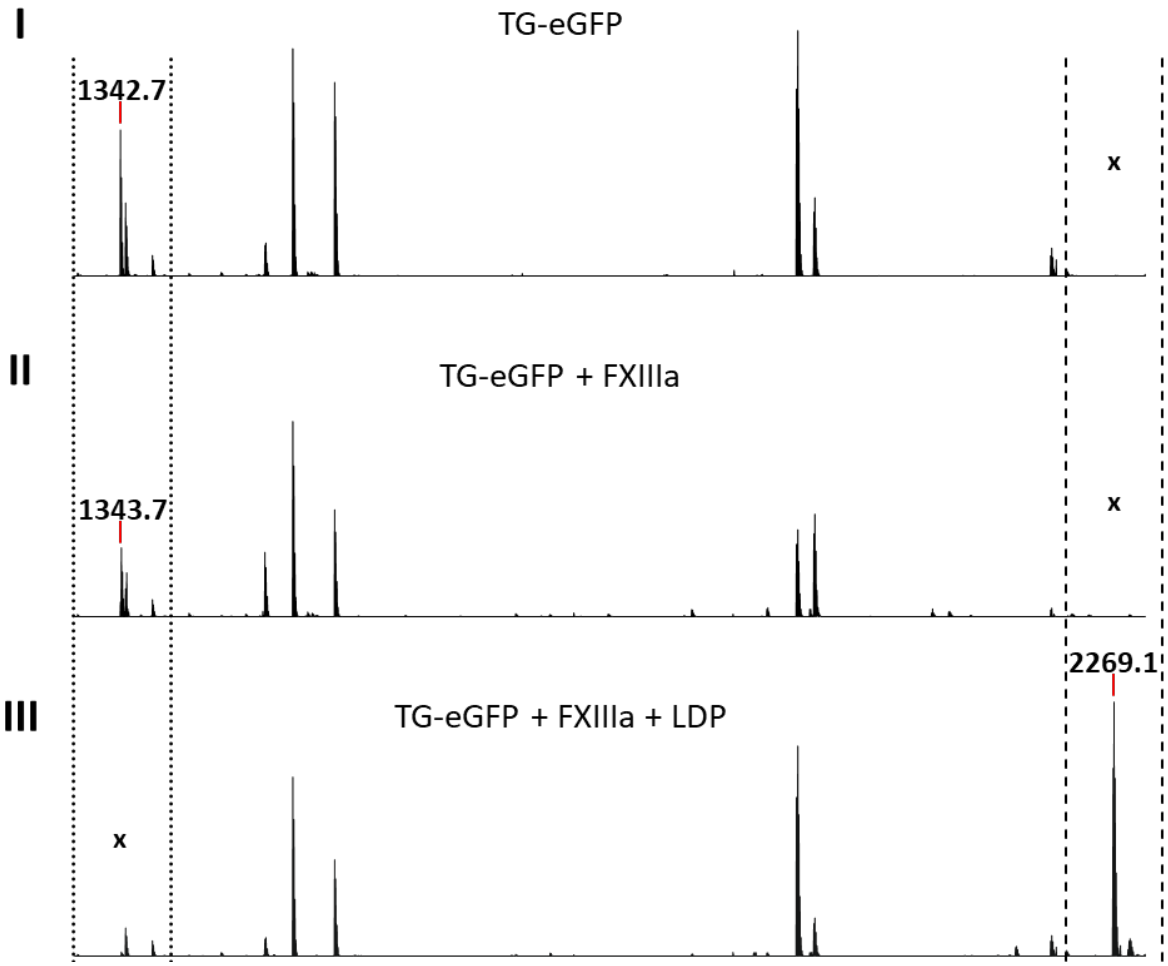

Figure 6.2.3 **ESI pos. MS data of iodoacetamide treated samples after trypsin digestion.** (**I**) TG-eGFP control, presenting the N-terminal fragment with a mass of 1342.7 Da. (**II**) Control reaction sample excluding the LDP, where the N-terminal fragment experienced a weight shift of 1 Da to result in 1343.7 Da. (**III**) Completed reaction sample. The initially found N-terminal fragment is no longer present. In turn, a signal emerged at 2269.1 Da, which matched the calculated mass of the crosslinked source fragment with a Cam-modified LDP (2268.8 Da).

This result showed that the chosen platform containing the FXIIIa-specific eGFP mutant and the lysine-providing peptide was suitable to successfully perform the crosslinking procedure with expected high selectivity.

6.2.1.3 Small Molecule Conjugates via FXIIIa Crosslinking

As the basic functionality of the conjugation reaction was proven by the results shown in Chapter 6.2.1.2, the purpose of the LDP was further extended to serve as a cargo carrier and

mediator, respectively. Biotin was chosen as an easily detectable sample small molecule to demonstrate the working principle. Since the LDP was designed to provide a unique thiol group through the integration of a C-terminal cysteine, it was possible to utilize the broad range of thiol-Michael addition reactions to connect any desired cargo with minor effort [35]. For the coupling of biotin to the LDP a maleimide addition strategy was deployed. In order to exclusively consume the present sulfhydryls and prevent any primary amines from interfering, acetic acid was used as the solvent. To compensate for the reduced reactivity at low pH values the incubation time was substantially increased to up to one week.

Figure 6.2.4 contours the process of ascertaining the required reaction time to fully load the deployed LDP with the biotin cargo. The respective samples were analyzed via ESI-MS and revealed that after three days of incubation, LDP was almost completely transformed into the biotin-LDP conjugate. Samples that were incubated for up to one week, were entirely free of initial LDP signals but seemed to accumulate by-products. The reaction was therefore limited to a maximum incubation time of five days.

Each reactant, a representative reaction, and the purified product were evaluated by HPLC (***Figure 6.2.5***). Since the preparation of biotin-LDP was solely meant to demonstrate the basic principle, the degree of purity achieved by spin-out processing was considered sufficient (***Figure 6.2.5 IV***). Furthermore, the observed disulfide-LDP peak emerged not until after the transfer to a higher pH environment, which might point towards a retro-Michael reaction that maleimides are known to be prone to, with subsequent oxidation of the sulfhydryl groups [119].

The obtained biotin-LDP was then used to create a crosslinked conjugate with TG-eGFP via the FXIIIa-mediated acyl transfer described earlier. ***Figure 6.2.6*** displays the successful coupling of the partner substrates. Minor unspecific labeling visible in the western blot strongly indicates the side reaction mentioned in the preceding paragraph. Therefore, any weak signaling is in all probability caused by either impurities (e.g. residual biotin-maleimide) in the biotin-LDP sample or complete thiol exchange of any of the protein's cysteines with biotin-LDP. Apart from this incidental deviation, which can be easily overcome by utilizing a more stable Michael acceptor and/or adapted reaction conditions for the desired cargo group, the viability of this flexible platform was proven for small molecules [120].

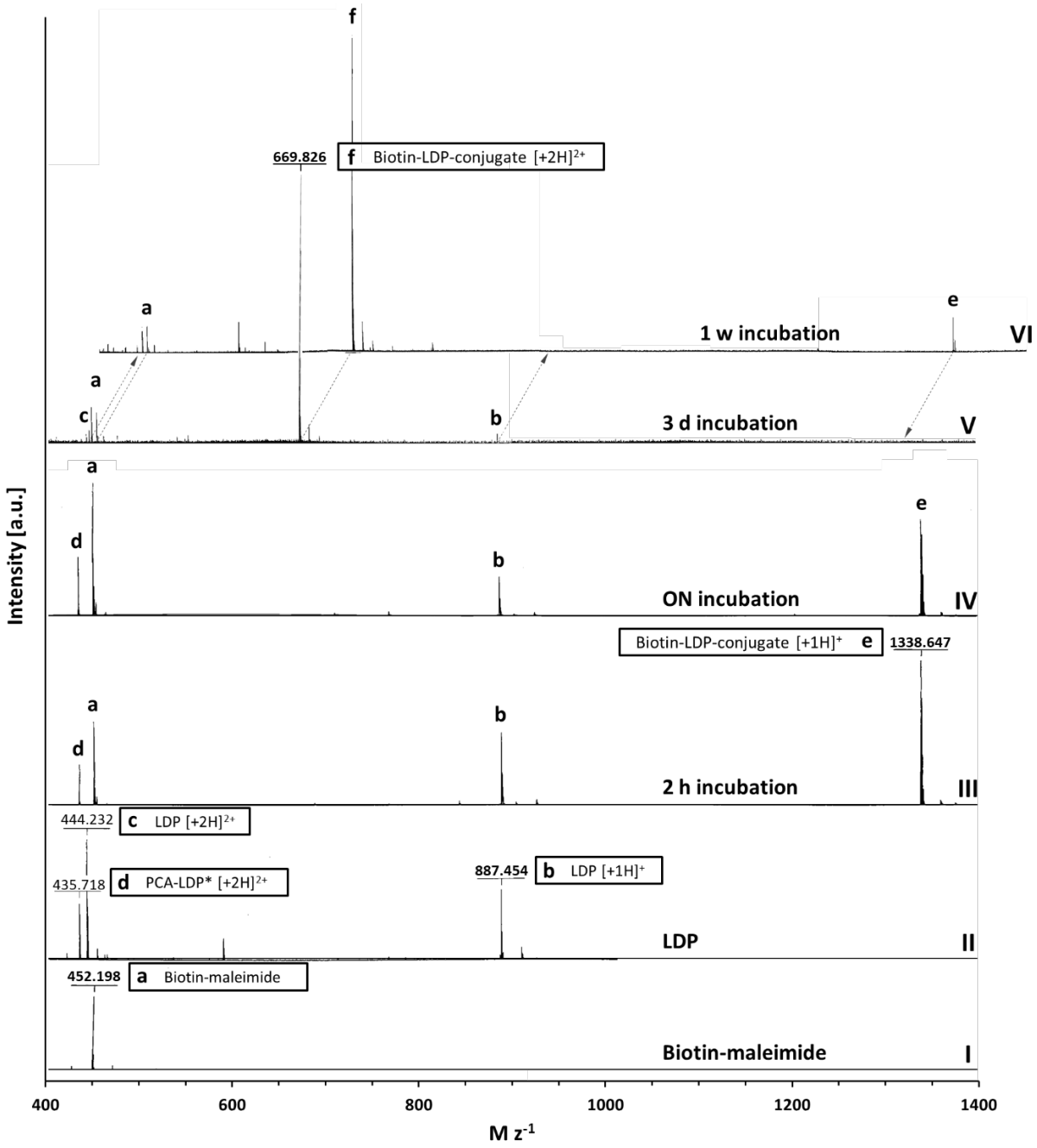

Figure 6.2.4 **Screening for the adequate incubation time for the pH-restricted thiol-Michael addition.** Stacked ESI pos. MS spectra with lowercase Latin letters to indicate the (re-)occurrence of a known substance, while single spectra show (**I**) biotin-maleimide source material (cal. mass 452.548 Da, obs. mass 452.198 Da) and (**II**) purified LDP (cal. mass 887.05 Da, obs. mass 887.454 Da). The signal at 435.718 Da was assigned to double-charged PCA-LDP (theoretical mass 435.512 Da), caused by a possible cyclization of glutamine during MS measurement, without further investigation or confirmation of this phenomenon [121]. The reaction progress at varying points of time are shown in (**III**) after 2 h of incubation, (**IV**) after over-night incubation, (**V**) after 3 days of incubation, and (**VI**) after 1 week of incubation, each containing the single charged and/or double charged Biotin-LDP product ($[+1H]^+$ cal. mass 1338.59 Da, obs. mass 1338.647 Da; $[+2H]^{2+}$ cal. mass 669.799 Da, obs. mass 669.826 Da. Due to negligible impact, the identity of signals marked with an asterisk (*) was not explicitly validated in subsequent experiments.

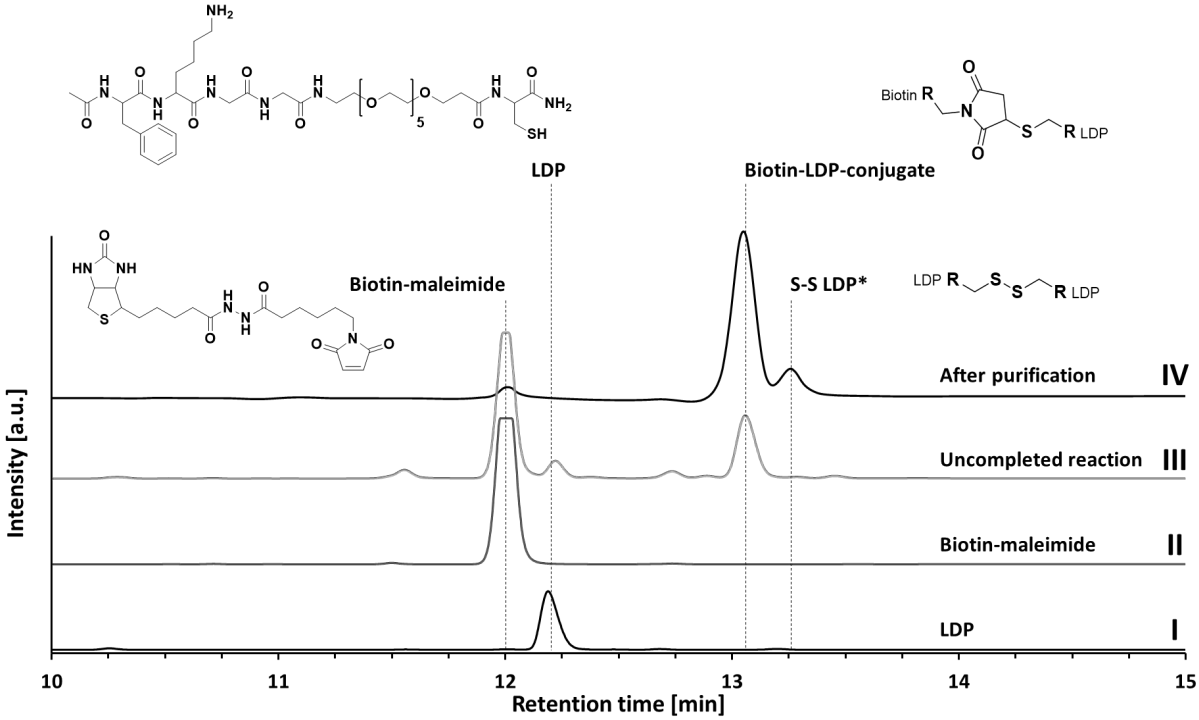

Figure 6.2.5 **Characterization of the Biotin-LDP conjugate and its reactants.** Stacked HPLC chromatograms with dotted vertical lines to indicate the (re-)occurrence of a known substance, while single runs show (**I**) isolated LDP, (**II**) biotin-maleimide source material, (**III**) a representative reaction after 2 days of incubation in acetic acid and (**IV**) the purified product in TBS pH 7.6. The peak at roughly 13.25 min in run IV was assigned to disulfide bonded LDP, as subsequent investigations (shown in ***Figure 6.2.7***) confirmed identical retention times. Due to negligible impact, the identity of signals marked with an asterisk (*) was not explicitly validated in subsequent experiments.

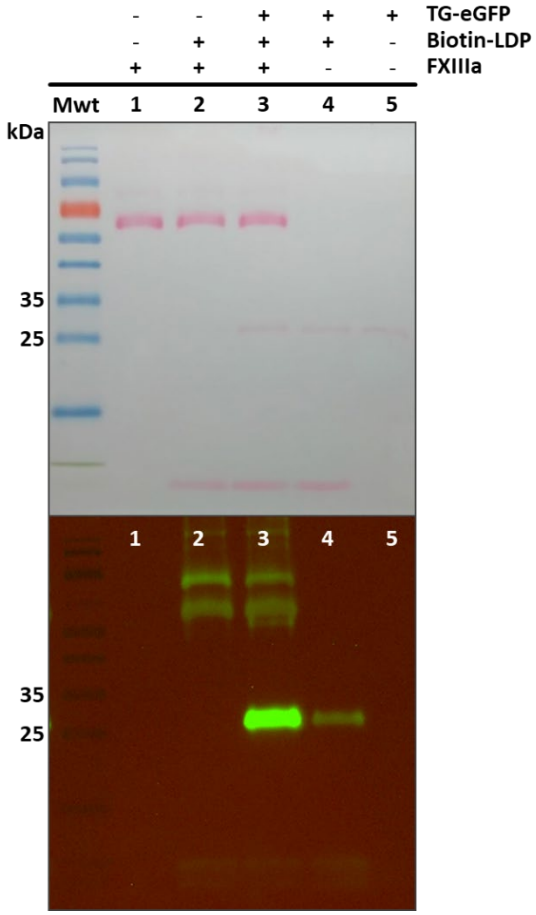

Figure 6.2.6 Ponceau red stain (top) and western blot visualization (bottom) of the FXIIIa mediated transfer reaction featuring TG-eGFP and biotin-LDP. Marks above the lanes indicate the (-) exclusion or (+) addition of the respective reactant or catalyst, respectively. The complete reaction (lane **3**) shows a specific labeling of TG-eGFP after streptavidin-HRP chemiluminescence activation, with minor side reactions visible in lanes **2**,**3,** and **4**.

6.2.1.4 High Molecular Weight Conjugates via FXIIIa Crosslinking

The applicability of the system at hand was further extended to feature an example of a larger cargo group. Because of its direct pharmaceutical utilization, a high molecular weight PEG (approximately 10 kDa) with an acrylamide modification was chosen, so that a Michael addition could serve once more as a labeling technique. The advantages and potential drawbacks of this method in general were shortly discussed in Chapter 6.2.1.3. As mass spectroscopy can at best yield broad signal distribution for PEG substances, developing a proper reaction protocol and adequate product characterization was challenging. Initially, the reactants and their isolated disulfide species if applicable, were individually analyzed by HPLC (***Figure 6.2.7 A I)***. As expected, acrylamide-PEG and DTT were able to form a

byproduct, whereas oxidized sulfhydryl groups are inert to the Michael acceptor (***Figure 6.2.7 A II-III***). The high pH-value dependency of the reaction was distinctively observable, as an overnight incubation at pH 7.7 generated significantly less product than a test reaction for 2 h at pH 8.8. A high pH environment however promoted the oxidation of the LDP's thiol groups (***Figure 6.2.7 A IV-V***). To reverse this effect, small quantities of DTT were added when residual LDP was expected to be fully oxidized and the desired reaction path would therefore be exhausted. This successive approach was used to keep the competing reaction between DTT and acrylamide-PEG at a minimum level and it was maintained until any initial acrylamide-PEG was depleted. The isolated product showed good purity except for a small peak which was assigned to a presumable DTT-PEG conjugate (***Figure 6.2.7 A II + IX***).

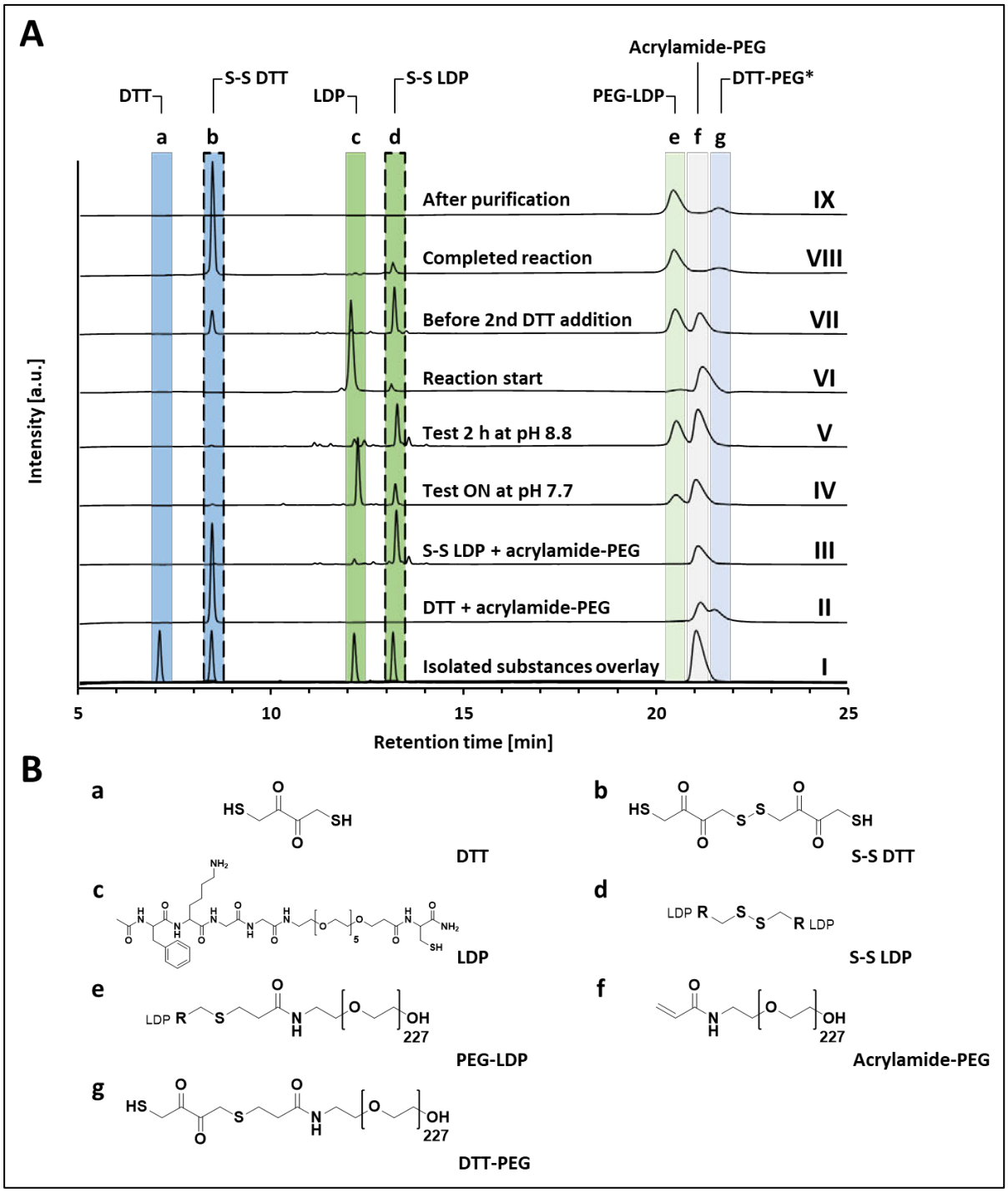

Figure 6.2.7 **Protocol development and characterization of the PEG-LDP.** (**A**) Stacked HPLC chromatograms with colored columns and lower-case Latin letters to indicate the (re-)occurrence of a known substance, while single runs show (**I**) the overlay of the individual substances, where disulfide species were purposely oxidized at first, (**II-IV**) test iterations to determine product specificity and optimal reaction conditions and (**V-IX**) chronologic stages throughout the PEG-LDP preparation. (**B**) Structural formulae of the deployed substances and generated products, respectively. DTT-PEG is marked with an asterisk as its identity was not confirmed by further analysis.

After obtaining PEG-LDP, the FXIIIa-mediated acyl transfer reaction was conducted with TG-eGFP and samples were analyzed by SDS-PAGE to assess the changes in molar weight. Contrary to expectations, the successful linkage was not achieved (***Figure 6.2.8***). As the general high performance of this reaction was already proven in the previous experiments, two possible causes were contemplated: (1) The preparation of PEG-LDP consumed the primary amine of LDP's lysine, thus rendering the peptide inert to the acyl transfer. (2) Spatial or structural obstructions may prevent the substrates from interacting with the active center of FXIIIa. While the direct examination of the latter consideration would have exceeded the scope of this work, the quality and responsiveness of PEG-LDP were studied in more detail.

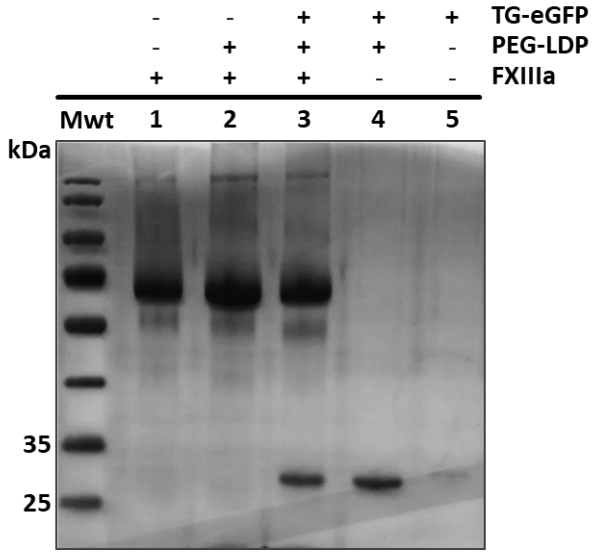

Figure 6.2.8 **Coomassie-stained SDS-PAGE of TG-eGFP and PEG-LDP using FXIIIa mediated acyl transfer reaction.** Signs above the lanes indicate the (-) exclusion or (+) addition of the respective reactant or catalyst, respectively. The complete reaction (lane **3**) showed no difference in size compared to TG-eGFP-containing controls (lanes **4** and **5**).

In order to validate the presence and accessibility of LDP's lysine, Folin's reagent was deployed, as it generates intensely colored derivatives with primary amines among other amino compounds [122]. For a comprehensive evaluation, every substance used in the PEG-LDP conjugation reaction was analyzed, albeit cysteine and lysine were assessed separately instead of source LDP to distinguish the effects of primary amines and amino acids in general (***Figure 6.2.9***). Although the result could serve as proof only to a limited extent, the

observable patterns revealed a decisive cogency. Analytes without any amino functionality remained colorless and pale. Cysteine exposed a slight orange coloration, hardly reflected by the photographic image. Exclusively lysine and PEG-LDP gave intensively colored derivates. Compared to the lysine sample, the stain appears somewhat brighter for PEG-LDP, which also shows a marginal white shadow, that matches with the characteristic of the unmodified PEG sample. This phenomenon, whether caused by still present acrylamide groups or PEG itself, in addition to a lower molar concentration, is a coherent rationale for a less saturated coloration. Overall, this investigation suggested the unrestricted reactivity of the peptide's lysines and the correct coupling between PEG and LDP.

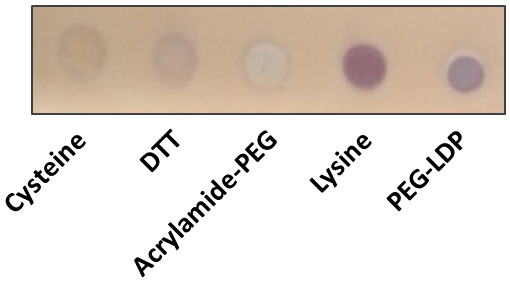

***Figure 6.2.9* PEG-LDP and reference substances treated with Folin's reagent.** The respective substances were applied to a TLC plate and briefly immersed into an alkaline aqueous solution of 1,2-naphthoquinon-4-sulphonate (Folins' reagent).

To further assess the structural integrity of PEG-LDP, MALDI mass spectroscopy data was gathered. PEG compounds typically exhibit substantial molar weight polydispersity, which increases with average polymer chain length. For this reason, spectra signals were expected to show broad distributions, so that the source PEG species was directly compared to PEG-LDP to give a better understanding of any observable changes. In comparison, PEG-LDP's spectrum was noticeably extended to higher m/z values, indicating a successful conjugation reaction, but the heterogenous signal occurrence did not allow for a distinctive assessment (***Figure 6.2.10 A***). Since many lower mass signals of both substances overlapped, it was assumable that PEG-LDP still contained residual acrylamide-PEG or DTT-PEG (cf. ***Figure 6.2.7 A***). For better visualization, the data was edited to exclusively display signal peaks (***Figure 6.2.10 B***). Subsequently, distributions were fitted with a basic Gaussian model. On the supposition that at least two compounds are present in the PEG-LDP sample, piecewise fittings were introduced to account for isolated PEG-LDP and possible DTT-PEG fractions.

Under this hypothesis, R^2 values indicated better coherence, when each subset was analyzed separately. While LDP should increase the average mass by 887 Da, the maximal difference between the mean acrylamide-PEG and the theoretical pure PEG-LDP mass accounted for approximately 500 Da. This deviation however might have been caused by the pronounced signal distribution and an analogously impaired readout. Despite the illustrated data consistency, MALDI MS data could only provide limited information about the exact sample composition and therefore PEG-LDP's reaction capacity.

In sum, there are strong indications that PEG-LDP was sufficiently available and reactive. Consequently, the unsuccessful coupling between PEG-LDP and TG-eGFP might have been a reaction-specific problem. It is conceivable that the structural properties of substrates may inhibit the correct coordination within the active site of FXIIIa. Additionally, the PEGylation of LDP itself might interfere with enzymatic recognition, as this modification can be used to shield proteins from enzymatic degradation [123]. Although successful PEG integration has been reported in the past, the mean molar weight of PEG deployed in this work was considerably higher [47]. Hence, a possible masking effect on substrate identification cannot be ruled out.

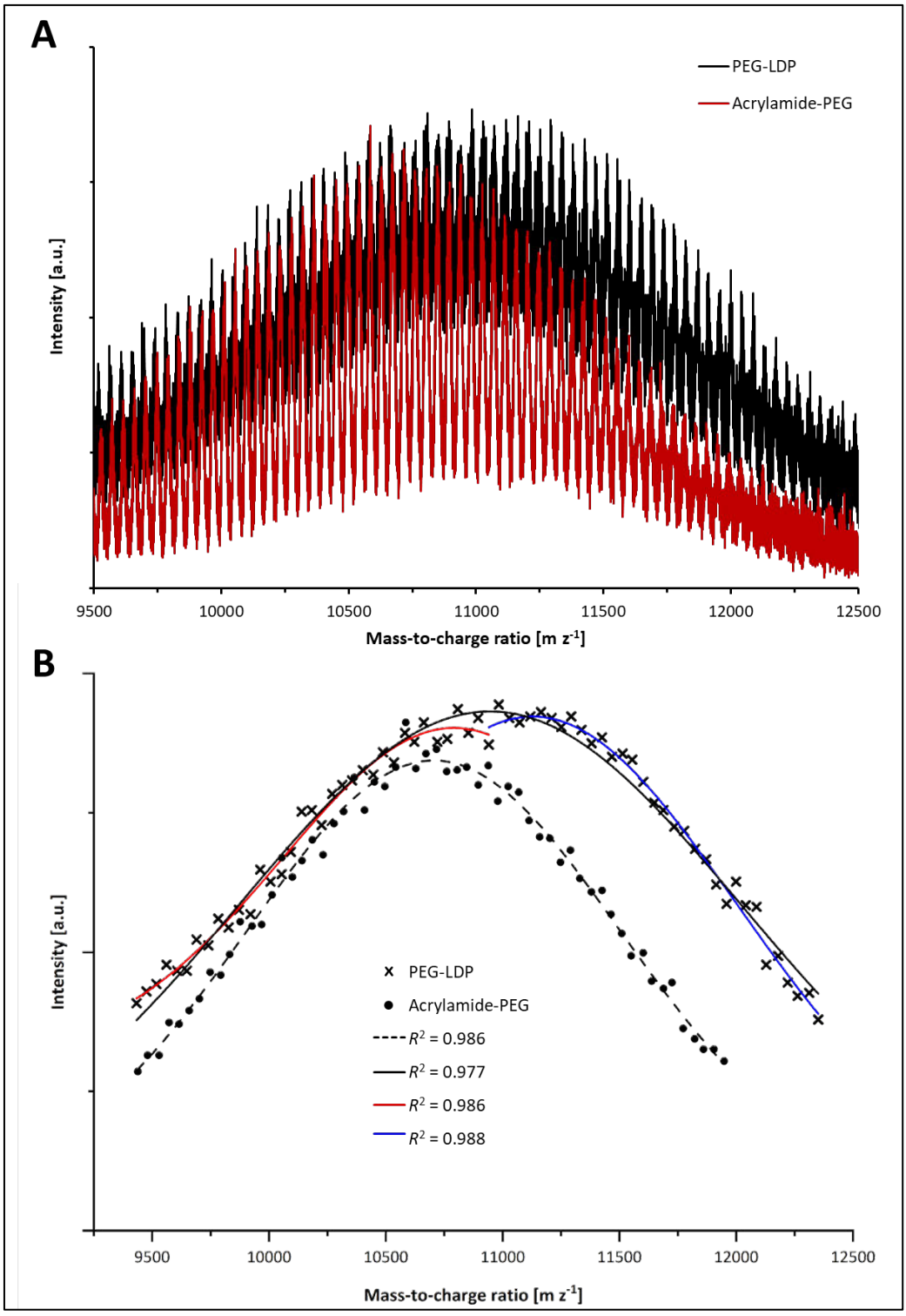

Figure 6.2.10 **MALDI-MS analysis and fitted distributions of acrylamide-PEG and PEG-LDP.** (**A**) MALDI mass spectra of acrylamide-PEG (red spectrum, expected apex at 10 kDA, observed apex at approximately 10.7 kDa) and PEG-LDP (black spectrum, expected apex at 10.9 kDA, observed apex at approximately 11 kDa). (**B**) Full and piecewise Gaussian fittings of acrylamide-PEG and PEG-LDP with their respective R^2 coefficients. Results are given in (blue) for a hypothetical pure PEG-LDP fraction (theoretical apex at approximately 11.2 kDa) and (red) for a possible DTT-PEG impurity (theoretical apex at approximately 10.8 kDa).

6.2.1.5 FXIIIa Reaction Studies

Despite the problems of linking high molecular weight PEG molecules described in the previous section, the platform presented is an exceptional tool for bioorthogonal conjugation reactions. To collect further details on the reaction-determining factors and thus to be able to further optimize the system, a series of experiments was conducted.

For this purpose, the substrates from the previous investigations were first exchanged or adapted. The cysteine in the lysine-bearing peptide (LDP) integrated for cargo coupling was replaced with phenylalanine, which reduced oxidation sensitivity and simplified UV detection at the same time. For more efficient experimental performance, the glutamine-presenting sequence NQEQVSPL, previously provided by the eGFP mutein TG-eGFP, was also represented by a synthesized peptide with an acylated N- and amidated C-terminus. Analogous to the lysine-donating peptide (LDP) the hereby obtained molecule was denominated glutamine-donating peptide (GDP). Since the hydrolytic deamidation of the glutamine substrate after consumption or in the absence of the lysine substrate is a pivotal reaction mechanism, a hydrolyzed variant was also generated for better identification and traceability in the intended HPLC analysis. The structure of the hydrolyzed glutamine-donating peptide (HGDP) is therefore determined by the conversion of glutamine into glutamic acid (Ac-NEEQVSPL-NH_2).

Figure 6.2.11 A shows ESI pos. MS spectra of the mentioned synthesized peptides, as well as the doubly hydrolyzed form of glutamine peptide (2HGDP) isolated by HPLC peak sampling, which, however, was detectable only in traces and thus had no significant influence on the course or evaluation of the experiments. When incubated with FXIIIa, in addition to the expected LDP-GDP crosslinked product (CLP), HCLP (CLP, but the second glutamine of the GDP sequence was deamidated) and CLP2, which corresponds to a compound of GDP and two LDPs, were detectable under certain reaction conditions (***Figure 6.2.11 B***). Again, however, both additional forms occurred only in negligible quantities, so that for evaluation purposes all product forms were summarized as CLP without further differentiation.

With the first series of experiments, in which a fixed concentration of GDP was offered varying concentrations of LDP, it could be demonstrated that calculational consumptions and remaining portions of both peptides were equivalent to each other (***Figure 6.2.12 A, B***), which first of all clarified the robustness and the adequate calibration of the analytical

method as well as the specificity of the enzymatic reaction. Furthermore, ***Figure 6.2.12 C*** shows that at mathematically identical initial concentrations, a conversion rate of about 80 % was achieved for both substrates, whereas an approximately twofold excess of one substrate already results in almost complete utilization of the opposing peptide. Subsequently, the characteristics of product formation were examined in more detail. For this purpose, equal concentrations of both peptides in different orders of magnitude were used and the course of product formation was recorded. It was shown that the reaction was completed within about one hour even at concentrations of 5.5 mM (***Figure 6.2.12 D***). For longer incubation times, it was assumed that hydrolytic events or other undesired (reverse) reactions could accumulate, but these could not be observed up to about three times the required duration of incubation (***Figure 6.2.12 E, F***).

Since the FXIIIa mediated reaction is a multi-substrate process, the required excess for both peptides, which is necessary to make the reaction rate solely dependent on the opposite substrate, was determined [124]. For this purpose, the concentration of one substrate was kept constant while the concentration of the second substrate was increased until the maximum product formation rate was reached. ***Figure 6.2.12 G*** shows that no further effect on the process speed could be achieved after the concentration exceeded a fivefold excess for either peptide.

With the collection of this knowledge for all structures involved in the reaction, elaborately and/or expensively produced biologicals can be modified with maximum efficiency in future projects.

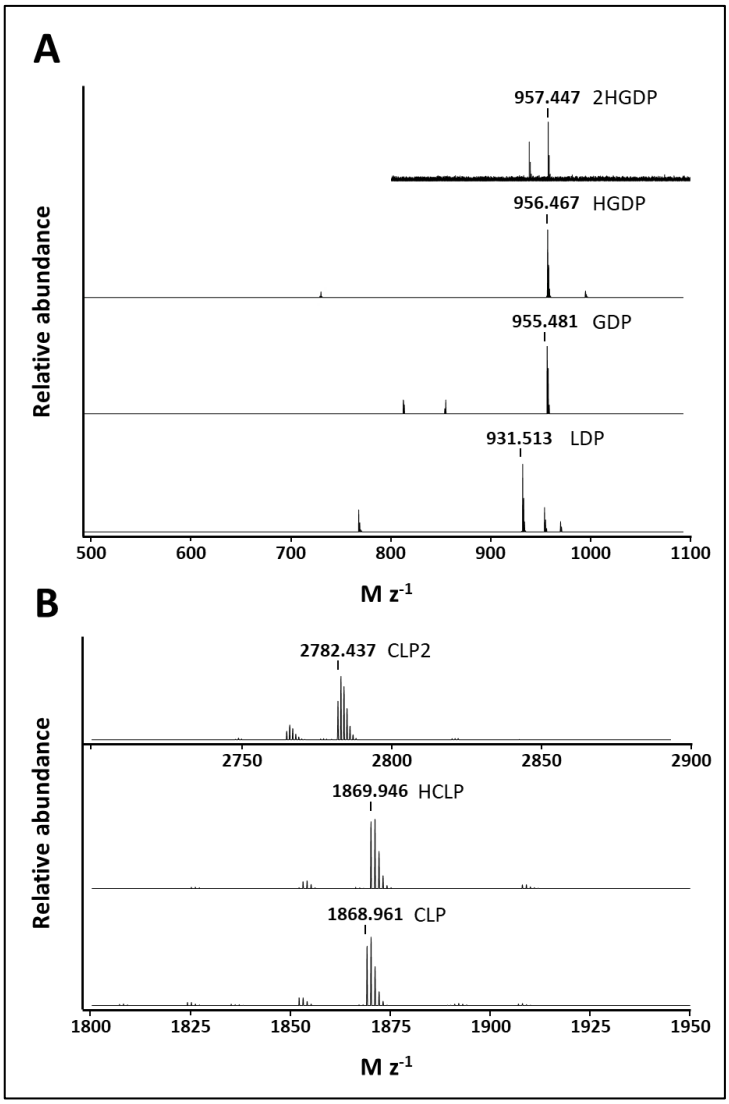

Figure 6.2.11 **ESI pos. MS data of substrates and products of the FXIIIa-mediated reaction.** (**A**) Spectra in ascending order showing (*LDP*) a purified sample of modified lysine providing peptide Ac-FKGG-PEG6-F-NH_2 (calculated mass 931.08 Da, found mass 931.513 Da), (*GDP*) a purified sample of glutamine donating peptide (Ac-NQEQVSPL-NH_2, calculated mass 955.01 Da, found mass 955.481 Da), (*HGDP*) a purified sample of a modified GDP, simulating a single hydrolytic deamidation (Ac-NEEQVSPL-NH_2, calculated mass 955.99 Da, found mass 956.467 Da) and (*2HGDP*) an isolated HPLC peak of a doubly hydrolyzed GDP (Ac-NEEEVSPL-NH_2, calculated mass 956.97 Da, found mass 957.447 Da). (**B**) Spectra of conjugates in ascending order showing (*CLP*) the crosslinked product of LDP and GDP (calculated mass 1869.06 Da, found mass 1868.961 Da), (*HCLP*) the conjugation of LDP and GDP, with one hydrolyzed glutamine (calculated mass 1870.04 Da, found mass 1869.946 Da) and (*CLP2*) a conjugation of two LDP and GDP (calculated mass 2783.11 Da, found mass 2782.437 Da).

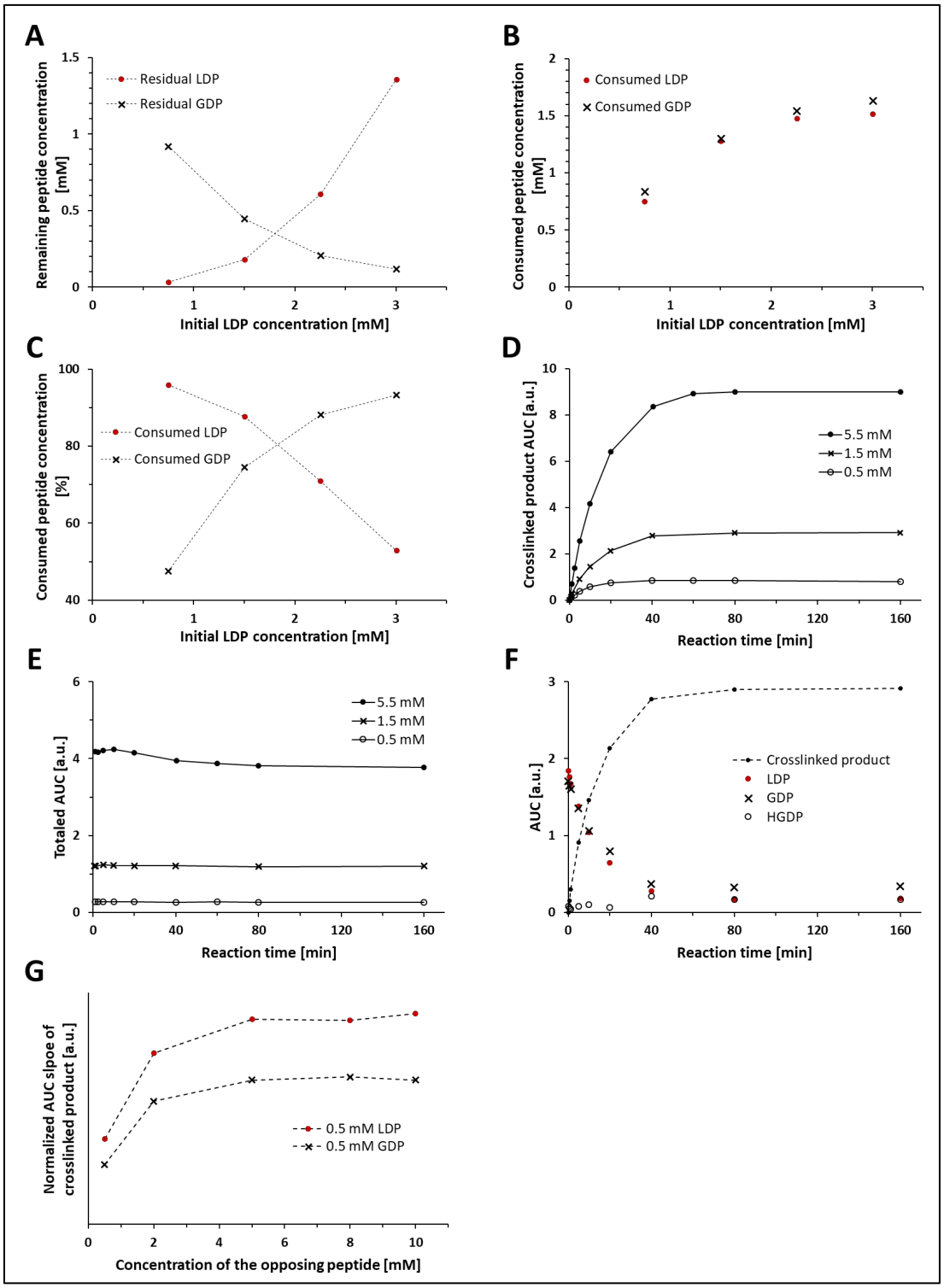

Figure 6.2.12 **Characterization of the FXIIIa-mediated reaction analyzed via HPLC.** Visualization of (**A**) the unconsumed substrate fractions, (**B**) the reduction of substrate concentration, and (**C**) the percental peptide consumption after an unvaried concentration of 1.75 mM GDP was incubated with varying concentrations of LDP. Deploying equal substrate concentrations, (**D**) shows the accumulation of conjugation product while (**E**) depicts the entirety of substrate and product AUCs over time. (**F**) Reaction progression with an initial substrate concentration of 1.5 mM. (**G**) AUC slope evaluation of conjugation product formation as a criterion for reaction speed in dependence of a concentration surplus of each substrate at a time.

6.2.2 Conjugation via Copper(I)-Catalyzed Azide-Alkyne Cycloaddition

The Huisgen cycloaddition is one of the most used click chemistry techniques to date and is extensively applied in the following chapters. It was also utilized as a comparison to the endogenous method perused in the previous sections. With a focus on the enzymatic approach in this part of this work, CuAAC primarily served as a well-established reference, since its effectiveness in labeling both small and large molecules to other proteins was particularized before [125]. Especially PEGylation, which failed for the FXIIIa-mediated reaction in the chosen constellation, is commonly achieved with this method. To determine the basic availability of the alkyne group in Plk-eGFP, introduced via the artificial amino acid Plk, the reactivity was tested employing an azide-modified biotin. ***Figure 6.2.13*** shows that the CuAAC reaction was specific and that the fluorescence intensity was increased depending on the molar excess of the azide entity's concentration.

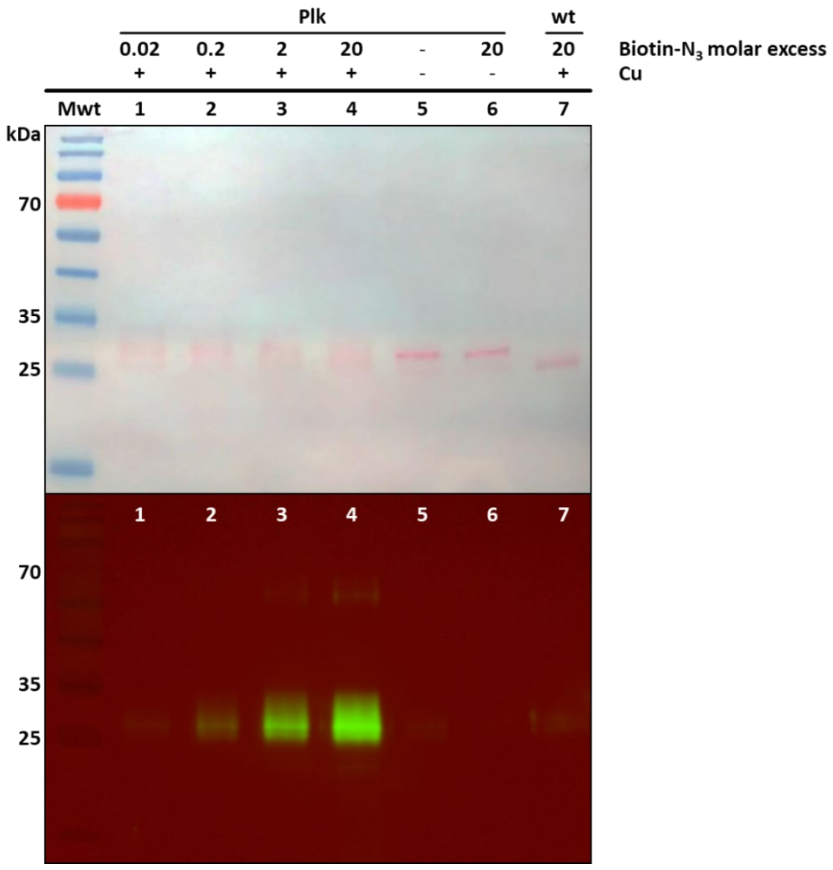

Figure 6.2.13 **Ponceau red stain (top) and Western blot visualization (bottom) of Plk-eGFP and Biotin-N_3 reaction using CuAAC.** The reaction shows an azide substrate-dependent increase in fluorescence with minimal to no side reaction in the absence of copper or alkyne group. The top brackets indicate the deployed eGFP variation.

6.3 Nano- and Micro-Surface Functionalization

Site-specific modifications can furthermore be utilized to facilitate directional surface decoration and hence serve a broad field of analytic and therapeutic applications [126]. To establish a connection, the carrier's surface needs to provide inherent or introduced functional groups. Determined by the presented functionality, a cargo molecule can adhere to the surface in several ways. Various modifications onto different materials and surfaces were examined within the framework of this thesis. For a better understanding, all surface-providing units are schematically illustrated in ***Scheme 4***.

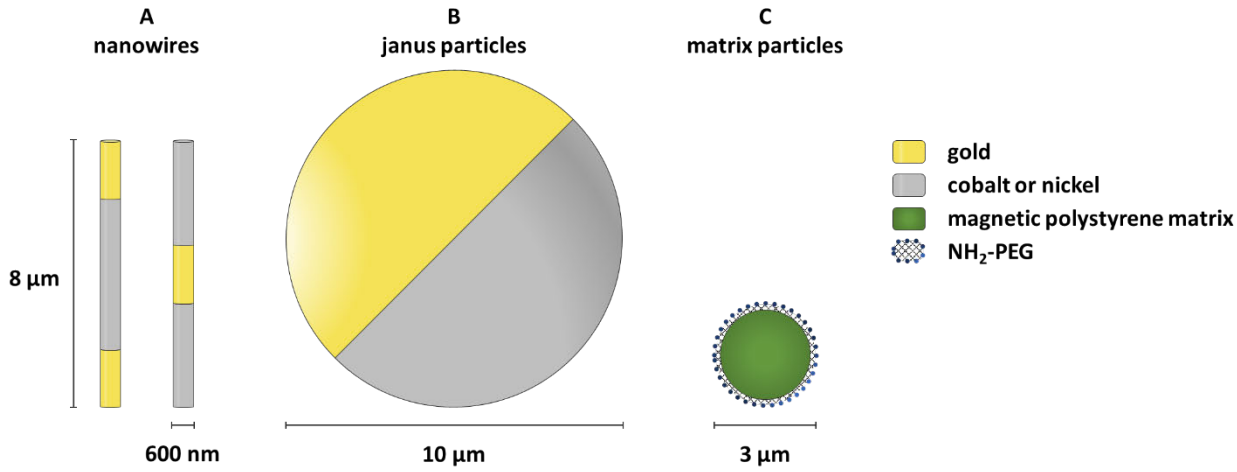

Scheme 4 **Overview of the deployed surface source materials.**

6.3.1 Gold-Thiol (Au-SH) Utilization

When a gold surface is available, connections with binding strengths comparable to covalent bonds can be acquired with thiol groups by single-stage incubation, generating a self-assembled monolayer (SAM) (see ***Scheme 5***) [127]. The geometry of the surface can be varied to fit the required conditions.

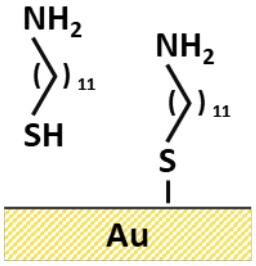

Scheme 5 **Simplified gold-thiol interaction with 1-Amino-11-undecanethiol.**

6.3.1.1 Alkanethiols Intermediates and Enoxaparin Functionalization

In this work, 1-Amino-11-undecanethiol (AUT) was used as the sulfur component, also providing a free primary amine for further functionalization. Initially, the availability of the amino group was verified by subsequent fluorescein isothiocyanate (FITC) staining. ***Figure 6.3.1 (A-C)*** shows the completed procedure, where the outer gold segments of an Au-Co-Au nanowire are specifically targeted.

In addition to that, available primary amines make a variety of functionalizations possible. To attach enoxaparin, a low molecular weight heparin with accessible carboxyl groups, to the nanowire's surface, a two-step EDC/Sulfo-NHS reaction was utilized as a basic approach. To render the successful decoration visible, the nanowires were incubated with fluorescein-labeled protamine. Through electrostatic attraction protamine attached to the negatively charged enoxaparin molecules, which resulted in fluorescent nanowire segments as can be seen in ***Figure 6.3.1 (D-F)***.

The identical procedure was applied to NH_2-PEG magnetic polystyrene-matrix particles, which were successfully used in an analytical setup to investigate molecular binding characteristics between Fibroblast growth factor 2 (FGF-2) and heparin [128].

However, unlike industrial-produced and purchased polymer particles, the deployed nanowires showed extremely inconsistent behavior regarding wetting properties and quality of functionalization, to the extent that many decoration attempts failed. Since respective batches exhibited extreme hydrophobicity, wettability was tried to improve by preponed silanization (see Chapter 6.3.2) with subsequent curing (in vacuo drying). Yet, nanowires treated in this way revealed no improvement (data not shown). Whilst super-hydrophobic and super-hydrophilic properties of especially nickel surfaces are well known, a direct connection to the failure of subsequent functionalization could not be investigated within the

scope of this work [129-131]. Most likely, the etching procedure applied during the nanowire template release has a huge impact on the hydrophilic properties as recent work of Qian *et al.* strongly suggests [132].

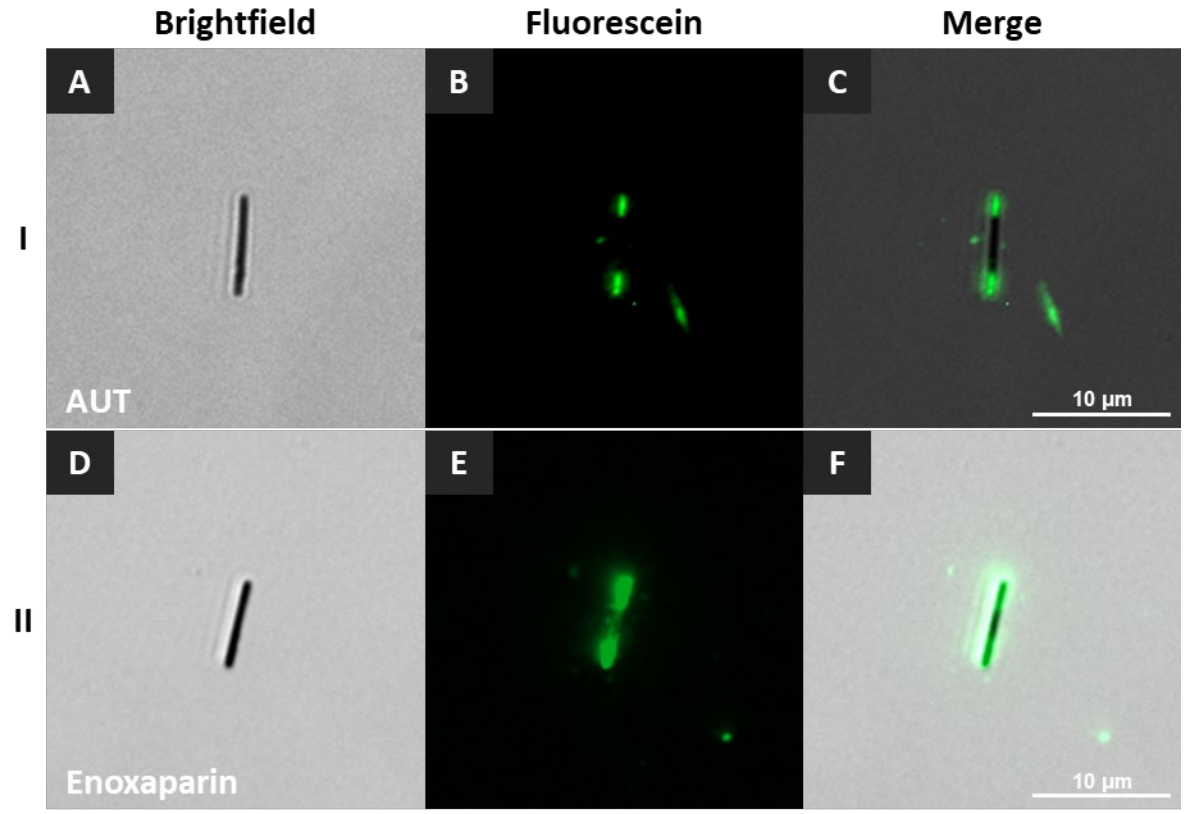

Figure 6.3.1 **Fluorescence microscopy images of functionalized Au-Co-Au nanowires marked with fluorescein.** Row **I** (images **A-C**): FITC staining revealed the formation of the AUT-SAM. Row **II** (images **D-F**): enoxaparin coupled to the AUT-treated nanowires visualized by fluorescein-labeled protamine.

6.3.1.2 DNA-Functionalization

When utilizing the interaction strength of gold and thiol groups, the additional functionality is not limited to a specific entity. Large biomolecules like nucleic acids and other complex compounds can be chosen as cargo. The modified DNA depicted in ***Scheme 6*** was used as a model molecule to be attached to Co-Au-Co type nanowires and gold/nickel Janus particles.

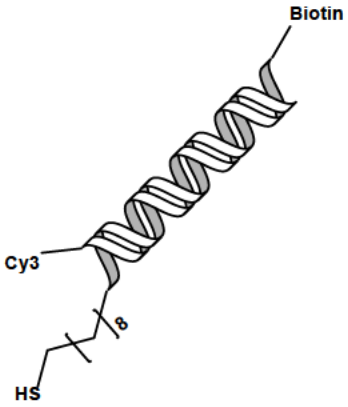

Scheme 6 **Modified sample DNA strain, comprising a biotin and a fluorescent Cy3 marker as well as a flexible thiol group.**

SsDNA was fused in a preparation step and incubated with the desired material in a TBS buffer with increased ionic strength to stabilize the dsDNA and interrupt unspecific ionic interactions. ***Figure 6.3.2 (A-C)*** shows a processed nanowire with a clearly visible attachment of Cy3-marked DNA. This decoration strategy was easily transferred to other surface geometries. ***Figure 6.3.2 (D-I)*** depicts single and clustered bifunctional Janus particles, which received the identical treatment.

Furthermore, a DNA species with duplicative thiol groups on one side, as well as two biotin markers on the opposing side, was created (***Scheme 7***). This array allowed for the rigid fixation of the molecule between the particle's surface and a potential analytical setup to investigate intramolecular properties [133, 134]. Since the inherent Cy3 marker was omitted, the successful attachment to the deployed surface was verified by propidium iodide (PI) DNA intercalation in ***Figure 6.3.2 (J-L)***.

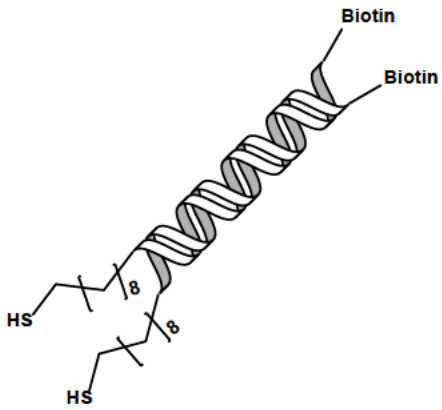

Scheme 7 **Modified sample DNA strain, with twin-functionalities on both ends.**

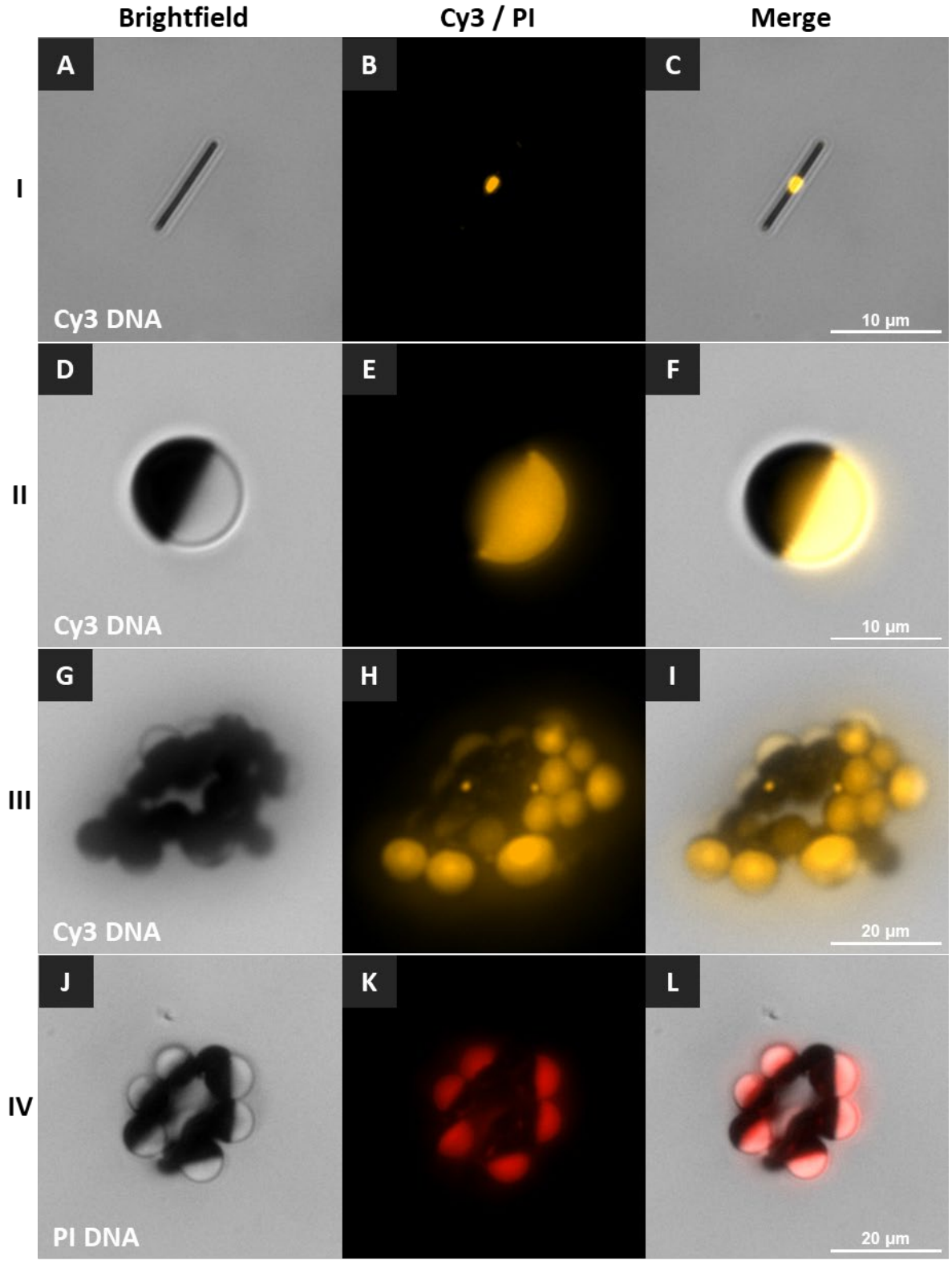

Figure 6.3.2 **Fluorescence microscopy recordings showing DNA decorated surfaces.** Row **I-III**: Cy3 marked DNA attached to (**A-C**) a Ni-Au-Ni nanowire and (**D-I**) Janus particles. Row **IV** (images **J-L**): DNA with twin functionalities, rigidly connected to the gold surface of the bifunctional particles, visualized with PI.

6.3.2 Silanization and PEGylation

Oxidized surfaces can be coated and masked with silanes. The cobalt or nickel surface provided by the nanowires featured enough hydroxyl groups due to the acid/base treatment during the template release (see Section 5.2.3.1) for a successful condensation reaction. (3-Aminopropyl)triethoxysilane (APTES) was used as silane with an additional primary amine as a functional group. ***Scheme 8*** offers an abridged version of the silanization process.

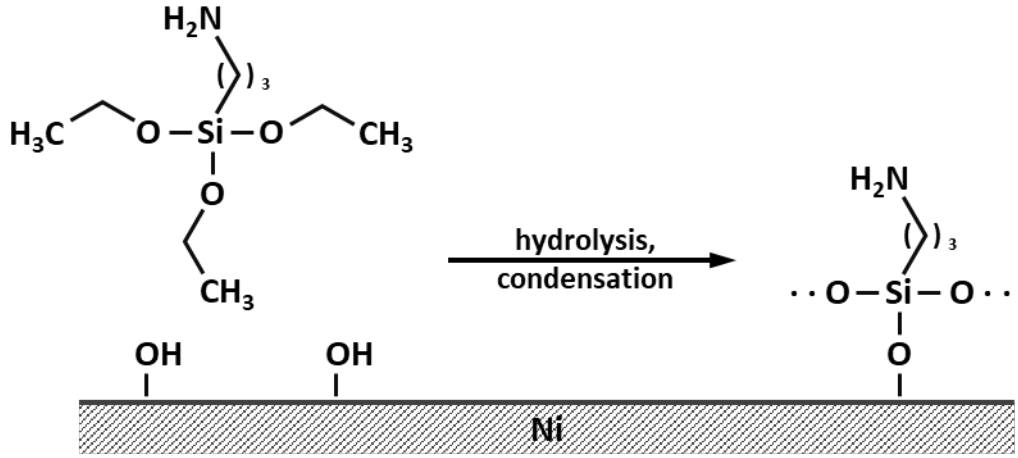

Scheme 8 **Oxidized nickel surface silanization with APTES.**

Figure 6.3.3 A-F displays the consummated attachment of APTES to the nickel segments visualized with FITC, whereas ***Figure 6.3.3 G-I*** shows the combined treatment of silanization and subsequent AUT functionalization described in Chapter 6.3.1.1, with the result of an entirely occupied nanowire.

After the silanization was confirmed, the provided amine functionality was used for PEGylation, which was achieved through an amine-reactive crosslinker reaction with Methoxypoly(ethylene glycol) succinate *N*-hydroxysuccinimide ester. No graphical data was plausible to verify this procedure, since subsequent FITC staining was still successful due to an undefined quantity of unreacted anime groups remaining on the nanowire's surface.

Nevertheless, the problem of hydrophobic nanowires described in section 6.3.1.1 also interfered heavily at this stage. Whenever possible functionalization steps were conducted in organic solvents to circumvent failure due to inadequate wettability. To improve silanization quality, the dipodal siloxane Bis(triethoxysilyl)ethane (BTESE) was added to

enhance surface bond strength [101]. As before the results were inconsistent: Among good results (***Figure 6.3.4***), the experiment often failed for no apparent reason even when all reaction conditions were unaltered without exception.

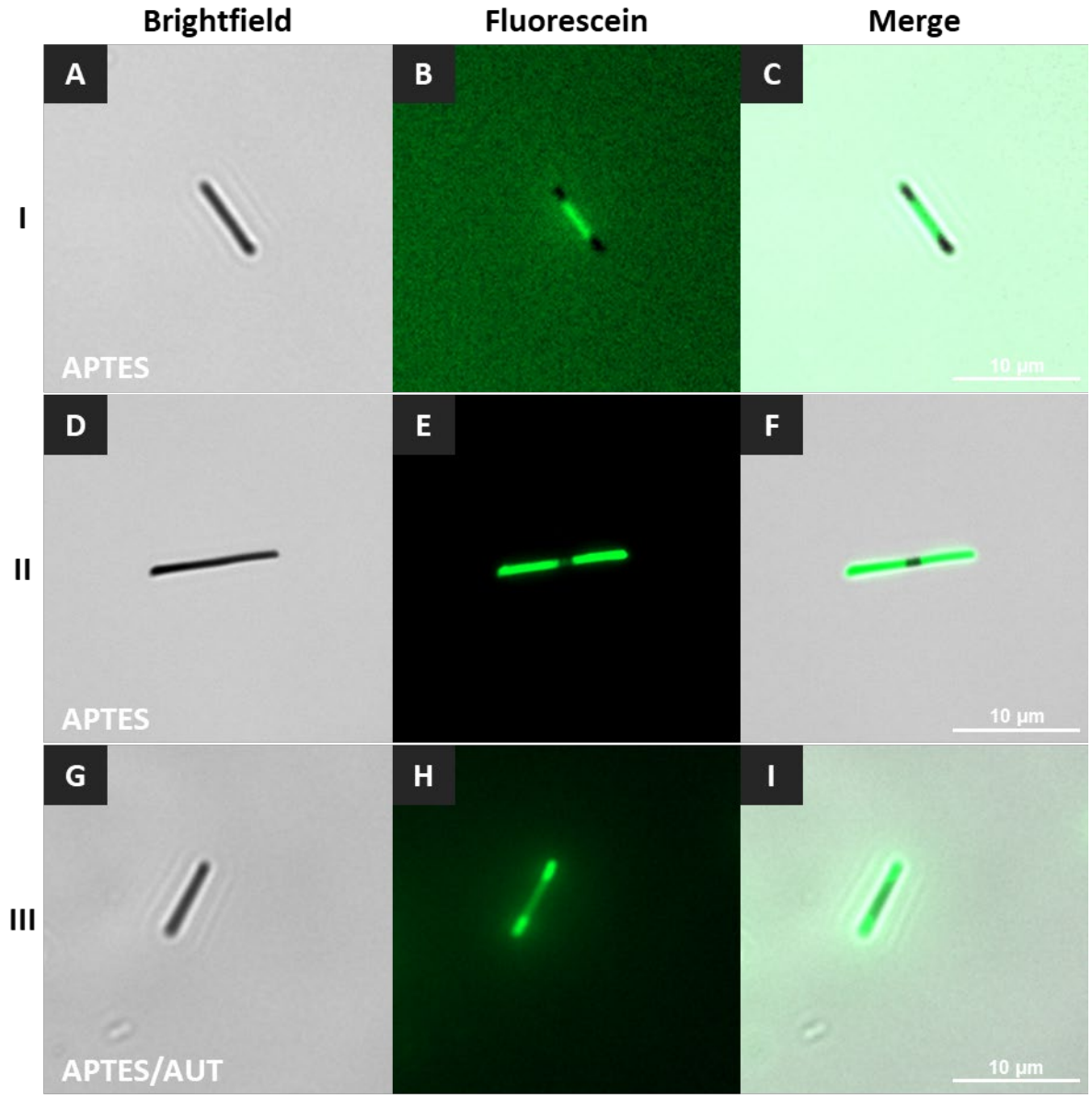

Figure 6.3.3 **Fluorescence microscopy images of fluorescein-labeled nanowires.** Row **I** and **II**: silanized and FITC-stained (**A**-**C**) Au-Co-Au and (**D**-**F**) Ni-Au-Ni nanowires, respectively. Row **III** (**G**-**I**): Au-Co-Au nanowire sample subjected to silanization and subsequent AUT treatment prior to FITC staining.

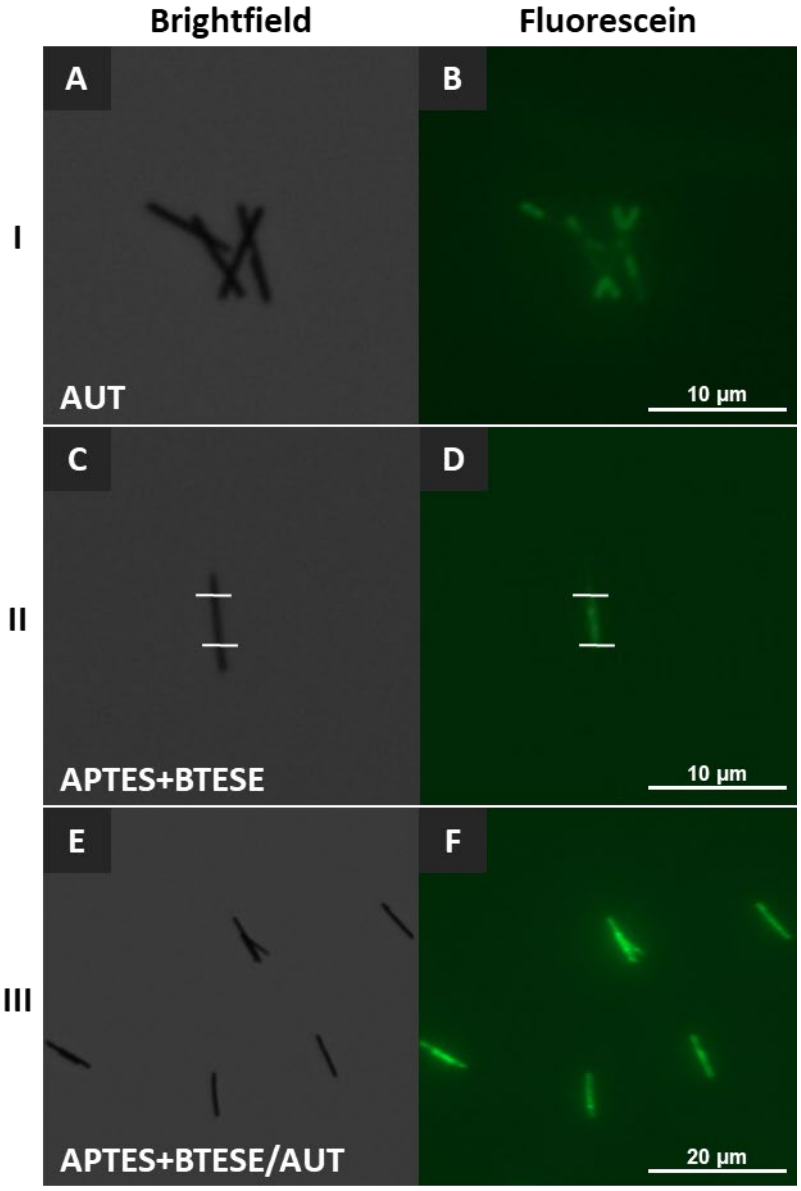

Figure 6.3.4 **Fluorescein-stained Gold-Nickel-Gold (Au-Ni-Au) nanowires analyzed by fluorescence microscopy.** Row **I** (**A**+**B**): after AUT treatment, with distinctly labeled gold ends. Row **II** (**C**+**D**): Silanized with APTES/BTESE, Nickel-segments distinctly labeled, emphasized with white marks. Row **III** (**E**-**F**): Silanization with APTES/BTESE and subsequent AUT incubation, resulting in a completely labeled nanowire.

6.3.3 Conversion of Primary Amines to Azides

As mentioned at the beginning of this chapter, the available functionality can be substituted to achieve a new spectrum of modifications. Via a diazo-transfer reaction utilizing imidazole-1-sulfonyl azide hydrochloride ($ImSO_2N_3 \cdot HCl$), present primary amines can be converted to azide groups making azide-alkyne "click" chemistry possible. $ImSO_2N_3$ as a diazo donor was prepared as described previously [102, 135]. Successful preparation and high purity were confirmed via LC-ESI-MS without further specification as shown in ***Figure 6.3.5***.

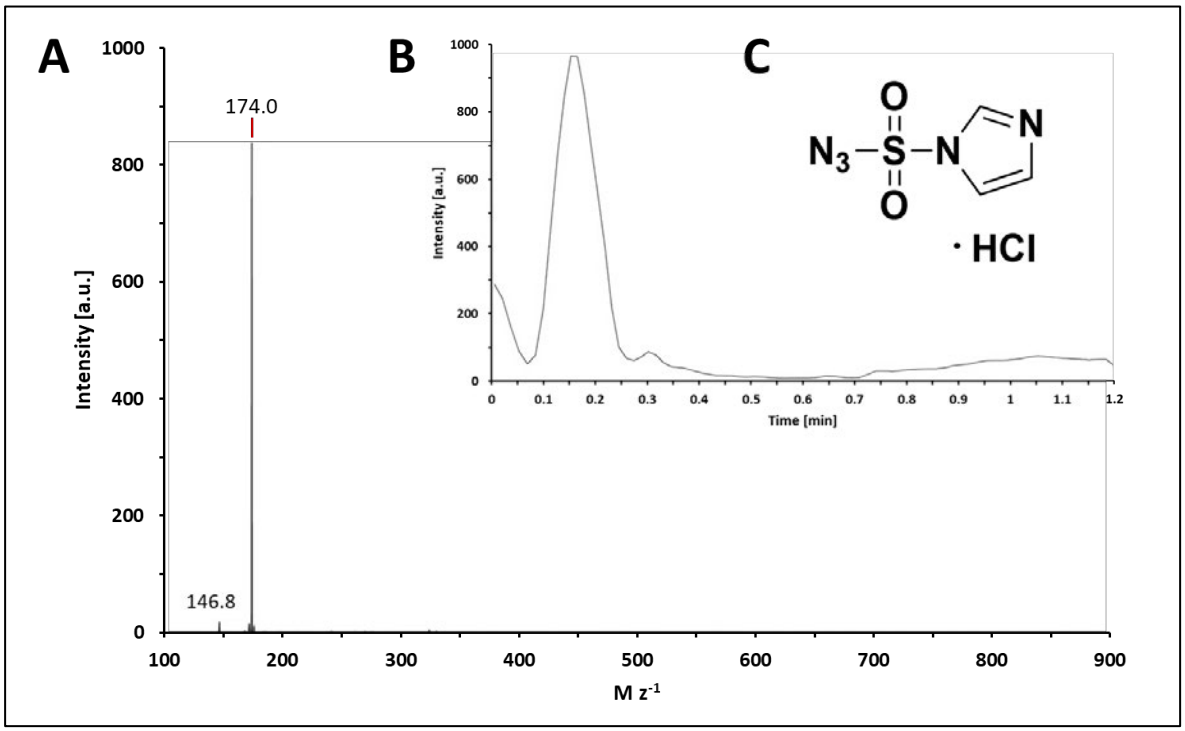

Figure 6.3.5 **Characterization of imidazole-1-sulfonyl azide hydrochloride.** (**A**) LC-ESI-MS chromatogram of $ImSO_2N_3$ (obs. mass 174.0 Da, calc. mass 174.0 Da). (**B**) Corresponding HPLC-UV chromatogram of $ImSO_2N_3$. (**C**) Chemical structure of $ImSO_2N_3 \cdot HCl$.

With the available azido-transfer agent, the conversion reaction was conducted as described previously with minor adaptions [102]. To determine the most appropriate catalytic salt, as it may hold different properties regarding the efficacy and oxidative effects, preliminary reaction compositions were prepared and analyzed via thin-layer chromatography (TLC) [136-138]. The catalytic salts in question were $CuSO_4$ and $ZnCl_2$. ***Figure 6.3.6*** shows the

resulting TLC separation, illustrating the complete consumption of the anime-presenting species AUT in both reaction mixtures yet yielding homogenous products with distinguishable polar properties [139, 140]. Reasoning that not only the desired azide conversion but also excessive oxidation of the existing thiols to disulfide groups may reduce the polarity of the resulting compounds, $ZnCl_2$ was chosen for subsequent experiments since it generated a product with anticipated chromatographic properties and less oxidative potential and was also reported to be the overall more efficient catalyst [137].

Albeit this approach was not qualified to rule out the possible creation of other compound compositions such as disulfide-linked AUT molecules with only a single converted azide or even none, there was no indication of their existence and it was assumed that their presence would have no significant effect on the outcome of the following experiments.

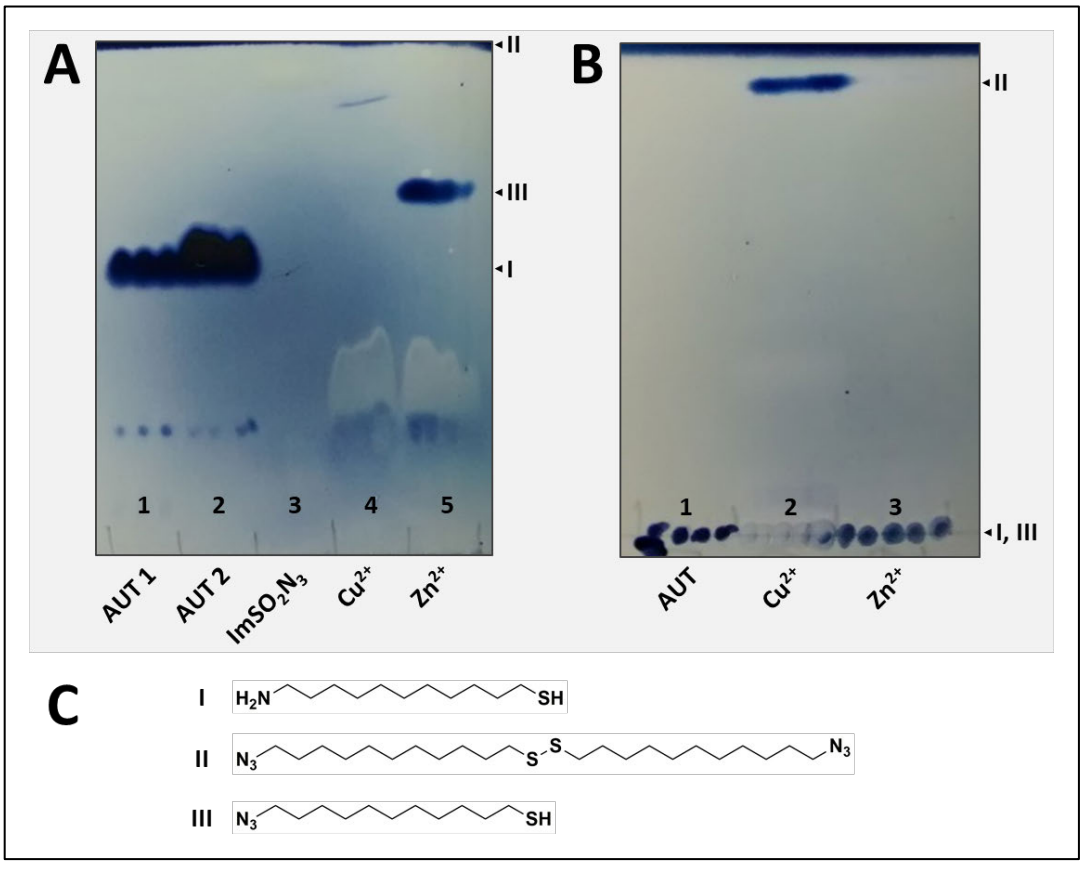

Figure 6.3.6 **TLC analysis of a diazo-transfer reaction and its reactants.** (**A**) Showing two different batches of AUT on lanes **1** and **2** and $ImSO_2N_3$ on lane **3**. Lanes **4** and **5** represent samples of completed reactions with either (Cu) copper or (Zn) zinc as catalysts. Separation was run with chloroform/methanol/20 % acetic acid (65:25:5, v/v/v) as a rather polar eluent. Marks on the right side indicate the R_f of the respective substances. (**B**) The second run omits one AUT batch and the diazo-transfer reagent while using hexane/ethyl acetate (4:1, v/v) as the solvent system. (**C**) Structual formulae of the anticipated compounds.

6.3.4 Directional Protein Functionalization via CuAAC

A small molecule like the fluorescent dye 5-FAM-alkyne was chosen as an example cargo molecule to be attached to azide-converted NH_2-PEG magnetic polystyrene-matrix particles using copper(I)-catalyzed azide-alkyne huisgen cycloaddition. ***Figure 6.3.7 (I)*** shows reactions with unconverted amine-presenting beads (**NH_2**) as a negative control, as well as the successful attachment of 5-FAM on the converted azide profile (**N_3**) when a copper(I) species is present (**+Cu**).

Furthermore, in ***Figure 6.3.7 (II)*** the experimental setup was applied to WT-eGFP to consider unspecific reactions or aggregation. As a result, the combination of azide-converted beads with Cu(I) in conjunction with the alkyne-free protein, generated a very weak and uneven fluorescence signal.

In ***Figure 6.3.7 (III)*** Plk-eGFP was used as the alkyne counterpart cargo molecule. In addition to the successful decoration under regular reaction conditions, the native amine functionality revealed a weak but uniform fluorescence signal.

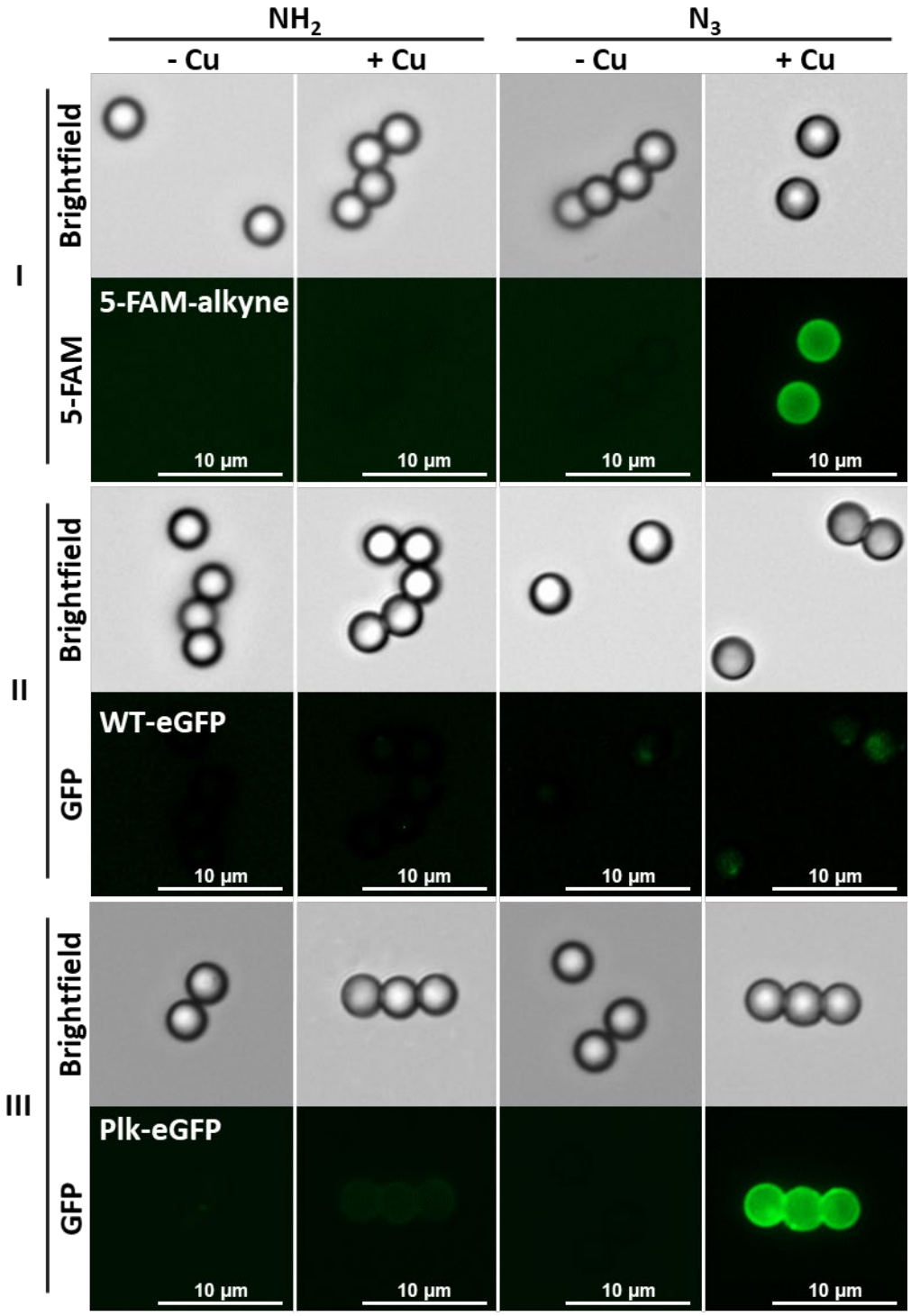

Figure 6.3.7 **Fluorescence microscopy images of CuAAC-mediated surface decoration.** Left double column **NH_2**: negative controls, where particles were not treated with Imidazole-1-sulfonyl azide, thus remaining with their initial amine functionality. Right double column **N_3**: particles with completed conversion treatment, presenting azide groups on their surface. Sub columns **-Cu/+Cu**: indication whether the reaction was supplemented with (+Cu) or without (-Cu) copper(I) as a reaction catalyzing agent. Row **I-III**: reflecting the potential cargo molecules, where reactions were conducted with (**I**) 5-FAM-alkyne, (**II**) WT-eGFP, and (**III**) Plk-eGFP imaging respective samples under brightfield and a 5-FAM or GFP filter, respectively.

6.3.5 Directional Protein Functionalization via FXIIIa

The presented primary amine groups of the untreated polystyrene-matrix beads (Chapter 6.3.4) were exploited to test the surface functionalization capacity of factor XIIIa. In the absence (***Figure 6.3.8 (I)***) and presence (***Figure 6.3.8 (II)***) of the transglutaminase, the beads were incubated with TG-eGFP. It was shown that there was no surface attachment without the addition of FXIIIa, except for some very minor aggregation that is hardly visible on the converted images. Under regular reaction conditions, the particles were evenly labeled with the fluorescent protein.

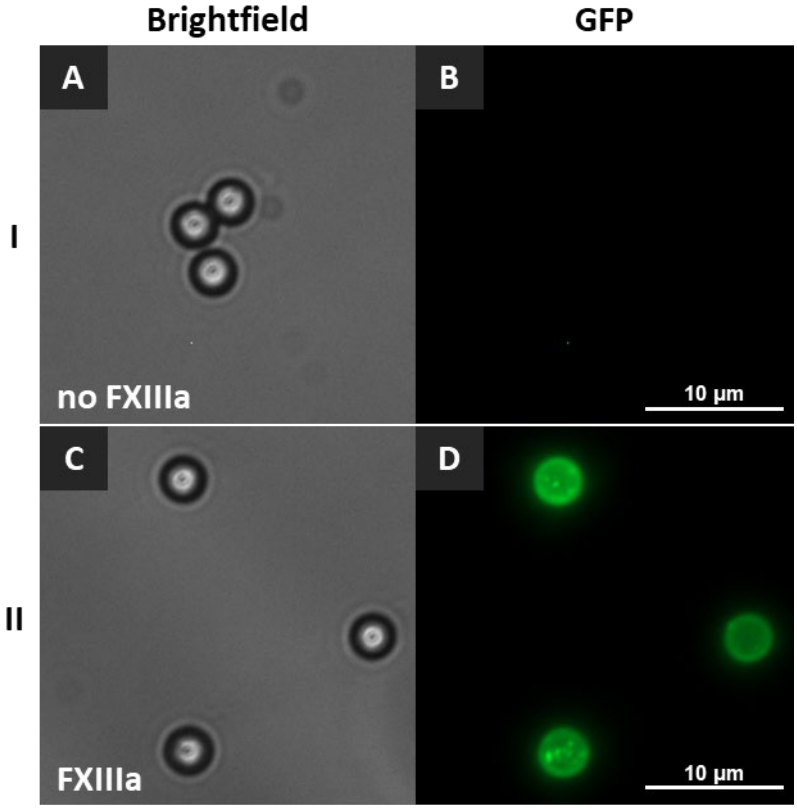

Figure 6.3.8 **Fluorescence microscopy images of FXIIIa-mediated surface decoration.** Row **I** (**A**+**B**): Magnetic PEG-NH_2 beads were incubated with TG-eGFP omitting the transglutaminase as a negative control. Row **II** (**C**+**D**): Identical incubation reaction but in the presence of FXIIIa.

7 Discussion and Outlook

Other than their ease of use, unspecific biofunctionalization strategies pose many disadvantages for innovative, highly sophisticated biologicals, especially in terms of homogeneity. To conquer these shortcomings, bioorthogonal, site-specific modifications will play an increasingly important role in the development of new pharmaceutical formulations. Even though a broad pool of contemplatable methods is available, choosing the most suitable system is a delicate task, as it will govern every aspect of the prospective process. To gain further insights into characteristic properties and essential differences, two potent representatives of opposing functionalization strategies, i.e., enzymatic conjugation via FXIIIa and chemical coupling through CuAAC, were chosen. Since the mutual hallmark of every site-directed reaction approach is a unique functionality within the protein of interest, various eGFP muteins were designed in the first part of this work. GFP and its many mutants are a great example of how minor changes in the amino acid sequence can significantly affect a protein's properties, in this case, emission wavelength and brightness [72, 141]. The accumulated knowledge about eGFP's structure allowed us to specifically target the flexible N- and C-termini for modifications, as they are not involved in the protein's folding and function.

Four different types of eGFP muteins were designed to create a comparable system for post-translational customization. Initially, a wild-type variant solely bearing an added His-Tag for efficient purification via affinity chromatography, was successfully expressed and characterized to establish a baseline construct, allowing the identification of potential deviations in the conjugation-primed mutants [142]. *Escherichia coli* as a reliable host was chosen for its convenient handling and high efficacy [143, 144]. Subcloning into the pET-11a vector was achieved after gene amplification via PCR, using primers harboring NdeI and BamHI restriction sites to allow for an oriented ligation through the creation of overlapping ends. Routinely, the inducible *E. coli* T7-polymerase-pET-system was used for all expressions, after the gene-carrying plasmid was amplified and transformed into the BL21(DE3) *E. coli* strain. WT-eGFP was obtained in high yields and purity, displaying characteristic properties regarding sequence, observed mass, and fluorescence features (***Figure 6.1.7***) [98]. Additionally, a linear concentration-dependent fluorescence intensity was shown, enabling active protein yield estimation for further experiments.

Subsequently, applying the identical subcloning procedure, the FXIIIa-dependent eGFP mutein containing the glutamine-presenting motif was successfully created. The recognition sequence was chosen from the endogenous conjugation substrate α-2 plasmin inhibitor known for its comparatively good affinity towards FXIIIa [58].

At first, a standard expression scheme (6-8 hours incubation at 37°C) failed to yield any protein at all [145, 146]. As shown in ***Figure 7.1*** a series of test expressions were conducted to find suitable expression parameters. No expression attempt in LB medium was successful. Although *E. coli* can grow within a large pH range (4.4 to 9.2), the environmental stress caused by pH values above 10 within samples taken after 24 hours, might be a reason for this phenomenon [147]. The aggregation of expression product into inclusion bodies because of rapid formation under high temperatures was not a reasonable explanation, as these would be solubilized during the denaturing SDS-PAGE preparation. Slow activation at low temperatures (20°C) exclusively, resulted in the desired overexpression in phosphate-buffed TB medium.

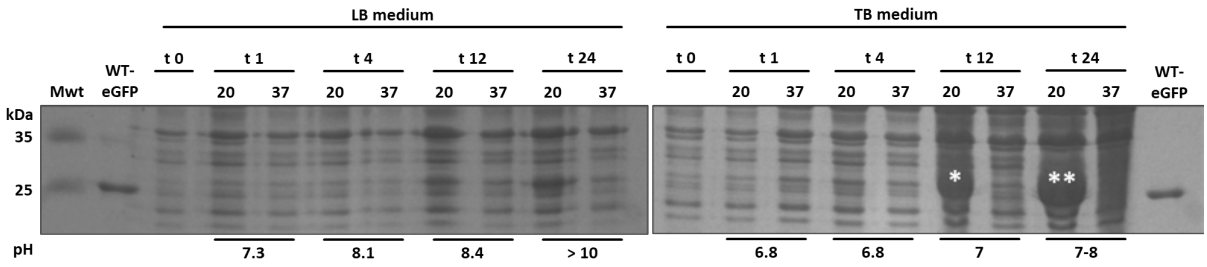

Figure 7.1 **SDS-PAGE of the expression condition screening for TG-eGFP.** Suitable expression conditions for TG-eGFP were analyzed in LB and TB medium at 20 and 37°C. Samples were taken before induction (t 0), and 1, 4, 12, and 24 hours after induction with IPTG (t 1, t 4, t 12, and t 24, respectively). Overexpression is solely visible in TB medium at 20°C past 12 hours (bands marked with asterisks).

The purified TG-eGFP matched the eGFP characteristic properties and no deviation to the WT-eGFP reference was found (***Figure 6.1.13***). Interestingly, even though the protein was obtained in high amounts after the adaptations, expression requirements were significantly influenced solely by the addition of the amino acid motif.

The subcloning procedure was repeated for amber stop codon containing plasmids enabling the subsequent translation into Plk-eGFP, following the same principles mentioned beforehand. Due to the substantially more complex expression mechanism comprising the

cell uptake of the unnatural amino acid, the critical induction of pyrrolysyl-tRNA synthetase, and the competitive stop codon suppression, considerably smaller expression yields were achieved (***Figure 6.1.18***). As a low availability of modified protein potentially poses a major drawback for UAA-based expressions, the identification and optimization of governing factors are of great importance. Meanwhile, several strategies were successfully pursued by other groups to improve the efficiency of UAA incorporation including (1) the genetic alteration of release factor 1 (RF1) and its recognition motifs to weaken its function to terminate the elongation process, (2) the utilization of optimized promotors to enhance the levels of tRNA and tRNA synthetase, (3) the customization of the deployed tRNAs or even ribosomes for better recognition and (4) the introduction of unnatural base pairs to create unassigned and uncontested codons [109]. Beyond that, UAAs have been integrated via alternative quadruplet codons [148, 149]. Since modifications to the translational machinery were not a focus of this work, attempts to facilitate the overexpression of Plk-eGFP were limited to codon optimization of the added gene information for the expression host using a codon usage table from the Kazusa data [150], the addition of 2 % glucose to uninduced cultures to prevent metabolic stress by leaked induction of the *lac* promoter, as well as the addition of polypropylene glycol as an antifoam agent to ensure sufficient oxygen supply during induction [144, 151]. Presented by Verma *et al.*, a comparatively simple way to further enhance translation initiation and therefore expression efficiency by modulation of the initial amino acid composition, could be beneficial in future studies [152]. Separate optimization in small-volume screening experiments conducted by Georg Wandrey provided additional information, especially regarding the most efficient amount of UAA supplementation.

Eventually, Plk-eGFP was obtained in sufficient yields, fully matching the functional characteristics of the wild-type (***Figure 6.1.25***). With the completion of all relevant muteins, a common platform for coherent comparison in the subsequent conjugation experiments was established. The interim conclusion is that the adequate implementation of UAA is potentially harder to achieve, although individual difficulties may arise from every gene-level protein modification. The use and improvement of specialized expression systems for UAA integration can potentially help this strategy to widen its field of application [153].

For FXIIIa-related studies, a peptide was synthesized that served as the lysine donating substrate (LDP) in the featured isopeptide bond formation as well as a potential cargo linker

(***Figure 6.2.1***). The design of this linker has a critical influence on the expectable product outcome in two ways. Its affinity towards the transglutaminase governs the reaction kinetics, especially as it competes with other lysines and water in the active site. In addition to that, it must be primed with a suitable mechanism to bind a desired cargo molecule. In this work, the implementation of a terminal cysteine enabled the utilization of thiol-Michael additions as a flexible loading strategy.

The coupling of TG-eGFP and LDP via FXIIIa was successfully conducted as shown in ***Figure 6.2.2*** and ***Figure 6.2.3***. The mass spectroscopy data suggests full conversion into the desired conjugated product. Moreover, there was no indication of unspecific coupling or dimerization, although eGFP features several free lysine residues on its surface (see ***Scheme 9***). At first, this might seem self-evident, given the high selectivity of natural enzymatic processes. However, a broad table of endogenous substrates has been reported for FXIII and potentially unknown targets had to be ruled out [56].

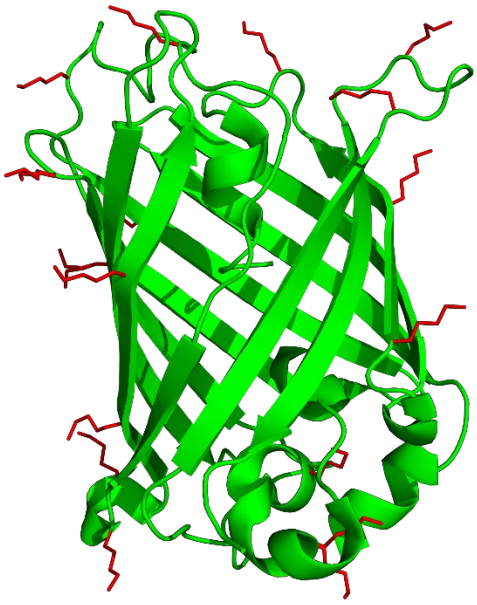

Scheme 9 **Free lysine residues (red) on eGFP**

Furthermore, the postulated clearing of the active site by hydrolytic cleavage of the bound glutamine substrate, when no lysine donor is available, effectively generating a glutamic acid entity, was observable through a 1 Da mass shift in ESI pos. MS data.

To demonstrate an exemplary loading process via the linker peptide, biotin maleimide was selected to serve as a small molecule cargo. To ensure the inertness of the primary amino group of LDP's lysine, the reaction between the sulfhydryl group of the cysteine residue and the maleimide was conducted in acetic acid for a prolonged time and the successful coupling was analyzed again via ESI pos. MS (***Figure 6.2.4***). Thiol-based conjugation kinetics and product stability vary significantly with the choice of the deployed electrophile. Recent studies revealed that maleimides may provide excellent reactivity but are very prone to subsequent hydrolysis and thiol-exchange reactions so other Michael acceptors like vinyl sulfones and acrylamides should preferentially be considered [119, 154-157]. These findings give a reasonable explanation for the somewhat fragmentary purification of the biotin-loaded LDP and consequently for the observed minor unspecific reactions with TG-eGFP and FXIIIa (***Figure 6.2.6***), too. Nonetheless, the small molecule conjugation via LDP was successfully completed.

The loading approach was transferred to a high molecular weight PEG, featuring an acrylamide functionality. With a series of HPLC runs, a protocol was developed to monitor the LDP labeling process (***Figure 6.2.7***). A pH of 8.8 was found to facilitate the reactivity of LDP's sulfhydryl groups, yet associated with increased oxidation, leading to the formation of disulfide bridges. Since the conversion stopped, when only the oxidized form was detectable, an intermittent addition of DTT was applied to reduce the S-S bond and reenable the conjugation reaction until LDP was completely processed. The PEG-loaded linker was purified while a small portion of presumably residual DTT-PEG compound was still present but found to have little influence on the subsequent reaction.

The SDS-PAGE analysis of the reaction between the PEG-labeled LDP and TG-eGFP did not result in an additional signal, indicating that the reaction did not take place (***Figure 6.2.8***).

Efforts were made to identify the reason for the unsuccessful conjugation. In the first instance, native PAGE would have been the preferable analyzation tool, since interactions between PEG and SDS are known to cause smearing and broadening of sample bands [158]. A complete suppression of a present signal, however, is not plausible. To validate the PEG-peptide construct's responsiveness, 1,2-naphthoquinon-4-sulphonate in alkaline solution was applied to detect available amino groups [159, 160]. The obtained colored derivates showed conclusive properties indicating successful PEG conjugation while preserving lysine's amino functionality (***Figure 6.2.9***). This finding corroborates the superior

nucleophilicity of cysteine's sulfhydryl group with a pK_a of 8.37 compared to lysine's amino group with a pK_a of 10.54 during the Michael addition of acrylamide PEG, which was purposely conducted without a catalyst to prevent the primary amine's reactivity [161, 162].

Furthermore, Maldi-spectra of both the pure PEG substance and the PEG-peptide were gathered to confirm expected mass changes (***Figure 6.2.10 A***). Due to the vast signal distribution, a defined mass addition was difficult to assign. As shown in ***Figure 6.2.10 B*** there was a discernible mass shift, and it was hypothesized that the analyte contains the correct peptide-bound PEG as well as a possible DTT-PEG byproduct or still unaltered acrylamide PEG. To improve the purity and overall quality of the linker constructs in future studies, on-resin peptide modification during peptide synthesis could prove highly advantageous. Accordingly, Sutherland *et al.* demonstrated a modification procedure using vinyl sulfonamides as thiol acceptors after selectively removing the Mmt (monomethoxytrityl) protective group of cysteine's side chain [163]. As Sinha *et al.* before, they also addressed the superior water stability of tertiary vinyl sulfonamides as an additional asset to this alkene regarding the Michael addition [164].

Aside from the peptide preparation, a potential steric hindrance or shielding effect by the comparably large PEG chain of 10 kDa, blocking the active site of the transglutaminase or preventing an optimal alignment, must be considered [165]. To our knowledge, a maximum of 5 kDa side chains in a coordinated multi-arm reagent was the largest PEG molecule used in an FXIIIa-related coupling [53]. Higher ionic strength to disrupt intramolecular interactions, more diluted reaction conditions, as well as increased incubation time, may help to improve poor conjugation with high molecular weight polymers.

To assess and gain detailed insight into the conjugation process of the factor XIIIa reaction, additional model peptides were synthesized, isolating the substrate-specific amino acids sequences and their conjugated product as well as the expected spectrum of byproducts for clear identification (***Figure 6.2.11***). Since there is only limited information about efficient substrate deployment and affinity rates, a reaction monitoring protocol was established to prospectively enable a comprehensive comparison among varying peptide candidates. The results of this model are shown in ***Figure 6.2.12,*** clearly illustrating the robustness of the assessment. The studied peptides showed an 80 % conversion when deployed at equal concentrations, exposing well beyond 90 % consumption when the concentration of one peptide was doubled, while an approximate fivefold molar excess marked the maximal conversion rate regarding the opposing substrate. Although in all scenarios the monitored

deamidation of the GDP was unincisive, Sivadó *et al.* suggest that it cannot be prevented completely, even under most optimal reaction conditions, comprising excessive acyl acceptor (lysine donor) substrate and high pH [166]. Furthermore, due to the isopeptidase activity of factor XIIIa, prolonged incubation may facilitate the hydrolyzation of the crosslinked product [167]. In this study, no such reaction was noticeable in the monitored time frame of up to 160 minutes. However, the incubation can readily be terminated after about an hour as the conjugation was reliably completed within 60 minutes at varying concentrations.

While several studies investigate glutamine donor site substrate properties, only a few tried to find patterns for high-affinity lysine donors [47, 48, 58, 118, 168-171]. Although factor XIIIa accepts substrates as simple as NH_4Cl [169], it was shown that most lysine sites exhibit no affinity at all (***Scheme 9***) [114]. More detailed information about effective lysine donor structures could greatly facilitate the use of this transglutaminase as a bioconjugation method.

In sum, the presented series of factor XIIIa-mediated reactions can conceivably serve as a platform to test potential substrate applicants and find their most efficient use conditions.

The successful incorporation of azide entities featuring Plk-eGFP was successfully demonstrated with biotin as a small molecule featuring the CuAAC reaction (***Figure 6.2.13***). Unsurprisingly, this archetype still represents the most prevalent technique among the entire click chemistry repertoire [172]. However, despite the high specificity, non-specific interactions are detectable due to the presence of the copper catalyst. The reaction and its application are further discussed in the following surface-modification-focused part of this work.

One of the strongest assets of site-specific modification and conjugation strategies is the paramount utility they bring to the field of surface functionalization. In this work, a variety of surfaces has been used to demonstrate different functionalization approaches. Depending on which type of surface is to be modified, several steps are needed to be performed to reach the desired level of functionalization. A variety of metals exposing stable oxide layers can undergo condensation reactions to form stable bonds with molecules like siloxanes or phosphonic acid derivates to serve as intermediary linkers. Within this work this trait was

shown with cobalt and nickel as ferromagnetic materials, to prevent or reduce aggregation and unwanted protein attachment (***Figure 6.3.3***). Identical approaches are utilized for metals like titanium, which can instead gain biological features when used as orthopedic or dental implants with pharmaceutically active agents attached to them [173-175]. However, the quality of these oxide films can vary strongly since their controlled formation is a delicate process [176]. Unfortunately, the deployed nickel-based nanowires were exposed to an aqueous ferric chloride solution during the template release treatment (Chapter 5.2.3.1) in a non-standardized fashion, which resulted in vastly different properties regarding their qualification for successive functionalization, given that uncontrolled growth of antiferromagnetic NiO rendered the cleaning procedure by magnetic tethering impossible or even caused nanowires to disintegrate (see Chapter 6.3.1.1). Just recently, Wang *et al.* corroborated this observation, stating that the nickel interface generated by electrochemical fabrication processes is prone to corrosion [177]. To improve the outcome of the surface coating a dipodal silane was added, as they allow for an increased crosslink density and hydrolysis resistance (***Figure 6.3.4***) [178]. Unfortunately, there was no notable or consistent improvement in the overall coating quality. It was hypothesized that the irregularities caused by the release procedure prevented a steady result. Nevertheless, silanization of Co and Ni nanowire segments with successive PEGylation or dye detection was successfully conducted in several experiments (***Figure 6.3.3*** and ***Figure 6.3.4***).

Furthermore, the ability of sulfur compounds to form well-structured self-assembled layers on noble metals like gold was exploited to functionalize nanowires and particles alike. It is up to current debate whether or not the thiol gold bond is of a covalent character or not [179, 180]. Irrespective of binding strength, DNA strands modified with terminal thiols were successfully bound in a free-to-rotate state as well as a rigidly attached formation by adding a second sulfur group to the opposing strand (***Figure 6.3.2***). More complex structured molecules with a tightly spaced sulfur group or shorter alkane chains take more time to be adsorbed to the gold surface than lengthier alkanethiols [91]. Despite having an unbranched alkane sequence, AUT was incubated for up to 18 h to develop a uniform monolayer due to its amino end groups, which were used to make ensuing freely selectable functionalization possible. Efficient AUT attachment was visualized by FITC coupling. Moreover, beads and nanowires were functionalized with enoxaparin via the AUT linker, and the successful conjunction was demonstrated with fluorescein-labeled protamine (***Figure 6.3.1***). In turn, Torun *et al.* used the enoxaparin-loaded particles in surveying the binding characteristics

between FGF-2 and low molecular weight heparin by AFM-assisted single molecule analysis [128].

Both priming surface modification strategies, namely silanization and sulfur adsorption, were successfully combined (***Figure 6.3.4***), giving inspiration for other potential multisegment surface functionalizations.

Due to the unsteady performance of the deployed nanowires, magnetic polystyrene beads with amino end groups were used for the succeeding surface conjugation experiments.

To attach Plk-eGFP to the particle surface, the amino groups had to be converted into azides. For this reason, the diazo-transfer reagent imidazole-1-sulfonyl azide hydrochloride was synthesized and characterized (***Figure 6.3.5***). The successful transformation was monitored via TLC (***Figure 6.3.6***).

The reaction itself along with several control experiments revealed the strengths and potential weaknesses of the CuAAC strategy. Separately, unmodified beads and azide-converted beads were incubated with 5-FAM alkyne, WT-eGFP, or Plk-eGFP including or omitting the copper catalyst, respectively (***Figure 6.3.7***).

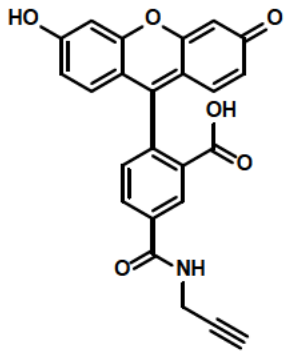

Scheme 10 **Structural formula of 5-FAM alkyne**

While the fluorescent dye showed no unspecific reaction, some diffuse signals were visible when alkyne-free WT-eGFP was incubated with copper and azide beads. On the other hand, the Cu-catalyzed incubation of PLK-eGFP and unmodified amino beads resulted in a weak but uniform signal. Reactive oxygen species (ROS) induced by copper and ascorbate as the initial reducing agent, are well-known causes for undesired side reactions resulting in unspecific outcomes as well as cytotoxic effects [181, 182]. Also, diynes can be formed as

by-products from Cu(I) catalyzed oxidative coupling of terminal alkynes [183]. Typically, histidine and arginine are prone to be attacked by these reactive compounds. This helps to explain why 5-FAM, being a small molecule with no susceptible functionalities (***Scheme 10***), does not expose visible side reactions. To effectively diminish these oxidizing effects in biomolecule-involved environments, THPTA is commonly used [184]. Moreover, it has been reported, that betaine as a nontoxic zwitterionic ligand can additionally improve the general result as its supplementation allows to reduce the necessary copper concentration even further [185]. Apart from that, it is known that non-specific reactivity can occur in a buffer with an excessive amount of alkyne reagents [186, 187]. This might explain the weak but uniform signal when Plk-eGFP was used with NH_2-beads. Since all of these unwanted side reactions are Cu(I) related, copper-free, strain-promoted azide-alkyne cycloaddition (SPAAC) appears to be the superior technique, as it circumvents most of the addressed issues. However, off-target azide-independent reactions between cyclooctynes and thiol groups in proteins are its major drawback [188-190]. Albeit the rate of this thiol-yne reaction is limited and can be observed in copper-catalyzed click chemistry, too, the extent of this undesirable interaction is significantly higher in SPAAC [63, 191]. While Zhong *et al.* completely prevented the thiol interference with hydrogen peroxide treatment in their CuAAC studies, this proceeding may not be applicable in every environment [192].

The decoration of NH_2-beads with TG-eGFP was successfully achieved via factor XIIIa (**Figure *6.3.8***), showcasing its potential use in surface modification tasks. Strictly speaking, the reaction is not completely site-directed in a bidirectional sense since the acceptance of the amino functionality is primarily governed by its structural environment and steric accessibility. However, as mentioned before the specificity is perfectly adequate in controlled bioconjugation strategies, illustrated by the multiple highlighted unreactive lysine residues of eGFP in ***Scheme 9***, leaving only the introduced lysine residue as conjugation competent substrate. Furthermore, as a naturally occurring reaction, it provides physiological reaction conditions making it a powerful tool for potential cell surface protein labeling or any conjugation projects that involves sensible biomolecules. Amine-presenting polymer-based applications could benefit immensely from this approach [193], while Yu *et al.* presented another implementation of this concept with microbial transglutaminase [80].

In summary, this work presented two biorthogonal modification strategies in a variety of possible use cases, elucidating their individual strengths and limitations. While there are promising new developments like the application of conformationally strained trans-cyclooctene as a new click chemistry [194] or the evolution of the sortase A enzyme [195], there is no universal technique to provide optimal ligation in every project design.

Consequently, this thesis encourages further elaboration on the specific challenges of the featured bioorthogonal functionalization strategies in order to expand their fields of application.

8 References

1. Renault, K., J.W. Fredy, P.Y. Renard and C. Sabot, *Covalent Modification of Biomolecules through Maleimide-Based Labeling Strategies.* Bioconjug Chem, 2018. **29**(8): p. 2497-2513.
2. Keeble, A.H., A. Banerjee, M.P. Ferla, S.C. Reddington, I. Anuar and M. Howarth, *Evolving Accelerated Amidation by SpyTag/SpyCatcher to Analyze Membrane Dynamics.* Angew Chem Int Ed Engl, 2017. **56**(52): p. 16521-16525.
3. Duckworth, B.P., J. Xu, T.A. Taton, A. Guo and M.D. Distefano, *Site-specific, covalent attachment of proteins to a solid surface.* Bioconjug Chem, 2006. **17**(4): p. 967-74.
4. Li, F. and R.I. Mahato, *Bioconjugate Therapeutics: Current Progress and Future Perspective.* Mol Pharm, 2017. **14**(5): p. 1321-1324.
5. Sevim, S., S. Ozer, L. Feng, J. Wurzel, A. Fakhraee, N. Shamsudhin, B. Jang, C. Alcantara*, et al.*, *Dually actuated atomic force microscope with miniaturized magnetic bead-actuators for single-molecule force measurements.* Nanoscale Horiz, 2016. **1**(6): p. 488-495.
6. Baumann, A.L. and C.P.R. Hackenberger, *Modern Ligation Methods to Access Natural and Modified Proteins.* Chimia (Aarau), 2018. **72**(11): p. 802-808.
7. Agarwal, P. and C.R. Bertozzi, *Site-specific antibody-drug conjugates: the nexus of bioorthogonal chemistry, protein engineering, and drug development.* Bioconjug Chem, 2015. **26**(2): p. 176-92.
8. Sakamoto, T., S. Sawamoto, T. Tanaka, H. Fukuda and A. Kondo, *Enzyme-mediated site-specific antibody-protein modification using a ZZ domain as a linker.* Bioconjug Chem, 2010. **21**(12): p. 2227-33.
9. Kolb, H.C., M.G. Finn and K.B. Sharpless, *Click Chemistry: Diverse Chemical Function from a Few Good Reactions.* Angewandte Chemie International Edition, 2001. **40**(11): p. 2004-2021.
10. Mao, H., S.A. Hart, A. Schink and B.A. Pollok, *Sortase-mediated protein ligation: a new method for protein engineering.* J Am Chem Soc, 2004. **126**(9): p. 2670-1.
11. Theile, C.S., M.D. Witte, A.E. Blom, L. Kundrat, H.L. Ploegh and C.P. Guimaraes, *Site-specific N-terminal labeling of proteins using sortase-mediated reactions.* Nat Protoc, 2013. **8**(9): p. 1800-7.
12. Tanaka, T., N. Kamiya and T. Nagamune, *N-terminal glycine-specific protein conjugation catalyzed by microbial transglutaminase.* FEBS Lett, 2005. **579**(10): p. 2092-6.
13. Strop, P., *Versatility of microbial transglutaminase.* Bioconjug Chem, 2014. **25**(5): p. 855-62.
14. Mootz, H.D., *Split inteins as versatile tools for protein semisynthesis.* Chembiochem, 2009. **10**(16): p. 2579-89.
15. Ludwig, C., D. Schwarzer, J. Zettler, D. Garbe, P. Janning, C. Czeslik and H.D. Mootz, *Semisynthesis of proteins using split inteins.* Methods in enzymology, 2009. **462**: p. 77-96.
16. Paulus, H., *Inteins as enzymes.* Bioorg Chem, 2001. **29**(3): p. 119-29.
17. Chang, T.K., D.Y. Jackson, J.P. Burnier and J.A. Wells, *Subtiligase: a tool for semisynthesis of proteins.* Proc Natl Acad Sci U S A, 1994. **91**(26): p. 12544-8.
18. Weeks, A.M. and J.A. Wells, *Subtiligase-Catalyzed Peptide Ligation.* Chem Rev, 2020. **120**(6): p. 3127-3160.

19. Hemu, X., X. Zhang, X. Bi, C.F. Liu and J.P. Tam, *Butelase 1-Mediated Ligation of Peptides and Proteins.* Methods Mol Biol, 2019. **2012**: p. 83-109.
20. Nguyen, G.K., Y. Cao, W. Wang, C.F. Liu and J.P. Tam, *Site-Specific N-Terminal Labeling of Peptides and Proteins using Butelase 1 and Thiodepsipeptide.* Angew Chem Int Ed Engl, 2015. **54**(52): p. 15694-8.
21. Cao, Y., G.K. Nguyen, J.P. Tam and C.F. Liu, *Butelase-mediated synthesis of protein thioesters and its application for tandem chemoenzymatic ligation.* Chem Commun (Camb), 2015. **51**(97): p. 17289-92.
22. Nguyen, U.T., J. Cramer, J. Gomis, R. Reents, M. Gutierrez-Rodriguez, R.S. Goody, K. Alexandrov and H. Waldmann, *Exploiting the substrate tolerance of farnesyltransferase for site-selective protein derivatization.* Chembiochem, 2007. **8**(4): p. 408-23.
23. Grunewald, J., A. Brock and B.H. Geierstanger, *Site-Specific Antibody Labeling Using Phosphopantetheinyl Transferase-Catalyzed Ligation.* Methods Mol Biol, 2019. **2012**: p. 237-278.
24. Appel, M.J. and C.R. Bertozzi, *Formylglycine, a post-translationally generated residue with unique catalytic capabilities and biotechnology applications.* ACS Chem Biol, 2015. **10**(1): p. 72-84.
25. Agarwal, P., R. Kudirka, A.E. Albers, R.M. Barfield, G.W. de Hart, P.M. Drake, L.C. Jones and D. Rabuka, *Hydrazino-Pictet-Spengler ligation as a biocompatible method for the generation of stable protein conjugates.* Bioconjug Chem, 2013. **24**(6): p. 846-51.
26. Gerlach, M., T. Stoschek, H. Leonhardt, C.P.R. Hackenberger, D. Schumacher and J. Helma, *Tubulin Tyrosine Ligase-Mediated Modification of Proteins.* Methods Mol Biol, 2019. **2012**: p. 327-355.
27. Schumacher, D., J. Helma, F.A. Mann, G. Pichler, F. Natale, E. Krause, M.C. Cardoso, C.P. Hackenberger*, et al.*, *Versatile and Efficient Site-Specific Protein Functionalization by Tubulin Tyrosine Ligase.* Angew Chem Int Ed Engl, 2015. **54**(46): p. 13787-91.
28. Zhou, S., S. Cao, G. Ma, T. Ding, J. Mu, W. Han, D. Sun and C. Chen, *Recombinant streptavidin fusion proteins as signal reporters in rapid test of human hepatitis C virus infection.* J Clin Lab Anal, 2019. **33**(3): p. e22701.
29. Gu, G.J., M. Friedman, C. Jost, K. Johnsson, M. Kamali-Moghaddam, A. Pluckthun, U. Landegren and O. Soderberg, *Protein tag-mediated conjugation of oligonucleotides to recombinant affinity binders for proximity ligation.* N Biotechnol, 2013. **30**(2): p. 144-52.
30. Wollschlaeger, C., I. Meinhold-Heerlein, X. Cong, K. Brautigam, S. Di Fiore, F. Zeppernick, T. Klockenbring, E. Stickeler*, et al.*, *Simultaneous and Independent Dual Site-Specific Self-Labeling of Recombinant Antibodies.* Bioconjug Chem, 2018. **29**(11): p. 3586-3594.
31. England, C.G., H. Luo and W. Cai, *HaloTag technology: a versatile platform for biomedical applications.* Bioconjug Chem, 2015. **26**(6): p. 975-86.
32. Fischer, M.J., *Amine coupling through EDC/NHS: a practical approach.* Methods Mol Biol, 2010. **627**: p. 55-73.
33. Xu, M.Q. and T.C. Evans, Jr., *Intein-mediated ligation and cyclization of expressed proteins.* Methods, 2001. **24**(3): p. 257-77.
34. Petri, L., P.A. Szijj, Á. Kelemen, T. Imre, Á. Gömöry, M.T.W. Lee, K. Hegedűs, P. Ábrányi-Balogh*, et al.*, *Cysteine specific bioconjugation with benzyl isothiocyanates.* RSC Advances, 2020. **10**(25): p. 14928-14936.

35. Nair, D.P., M. Podgórski, S. Chatani, T. Gong, W. Xi, C.R. Fenoli and C.N. Bowman, *The Thiol-Michael Addition Click Reaction: A Powerful and Widely Used Tool in Materials Chemistry.* Chemistry of Materials, 2013. **26**(1): p. 724-744.
36. Lallana, E., R. Riguera and E. Fernandez-Megia, *Reliable and efficient procedures for the conjugation of biomolecules through Huisgen azide-alkyne cycloadditions.* Angew Chem Int Ed Engl, 2011. **50**(38): p. 8794-804.
37. Palomo, J.M., *Diels–Alder Cycloaddition in Protein Chemistry.* European Journal of Organic Chemistry, 2010. **2010**(33): p. 6303-6314.
38. Pozsgay, V., N.E. Vieira and A. Yergey, *A method for bioconjugation of carbohydrates using Diels-Alder cycloaddition.* Org Lett, 2002. **4**(19): p. 3191-4.
39. St. Amant, A.H., F. Huang, J. Lin, K. Rickert, V. Oganesyan, D. Lemen, S. Mao, J. Harper*, et al.*, *A Diene-Containing Noncanonical Amino Acid Enables Dual Functionality in Proteins: Rapid Diels–Alder Reaction with Maleimide or Proximity-Based Dimerization.* Angewandte Chemie, 2019.
40. Tam, A. and R.T. Raines, *Protein engineering with the traceless Staudinger ligation.* Methods in enzymology, 2009. **462**: p. 25-44.
41. Kiick, K.L., E. Saxon, D.A. Tirrell and C.R. Bertozzi, *Incorporation of azides into recombinant proteins for chemoselective modification by the Staudinger ligation.* Proc Natl Acad Sci U S A, 2002. **99**(1): p. 19-24.
42. Tsao, M.L., F. Tian and P.G. Schultz, *Selective Staudinger modification of proteins containing p-azidophenylalanine.* Chembiochem, 2005. **6**(12): p. 2147-9.
43. Shih, H., A.K. Fraser and C.C. Lin, *Interfacial thiol-ene photoclick reactions for forming multilayer hydrogels.* ACS Appl Mater Interfaces, 2013. **5**(5): p. 1673-80.
44. Grim, J.C., I.A. Marozas and K.S. Anseth, *Thiol-ene and photo-cleavage chemistry for controlled presentation of biomolecules in hydrogels.* J Control Release, 2015. **219**: p. 95-106.
45. Richardson, V.R., P. Cordell, K.F. Standeven and A.M. Carter, *Substrates of Factor XIII-A: roles in thrombosis and wound healing.* Clin Sci (Lond), 2013. **124**(3): p. 123-37.
46. de Góes-Favoni, S.P. and F.R. Bueno, *Microbial Transglutaminase: General Characteristics and Performance in Food Processing Technology.* Food Biotechnology, 2014. **28**(1): p. 1-24.
47. Hu, B.H. and P.B. Messersmith, *Rational design of transglutaminase substrate peptides for rapid enzymatic formation of hydrogels.* J Am Chem Soc, 2003. **125**(47): p. 14298-9.
48. Gorman, J.J. and J.E. Folk, *Structural features of glutamine substrates for transglutaminases. Specificities of human plasma factor XIIIa and the guinea pig liver enzyme toward synthetic peptides.* J Biol Chem, 1981. **256**(6): p. 2712-5.
49. Ando, H., M. Adachi, K. Umeda, A. Matsuura, M. Nonaka, R. Uchio, H. Tanaka and M. Motoki, *Purification and Characteristics of a Novel Transglutaminase Derived from Microorganisms.* Agricultural and Biological Chemistry, 2014. **53**(10): p. 2613-2617.
50. Torsten, M. and L. Aaron, *Microbial Transglutaminase Is Immunogenic and Potentially Pathogenic in Pediatric Celiac Disease.* Front Pediatr, 2018. **6**: p. 389.
51. Sjober, K., S. Eriksson, B. Tenngart, E.B. Roth, H. Leffler and P. Stenberg, *Factor XIII and tissue transglutaminase antibodies in coeliac and inflammatory bowel disease.* Autoimmunity, 2002. **35**(5): p. 357-64.
52. Ehrbar, M., S.C. Rizzi, R. Hlushchuk, V. Djonov, A.H. Zisch, J.A. Hubbell, F.E. Weber and M.P. Lutolf, *Enzymatic formation of modular cell-instructive fibrin analogs for tissue engineering.* Biomaterials, 2007. **28**(26): p. 3856-66.

53. Ehrbar, M., S.C. Rizzi, R.G. Schoenmakers, B.S. Miguel, J.A. Hubbell, F.E. Weber and M.P. Lutolf, *Biomolecular hydrogels formed and degraded via site-specific enzymatic reactions.* Biomacromolecules, 2007. **8**(10): p. 3000-7.
54. Muszbek, L., Z. Bereczky, Z. Bagoly, I. Komaromi and E. Katona, *Factor XIII: a coagulation factor with multiple plasmatic and cellular functions.* Physiol Rev, 2011. **91**(3): p. 931-72.
55. Pedersen, L.C., V.C. Yee, P.D. Bishop, I. Le Trong, D.C. Teller and R.E. Stenkamp, *Transglutaminase factor XIII uses proteinase-like catalytic triad to crosslink macromolecules.* Protein Sci, 1994. **3**(7): p. 1131-5.
56. Nikolajsen, C.L., T.F. Dyrlund, E.T. Poulsen, J.J. Enghild and C. Scavenius, *Coagulation factor XIIIa substrates in human plasma: identification and incorporation into the clot.* J Biol Chem, 2014. **289**(10): p. 6526-34.
57. Penzes, K., K.E. Kover, F. Fazakas, G. Haramura and L. Muszbek, *Molecular mechanism of the interaction between activated factor XIII and its glutamine donor peptide substrate.* J Thromb Haemost, 2009. **7**(4): p. 627-33.
58. Cleary, D.B. and M.C. Maurer, *Characterizing the specificity of activated Factor XIII for glutamine-containing substrate peptides.* Biochim Biophys Acta, 2006. **1764**(7): p. 1207-17.
59. Breugst, M. and H.U. Reissig, *The Huisgen Reaction: Milestones of the 1,3-Dipolar Cycloaddition.* Angew Chem Int Ed Engl, 2020. **59**(30): p. 12293-12307.
60. Li, L. and Z. Zhang, *Development and Applications of the Copper-Catalyzed Azide-Alkyne Cycloaddition (CuAAC) as a Bioorthogonal Reaction.* Molecules, 2016. **21**(10).
61. Besanceney-Webler, C., H. Jiang, T. Zheng, L. Feng, D. Soriano del Amo, W. Wang, L.M. Klivansky, F.L. Marlow*, et al.*, *Increasing the efficacy of bioorthogonal click reactions for bioconjugation: a comparative study.* Angew Chem Int Ed Engl, 2011. **50**(35): p. 8051-6.
62. Hamlin, T.A., B.J. Levandowski, A.K. Narsaria, K.N. Houk and F.M. Bickelhaupt, *Structural Distortion of Cycloalkynes Influences Cycloaddition Rates both by Strain and Interaction Energies.* Chemistry, 2019. **25**(25): p. 6342-6348.
63. Li, S., H. Zhu, J. Wang, X. Wang, X. Li, C. Ma, L. Wen, B. Yu*, et al.*, *Comparative analysis of Cu (I)-catalyzed alkyne-azide cycloaddition (CuAAC) and strain-promoted alkyne-azide cycloaddition (SPAAC) in O-GlcNAc proteomics.* Electrophoresis, 2016. **37**(11): p. 1431-6.
64. Kele, P., G. Mezo, D. Achatz and O.S. Wolfbeis, *Dual labeling of biomolecules by using click chemistry: a sequential approach.* Angew Chem Int Ed Engl, 2009. **48**(2): p. 344-7.
65. Khan, I. and M. Waheed Akhtar, *Different Approaches For Protein Engineering In Industrial Biotechnology.* Nature Precedings, 2011.
66. Smith, S.N., Y. Wang, J.L. Baylon, N.K. Singh, B.M. Baker, E. Tajkhorshid and D.M. Kranz, *Changing the peptide specificity of a human T-cell receptor by directed evolution.* Nat Commun, 2014. **5**: p. 5223.
67. Ren, C., X. Wen, J. Mencius and S. Quan, *Selection and screening strategies in directed evolution to improve protein stability.* Bioresources and Bioprocessing, 2019. **6**(1).
68. Dhanjal, J.K., V. Malik, N. Radhakrishnan, M. Sigar, A. Kumari and D. Sundar, *Computational Protein Engineering Approaches for Effective Design of New Molecules*, in *Encyclopedia of Bioinformatics and Computational Biology*. 2019, Elsevier. p. 631-643.

69. Shin, J.E., A.J. Riesselman, A.W. Kollasch, C. McMahon, E. Simon, C. Sander, A. Manglik, A.C. Kruse*, et al.*, *Protein design and variant prediction using autoregressive generative models.* Nat Commun, 2021. **12**(1): p. 2403.
70. Zhang, G., V. Gurtu and S.R. Kain, *An enhanced green fluorescent protein allows sensitive detection of gene transfer in mammalian cells.* Biochem Biophys Res Commun, 1996. **227**(3): p. 707-11.
71. Jackson, S.E., T.D. Craggs and J.R. Huang, *Understanding the folding of GFP using biophysical techniques.* Expert Rev Proteomics, 2006. **3**(5): p. 545-59.
72. Nakatani, T., N. Yasui, I. Tamura and A. Yamashita, *Specific modification at the C-terminal lysine residue of the green fluorescent protein variant, GFPuv, expressed in Escherichia coli.* Sci Rep, 2019. **9**(1): p. 4722.
73. Zimmer, M., *Green Fluorescent Protein (GFP): Applications, Structure, and Related Photophysical Behavior.* Chemical Reviews, 2002. **102**(3): p. 759-782.
74. Manandhar, M., E. Chun and F.E. Romesberg, *Genetic Code Expansion: Inception, Development, Commercialization.* J Am Chem Soc, 2021. **143**(13): p. 4859-4878.
75. Eger, S., M. Scheffner, A. Marx and M. Rubini, *Formation of ubiquitin dimers via azide-alkyne click reaction.* Methods Mol Biol, 2012. **832**: p. 589-96.
76. Eger, S., M. Scheffner, A. Marx and M. Rubini, *Synthesis of defined ubiquitin dimers.* J Am Chem Soc, 2010. **132**(46): p. 16337-9.
77. Tharp, J.M., A. Ehnbom and W.R. Liu, *tRNA(Pyl): Structure, function, and applications.* RNA Biol, 2018. **15**(4-5): p. 441-452.
78. Braun, A.C., M. Gutmann, T. Luhmann and L. Meinel, *Bioorthogonal strategies for site-directed decoration of biomaterials with therapeutic proteins.* J Control Release, 2018. **273**: p. 68-85.
79. Lin, P.-C., D. Weinrich and H. Waldmann, *Protein Biochips: Oriented Surface Immobilization of Proteins.* Macromolecular Chemistry and Physics, 2010. **211**(2): p. 136-144.
80. Yu, C.M., H. Zhou, W.F. Zhang, H.M. Yang and J.B. Tang, *Site-specific, covalent immobilization of BirA by microbial transglutaminase: A reusable biocatalyst for in vitro biotinylation.* Anal Biochem, 2016. **511**: p. 10-2.
81. Noor, M., T. Dworeck, A. Schenk, P. Shinde, M. Fioroni and U. Schwaneberg, *Polymersome surface decoration by an EGFP fusion protein employing Cecropin A as peptide "anchor".* J Biotechnol, 2012. **157**(1): p. 31-7.
82. Bobo, D., K.J. Robinson, J. Islam, K.J. Thurecht and S.R. Corrie, *Nanoparticle-Based Medicines: A Review of FDA-Approved Materials and Clinical Trials to Date.* Pharm Res, 2016. **33**(10): p. 2373-87.
83. Trilling, A.K., J. Beekwilder and H. Zuilhof, *Antibody orientation on biosensor surfaces: a minireview.* Analyst, 2013. **138**(6): p. 1619-27.
84. Thiesen, B. and A. Jordan, *Clinical applications of magnetic nanoparticles for hyperthermia.* Int J Hyperthermia, 2008. **24**(6): p. 467-74.
85. Shukla, A., N. Dasgupta, S. Ranjan, S. Singh and R. Chidambram, *Nanotechnology towards prevention of anaemia and osteoporosis: from concept to market.* Biotechnology & Biotechnological Equipment, 2017. **31**(5): p. 863-879.
86. Gupta, A.K. and A.S. Curtis, *Lactoferrin and ceruloplasmin derivatized superparamagnetic iron oxide nanoparticles for targeting cell surface receptors.* Biomaterials, 2004. **25**(15): p. 3029-40.
87. Gupta, A.K. and M. Gupta, *Synthesis and surface engineering of iron oxide nanoparticles for biomedical applications.* Biomaterials, 2005. **26**(18): p. 3995-4021.

88. Shamsudhin, N., Y. Tao, J. Sort, B. Jang, C.L. Degen, B.J. Nelson and S. Pane, *Magnetometry of Individual Polycrystalline Ferromagnetic Nanowires.* Small, 2016. **12**(46): p. 6363-6369.
89. Ramulu, T.S., R. Venu, B. Sinha, S.S. Yoon and C.G. Kim, *Electrodeposition of CoPtP/Au Multisegment Nanowires: Synthesis and DNA Functionalization.* International Journal of Electrochemical Science, 2012. **7**(9): p. 7762-7769.
90. Anguelouch, A., R.L. Leheny and D.H. Reich, *Application of ferromagnetic nanowires to interfacial microrheology.* Applied Physics Letters, 2006. **89**(11).
91. Vericat, C., M.E. Vela, G. Benitez, P. Carro and R.C. Salvarezza, *Self-assembled monolayers of thiols and dithiols on gold: new challenges for a well-known system.* Chem Soc Rev, 2010. **39**(5): p. 1805-34.
92. Wildt, B., P. Mali and P.C. Searson, *Electrochemical template synthesis of multisegment nanowires: fabrication and protein functionalization.* Langmuir, 2006. **22**(25): p. 10528-34.
93. Beck, A., L. Goetsch, C. Dumontet and N. Corvaïa, *Strategies and challenges for the next generation of antibody–drug conjugates.* Nature Reviews Drug Discovery, 2017. **16**(5): p. 315-337.
94. Kibbe, W.A., *OligoCalc: an online oligonucleotide properties calculator.* Nucleic Acids Res, 2007. **35**(Web Server issue): p. W43-6.
95. Cranenburgh, R.M., *An equation for calculating the volumetric ratios required in a ligation reaction.* Appl Microbiol Biotechnol, 2004. **65**(2): p. 200-2.
96. He, F., *Laemmli-SDS-PAGE.* Bio-Protocol, 2011. **1**(11).
97. Neuhoff, V., N. Arold, D. Taube and W. Ehrhardt, *Improved staining of proteins in polyacrylamide gels including isoelectric focusing gels with clear background at nanogram sensitivity using Coomassie Brilliant Blue G-250 and R-250.* Electrophoresis, 1988. **9**(6): p. 255-62.
98. Tsien, R.Y., *The green fluorescent protein.* Annu Rev Biochem, 1998. **67**: p. 509-44.
99. Jang, B., E. Pellicer, M. Guerrero, X. Chen, H. Choi, B.J. Nelson, J. Sort and S. Pane, *Fabrication of segmented Au/Co/Au nanowires: insights in the quality of Co/Au junctions.* ACS Appl Mater Interfaces, 2014. **6**(16): p. 14583-9.
100. S, I., M. K and K. S, *Fabrication and Magnetoresistance of Single Au-Ni-Au Nanowire.* International Journal of Nano Studies & Technology, 2014: p. 45-49.
101. B., A., *Silane Coupling Agents: Connecting Across Boundaries (Version 3.0)*. 2014: Gelest.
102. McCarthy, S.A., G.L. Davies and Y.K. Gun'ko, *Preparation of multifunctional nanoparticles and their assemblies.* Nat Protoc, 2012. **7**(9): p. 1677-93.
103. den Dunnen, J.T. and S.E. Antonarakis, *Nomenclature for the description of human sequence variations.* Hum Genet, 2001. **109**(1): p. 121-4.
104. Aronson, D.E., L.M. Costantini and E.L. Snapp, *Superfolder GFP is fluorescent in oxidizing environments when targeted via the Sec translocon.* Traffic, 2011. **12**(5): p. 543-8.
105. Zacharias, D.A., J.D. Violin, A.C. Newton and R.Y. Tsien, *Partitioning of lipid-modified monomeric GFPs into membrane microdomains of live cells.* Science, 2002. **296**(5569): p. 913-6.
106. Hirel, P.H., J.M. Schmitter, P. Dessen, G. Fayat and S. Blanquet, *Extent of N-Terminal Methionine Excision from Escherichia-Coli Proteins Is Governed by the Side-Chain Length of the Penultimate Amino-Acid.* Proceedings of the National Academy of Sciences of the United States of America, 1989. **86**(21): p. 8247-8251.

107. Liao, Y.D., J.C. Jeng, C.F. Wang, S.C. Wang and S.T. Chang, *Removal of N-terminal methionine from recombinant proteins by engineered E. coli methionine aminopeptidase.* Protein Sci, 2004. **13**(7): p. 1802-10.
108. Wang, Y.S., W.K. Russell, Z. Wang, W. Wan, L.E. Dodd, P.J. Pai, D.H. Russell and W.R. Liu, *The de novo engineering of pyrrolysyl-tRNA synthetase for genetic incorporation of L-phenylalanine and its derivatives.* Mol Biosyst, 2011. **7**(3): p. 714-7.
109. Roy, G., J. Reier, A. Garcia, T. Martin, M. Rice, J. Wang, M. Prophet, R. Christie, *et al.*, *Development of a high yielding expression platform for the introduction of non-natural amino acids in protein sequences.* MAbs, 2020. **12**(1): p. 1684749.
110. Nguyen, D.P., H. Lusic, H. Neumann, P.B. Kapadnis, A. Deiters and J.W. Chin, *Genetic encoding and labeling of aliphatic azides and alkynes in recombinant proteins via a pyrrolysyl-tRNA Synthetase/tRNA(CUA) pair and click chemistry.* J Am Chem Soc, 2009. **131**(25): p. 8720-1.
111. Wan, W., J.M. Tharp and W.R. Liu, *Pyrrolysyl-tRNA synthetase: an ordinary enzyme but an outstanding genetic code expansion tool.* Biochim Biophys Acta, 2014. **1844**(6): p. 1059-70.
112. Zane, H.K., J.K. Doh, C.A. Enns and K.E. Beatty, *Versatile Interacting Peptide (VIP) Tags for Labeling Proteins with Bright Chemical Reporters.* Chembiochem, 2017. **18**(5): p. 470-474.
113. Milczek, E.M., *Commercial Applications for Enzyme-Mediated Protein Conjugation: New Developments in Enzymatic Processes to Deliver Functionalized Proteins on the Commercial Scale.* Chem Rev, 2018. **118**(1): p. 119-141.
114. Sobel, J.H. and M.A. Gawinowicz, *Identification of the Alpha Chain Lysine Donor Sites Involved in Factor XIIIa Fibrin Cross-linking.* Journal of Biological Chemistry, 1996. **271**(32): p. 19288-19297.
115. Toda, N., S. Asano and C.F. Barbas, 3rd, *Rapid, stable, chemoselective labeling of thiols with Julia-Kocienski-like reagents: a serum-stable alternative to maleimide-based protein conjugation.* Angew Chem Int Ed Engl, 2013. **52**(48): p. 12592-6.
116. Arnesen, T., *Towards a functional understanding of protein N-terminal acetylation.* PLoS Biol, 2011. **9**(5): p. e1001074.
117. Kim, K.-H. and B.L. Seong, *Peptide amidation: Production of peptide hormonesin vivo andin vitro.* Biotechnology and Bioprocess Engineering, 2001. **6**(4): p. 244-251.
118. Gorman, J.J. and J.E. Folk, *Structural features of glutamine substrates for human plasma factor XIIIa (activated blood coagulation factor XIII).* J Biol Chem, 1980. **255**(2): p. 419-27.
119. Ravasco, J., H. Faustino, A. Trindade and P.M.P. Gois, *Bioconjugation with Maleimides: A Useful Tool for Chemical Biology.* Chemistry, 2019. **25**(1): p. 43-59.
120. Frayne, S.H., *The Thiol-Michael Reaction: From First Principles to Applications in Macromolecular Synthesis*. 2018, Wesleyan University.
121. Purwaha, P., L.P. Silva, D.H. Hawke, J.N. Weinstein and P.L. Lorenzi, *An artifact in LC-MS/MS measurement of glutamine and glutamic acid: in-source cyclization to pyroglutamic acid.* Anal Chem, 2014. **86**(12): p. 5633-7.
122. Spangenberg, B., C.F. Poole and C. Weins, *Quantitative Thin-Layer Chromatography*. 2011.
123. Santos, J.H.P.M., K.M. Torres-Obreque, G.P. Meneguetti, B.P. Amaro and C.O. Rangel-Yagui, *Protein PEGylation for the design of biobetters: from reaction to purification processes.* Brazilian Journal of Pharmaceutical Sciences, 2018. **54**(spe).

124. Cleland, W.W., *The kinetics of enzyme-catalyzed reactions with two or more substrates or products.* Biochimica et Biophysica Acta (BBA) - Specialized Section on Enzymological Subjects, 1963. **67**: p. 188-196.
125. Presolski, S.I., V. Hong, S.H. Cho and M.G. Finn, *Tailored ligand acceleration of the Cu-catalyzed azide-alkyne cycloaddition reaction: practical and mechanistic implications.* J Am Chem Soc, 2010. **132**(41): p. 14570-6.
126. Solanki, P.R., S.K. Arya, Y. Nishimura, M. Iwamoto and B.D. Malhotra, *Cholesterol biosensor based on amino-undecanethiol self-assembled monolayer using surface plasmon resonance technique.* Langmuir, 2007. **23**(13): p. 7398-403.
127. Hakkinen, H., *The gold-sulfur interface at the nanoscale.* Nat Chem, 2012. **4**(6): p. 443-55.
128. Sevim, S., S. Ozer, G. Jones, J. Wurzel, L. Feng, A. Fakhraee, N. Shamsudhin, O. Ergeneman*, et al.*, *Nanomechanics on FGF-2 and Heparin Reveal Slip Bond Characteristics with pH Dependency.* ACS Biomater Sci Eng, 2017. **3**(6): p. 1000-1007.
129. Hang, T., A. Hu, H. Ling, M. Li and D. Mao, *Super-hydrophobic nickel films with micro-nano hierarchical structure prepared by electrodeposition.* Applied Surface Science, 2010. **256**(8): p. 2400-2404.
130. Khorsand, S., K. Raeissi, F. Ashrafizadeh and M.A. Arenas, *Super-hydrophobic nickel–cobalt alloy coating with micro-nano flower-like structure.* Chemical Engineering Journal, 2015. **273**: p. 638-646.
131. Xu, M., L. Shen, W. Jiang, M. Qiu and Z. Tian, *Study on the properties of superhydrophobic nickel coating prepared by jet electrodeposition in a parallel magnetic field.* Materials Research Express, 2019. **6**(8).
132. Qian, X., T. Tang, H. Wang, C. Chen, J. Luo and D. Luo, *Fabrication of Hydrophobic Ni Surface by Chemical Etching.* Materials (Basel), 2019. **12**(21).
133. Ritzefeld, M., V. Walhorn, D. Anselmetti and N. Sewald, *Analysis of DNA interactions using single-molecule force spectroscopy.* Amino Acids, 2013. **44**(6): p. 1457-75.
134. Almaqwashi, A.A., T. Paramanathan, I. Rouzina and M.C. Williams, *Mechanisms of small molecule-DNA interactions probed by single-molecule force spectroscopy.* Nucleic Acids Res, 2016. **44**(9): p. 3971-88.
135. Goddard-Borger, E.D. and R.V. Stick, *An efficient, inexpensive, and shelf-stable diazotransfer reagent: imidazole-1-sulfonyl azide hydrochloride.* Org Lett, 2007. **9**(19): p. 3797-800.
136. Lee, S.R., *Critical Role of Zinc as Either an Antioxidant or a Prooxidant in Cellular Systems.* Oxid Med Cell Longev, 2018. **2018**: p. 9156285.
137. Nyffeler, P.T., C.H. Liang, K.M. Koeller and C.H. Wong, *The chemistry of amine-azide interconversion: catalytic diazotransfer and regioselective azide reduction.* J Am Chem Soc, 2002. **124**(36): p. 10773-8.
138. Rakshit, A., K. Khatua, V. Shanbhag, P. Comba and A. Datta, *Cu(2+) selective chelators relieve copper-induced oxidative stress in vivo.* Chem Sci, 2018. **9**(41): p. 7916-7930.
139. Saunders, A.J., G.B. Young and G.J. Pielak, *Polarity of disulfide bonds.* Protein Sci, 1993. **2**(7): p. 1183-4.
140. Tanimoto, H. and K. Kakiuchi, *Recent Applications and Developments of Organic Azides in Total Synthesis of Natural Products.* ChemInform, 2013. **44**(49): p. no-no.
141. Heim, R. and R.Y. Tsien, *Engineering green fluorescent protein for improved brightness, longer wavelengths and fluorescence resonance energy transfer.* Current Biology, 1996. **6**(2): p. 178-182.

142. LaVallie, E.R. and J.M. McCoy, *Gene fusion expression systems in Escherichia coli.* Current Opinion in Biotechnology, 1995. **6**(5): p. 501-506.
143. Baneyx, F., *Recombinant protein expression in Escherichia coli.* Current Opinion in Biotechnology, 1999. **10**(5): p. 411-421.
144. Rosano, G.L. and E.A. Ceccarelli, *Recombinant protein expression in Escherichia coli: advances and challenges.* Front Microbiol, 2014. **5**: p. 172.
145. Mierendorf, R.C.M., B. B.; Hammer, B.; Novy, R. E., *Expression and Purification of Recombinant Proteins Using the pET System*, in *Molecular Diagnosis of Infectious Diseases*, U. Reischl, Editor. 1998.
146. QIAGEN, *The QIAexpressionist™*, in *A handbook for high-level expression and purification of 6xHis-tagged proteins*. 2003.
147. Stancik, L.M., D.M. Stancik, B. Schmidt, D.M. Barnhart, Y.N. Yoncheva and J.L. Slonczewski, *pH-dependent expression of periplasmic proteins and amino acid catabolism in Escherichia coli.* J Bacteriol, 2002. **184**(15): p. 4246-58.
148. Anderson, J.C., N. Wu, S.W. Santoro, V. Lakshman, D.S. King and P.G. Schultz, *An expanded genetic code with a functional quadruplet codon.* Proc Natl Acad Sci U S A, 2004. **101**(20): p. 7566-71.
149. Rodriguez, E.A., H.A. Lester and D.A. Dougherty, *In vivo incorporation of multiple unnatural amino acids through nonsense and frameshift suppression.* Proc Natl Acad Sci U S A, 2006. **103**(23): p. 8650-5.
150. Nakamura, Y., T. Gojobori and T. Ikemura, *Codon usage tabulated from international DNA sequence databases: status for the year 2000.* Nucleic Acids Res, 2000. **28**(1): p. 292.
151. Routledge, S.J., C.J. Hewitt, N. Bora and R.M. Bill, *Antifoam addition to shake flask cultures of recombinant Pichia pastoris increases yield.* Microb Cell Fact, 2011. **10**: p. 17.
152. Verma, M., J. Choi, K.A. Cottrell, Z. Lavagnino, E.N. Thomas, S. Pavlovic-Djuranovic, P. Szczesny, D.W. Piston*, et al.*, *A short translational ramp determines the efficiency of protein synthesis.* Nat Commun, 2019. **10**(1): p. 5774.
153. Chatterjee, A., S.B. Sun, J.L. Furman, H. Xiao and P.G. Schultz, *A versatile platform for single- and multiple-unnatural amino acid mutagenesis in Escherichia coli.* Biochemistry, 2013. **52**(10): p. 1828-37.
154. Chatani, S., D.P. Nair and C.N. Bowman, *Relative reactivity and selectivity of vinyl sulfones and acrylates towards the thiol–Michael addition reaction and polymerization.* Polym. Chem., 2013. **4**(4): p. 1048-1055.
155. Long, K.F., H. Wang, T.T. Dimos and C.N. Bowman, *Effects of Thiol Substitution on the Kinetics and Efficiency of Thiol-Michael Reactions and Polymerizations.* Macromolecules, 2021. **54**(7): p. 3093-3100.
156. Gennari, A., J. Wedgwood, E. Lallana, N. Francini and N. Tirelli, *Thiol-based michael-type addition. A systematic evaluation of its controlling factors.* Tetrahedron, 2020. **76**(47).
157. Hermanson, G.T., *Bioconjugate Techniques*. 3 ed. 2013: Academic Press.
158. Zheng, C., G. Ma and Z. Su, *Native PAGE eliminates the problem of PEG-SDS interaction in SDS-PAGE and provides an alternative to HPLC in characterization of protein PEGylation.* Electrophoresis, 2007. **28**(16): p. 2801-7.
159. Elbashir, A.A., A.A. Ahmed, S.M. Ali Ahmed and H.Y. Aboul-Enein, *1,2-Naphthoquinone-4-Sulphonic Acid Sodium Salt (NQS) as an Analytical Reagent for the Determination of Pharmaceutical Amine by Spectrophotometry.* Applied Spectroscopy Reviews, 2012. **47**(3): p. 219-232.

160. Feldmann, E.G., *The colorimetric determination of certain local anesthetics with sodium 1,2-naphthoquinone-4-sulfonate.* Journal of the American Pharmaceutical Association (Scientific ed.), 1959. **48**(4): p. 197-201.
161. Gunnoo, S.B. and A. Madder, *Chemical Protein Modification through Cysteine.* Chembiochem, 2016. **17**(7): p. 529-53.
162. Chen, H., R. Huang, Z. Li, W. Zhu, J. Chen, Y. Zhan and B. Jiang, *Selective lysine modification of native peptides via aza-Michael addition.* Org Biomol Chem, 2017. **15**(35): p. 7339-7345.
163. Sutherland, B.P., B.M. El-Zaatari, N.I. Halaszynski, J.M. French, S. Bai and C.J. Kloxin, *On-Resin Macrocyclization of Peptides Using Vinyl Sulfonamides as a Thiol-Michael "Click" Acceptor.* Bioconjug Chem, 2018. **29**(12): p. 3987-3992.
164. Sinha, J., M. Podgorski, S. Huang and C.N. Bowman, *Multifunctional monomers based on vinyl sulfonates and vinyl sulfonamides for crosslinking thiol-Michael polymerizations: monomer reactivity and mechanical behavior.* Chem Commun (Camb), 2018. **54**(24): p. 3034-3037.
165. Wang, J., T. Deng, Y. Liu, K. Chen, Z. Yang and Z.X. Jiang, *Monodisperse and Polydisperse PEGylation of Peptides and Proteins: A Comparative Study.* Biomacromolecules, 2020. **21**(8): p. 3134-3139.
166. Sivado, E., M. El Alaoui, R. Kiraly, L. Fesus, F. Delolme, A. Page and S. El Alaoui, *Optimised methods (SDS/PAGE and LC-MS) reveal deamidation in all examined transglutaminase-mediated reactions.* FEBS Open Bio, 2019. **9**(2): p. 396-404.
167. Durda, M.A., A.S. Wolberg and B.A. Kerlin, *State of the art in factor XIII laboratory assessment.* Transfus Apher Sci, 2018. **57**(6): p. 700-704.
168. Doiphode, P.G., M.V. Malovichko, K.N. Mouapi and M.C. Maurer, *Evaluating factor XIII specificity for glutamine-containing substrates using a matrix-assisted laser desorption/ionization time-of-flight mass spectrometry assay.* Anal Biochem, 2014. **457**: p. 74-84.
169. Bell, J., *Examining the substrate specificity of factor XIIIa towards peptide substrate modelsaC fibrin domains.* 2013.
170. McDonagh, J. and H. Fukue, *Determinants of substrate specificity for factor XIII.* Semin Thromb Hemost, 1996. **22**(5): p. 369-76.
171. Gorman, J.J. and J.E. Folk, *Structural features of glutamine substrates for transglutaminases. Role of extended interactions in the specificity of human plasma factor XIIIa and of the guinea pig liver enzyme.* J Biol Chem, 1984. **259**(14): p. 9007-10.
172. Neumann, S., M. Biewend, S. Rana and W.H. Binder, *The CuAAC: Principles, Homogeneous and Heterogeneous Catalysts, and Novel Developments and Applications.* Macromol Rapid Commun, 2020. **41**(1): p. e1900359.
173. Nanci, A., J.D. Wuest, L. Peru, P. Brunet, V. Sharma, S. Zalzal and M.D. McKee, *Chemical modification of titanium surfaces for covalent attachment of biological molecules.* Journal of Biomedical Materials Research, 1998. **40**(2): p. 324-335.
174. Aresti, A., J. Aragoneses, N. Lopez-Valverde, A. Suarez and J.M. Aragoneses, *Effectiveness of Biofunctionalization of Titanium Surfaces with Phosphonic Acid.* Biomedicines, 2021. **9**(11).
175. Li, J., X. Cui, G.J. Hooper, K.S. Lim and T.B.F. Woodfield, *Rational design, bio-functionalization and biological performance of hybrid additive manufactured titanium implants for orthopaedic applications: A review.* J Mech Behav Biomed Mater, 2020. **105**: p. 103671.

176. El Boujlaidi, A., N. Rochdi, R. Tchalala, H. Enriquez, A.J. Mayne and H. Oughaddou, *Growth and characterization of nickel oxide ultra-thin films.* Surfaces and Interfaces, 2020. **18**.
177. Wang, L., M. Ye, Y. Wang, D. Tian, z. Ye and C. Wang, *Corrosion Behavior of the Nickel/nickel Interface During the Copper Sacrificial Layer Releasing Process in Micro-Electroforming.* 2021.
178. Singh, M.P., H.K. Keister, J.G. Matisons, Y. Pan, J. Zazyczny and B. Arkles, *Dipodal Silanes: Important Tool for Surface Modification to Improve Durability.* MRS Proceedings, 2014. **1648**.
179. Inkpen, M.S., Z.F. Liu, H. Li, L.M. Campos, J.B. Neaton and L. Venkataraman, *Non-chemisorbed gold-sulfur binding prevails in self-assembled monolayers.* Nat Chem, 2019. **11**(4): p. 351-358.
180. Pacchioni, G., *A not-so-strong bond.* Nature Reviews Materials, 2019. **4**(4): p. 226-226.
181. Li, S., H. Cai, J. He, H. Chen, S. Lam, T. Cai, Z. Zhu, S.J. Bark*, et al.*, *Extent of the Oxidative Side Reactions to Peptides and Proteins During the CuAAC Reaction.* Bioconjug Chem, 2016. **27**(10): p. 2315-2322.
182. Gaetke, L.M. and C.K. Chow, *Copper toxicity, oxidative stress, and antioxidant nutrients.* Toxicology, 2003. **189**(1-2): p. 147-63.
183. Wang, Q., T.R. Chan, R. Hilgraf, V.V. Fokin, K.B. Sharpless and M.G. Finn, *Bioconjugation by copper(I)-catalyzed azide-alkyne [3 + 2] cycloaddition.* J Am Chem Soc, 2003. **125**(11): p. 3192-3.
184. Presolski, S.I., V.P. Hong and M.G. Finn, *Copper-Catalyzed Azide-Alkyne Click Chemistry for Bioconjugation.* Curr Protoc Chem Biol, 2011. **3**(4): p. 153-162.
185. Shin, J.-A., S.-J. Oh, H.-Y. Lee and Y.-G. Lim, *An efficient Cu-catalyzed azide–alkyne cycloaddition (CuAAC) reaction in aqueous medium with a zwitterionic ligand, betaine.* Catalysis Science & Technology, 2017. **7**(12): p. 2450-2456.
186. Link, A.J. and D.A. Tirrell, *Cell surface labeling of Escherichia coli via copper(I)-catalyzed [3+2] cycloaddition.* J Am Chem Soc, 2003. **125**(37): p. 11164-5.
187. Speers, A.E., G.C. Adam and B.F. Cravatt, *Activity-based protein profiling in vivo using a copper(i)-catalyzed azide-alkyne [3 + 2] cycloaddition.* J Am Chem Soc, 2003. **125**(16): p. 4686-7.
188. Kim, E.J., D.W. Kang, H.F. Leucke, M.R. Bond, S. Ghosh, D.C. Love, J.S. Ahn, D.O. Kang*, et al.*, *Optimizing the selectivity of DIFO-based reagents for intracellular bioorthogonal applications.* Carbohydr Res, 2013. **377**: p. 18-27.
189. Chang, P.V., J.A. Prescher, E.M. Sletten, J.M. Baskin, I.A. Miller, N.J. Agard, A. Lo and C.R. Bertozzi, *Copper-free click chemistry in living animals.* Proc Natl Acad Sci U S A, 2010. **107**(5): p. 1821-6.
190. van Geel, R., G.J. Pruijn, F.L. van Delft and W.C. Boelens, *Preventing thiol-yne addition improves the specificity of strain-promoted azide-alkyne cycloaddition.* Bioconjug Chem, 2012. **23**(3): p. 392-8.
191. Dommerholt, J., F. Rutjes and F.L. van Delft, *Strain-Promoted 1,3-Dipolar Cycloaddition of Cycloalkynes and Organic Azides.* Top Curr Chem (Cham), 2016. **374**(2): p. 16.
192. Zhong, W., B. Sun, C. Lu, H. Yu, C. Wang, L. He, J. Gu, S. Chen*, et al.*, *Problems and Solutions in Click Chemistry Applied to Drug Probes.* Sci Rep, 2016. **6**: p. 35579.
193. Nicolas, J., S. Mura, D. Brambilla, N. Mackiewicz and P. Couvreur, *Design, functionalization strategies and biomedical applications of targeted biodegradable/biocompatible polymer-based nanocarriers for drug delivery.* Chem Soc Rev, 2013. **42**(3): p. 1147-235.

194. Wang, M., D. Svatunek, K. Rohlfing, Y. Liu, H. Wang, B. Giglio, H. Yuan, Z. Wu, *et al.*, *Conformationally Strained trans-Cyclooctene (sTCO) Enables the Rapid Construction of (18)F-PET Probes via Tetrazine Ligation.* Theranostics, 2016. **6**(6): p. 887-95.
195. Dorr, B.M., H.O. Ham, C. An, E.L. Chaikof and D.R. Liu, *Reprogramming the specificity of sortase enzymes.* Proc Natl Acad Sci U S A, 2014. **111**(37): p. 13343-8.

9 Abbreviations

aa	Amino acids
ACN	Acetonitrile
AFM	Atomic force microscope
APTES	(3-Aminopropyl)triethoxysilane
AUT	11-Amino-1-undecanethiol hydrochloride
BTESE	1,2-bis(triethoxysilyl)ethane
BTTAA	2-(4-((Bis((1-(tert-butyl)-1H-1,2,3-triazol-4-yl)methyl)amino)methyl)-1H-1,2,3-triazol-1-yl)acetic acid
CuAAC	Copper(I)-catalyzed azide alkyne cycloaddition
DIPEA	N,N-Diisopropylethylamine
DMF	Dimethylformamide
DNA	Deoxyribonucleic acid
DTT	Dithiothreitol
EDC	1-Ethyl-3-(3-dimethylaminopropyl)carbodiimide
EDTA	Ethylenediaminetetraacetic acid
eGFP	Enhanced green fluorescent protein
EMA	European Medicines Agency
FDA	Food and Drug Administration
FITC	Fluorescein isothiocyanate
FXIIIa	Factor XIII activated
HCCA	α-Cyano-4-Hydroxycinnamic acid
HPLC	High performance liquid chromatography
$ImSO_2N_3$	Imidazole sulphonyl azide hydrochloride
IPTG	Isopropyl β-D-1-thiogalactopyranoside
LB	Lysogeny broth
LC-MS	Liquid chromatography-mass spectrometry
MALDI	Matrix-assisted laser desorption/ionization
MANAQA	Magnetic nano actuators for quantitative analysis
MES	2-(N-morpholino)ethanesulfonic acid
MethoxyPEG-NHS	Methoxypoly(ethylene glycol) succinate *N*-hydroxysuccinimide ester
NHS	N-Hydroxysuccinimide
PEG	Polyethylene glycol
PMSF	Phenylmethylsulfonyl fluoride
rpm	Rotations per minute
SAM	Self-assembled monolayer
SDS-PAGE	Sodium dodecyl sulfate-polyacrylamide gel electrophoresis
SPAAC	Strain-promoted alkyne-azide cycloaddition
SPPS	Solid phase peptide synthesis
TB	Terrific broth
TBTA	Tris(benzyltriazolylmethyl)amine
TFA	Trifluoroacetic acid
TG	Transglutaminase
THPTA	Tris(3-hydroxypropyltriazolylmethyl)amine
tris	Tris(hydroxymethyl) aminomethane
UHPLC	Ultra-high performance liquid chromatography

10 Publications and Presentations

10.1 Publications

Sevim, S., S. Ozer, G. Jones, J. Wurzel, L. Feng, A. Fakhraee, N. Shamsudhin, O. Ergeneman, *et al.*, Nanomechanics on FGF-2 and Heparin Reveal Slip Bond Characteristics with pH Dependency. ACS Biomater Sci Eng, 2017. 3(6): p. 1000-1007.

Wandrey, G., J. Wurzel, K. Hoffmann, T. Ladner, J. Buchs, L. Meinel and T. Luhmann, Probing unnatural amino acid integration into enhanced green fluorescent protein by genetic code expansion with a high-throughput screening platform. J Biol Eng, 2016. 10: p. 11.

Sevim, S., S. Ozer, L. Feng, J. Wurzel, A. Fakhraee, N. Shamsudhin, B. Jang, C. Alcantara, *et al.*, Dually actuated atomic force microscope with miniaturized magnetic bead-actuators for single-molecule force measurements. Nanoscale Horiz, 2016. 1(6): p. 488-495.

Schultz, I., J. Wurzel and L. Meinel, Drug delivery of Insulin-like growth factor I. Eur J Pharm Biopharm, 2015. 97(Pt B): p. 329-37.

10.2 Presentations

Wandrey, G., J. Wurzel, K. Hoffmann, T. Ladner, J. Büchs, L. Meinel, T. Lühmann, Online monitoring and high throughput screening of unnatural amino acid integration by genetic code expansion in Escherichia coli. 67th Mosbacher Kolloquium 2016

Wurzel, J., M. Gutmann, T. Lühmann, L. Meinel, Spatially controlled decoration of biologics using enhanced green fluorescent protein as model protein. German Pharmaceutical Society (DPhG) Annual Meeting 2015

12 Acknowledgments

First of all, I would like to thank Prof. Dr. Dr. Lorenz Meinel, who gave me the opportunity to do my Ph.D. thesis in his work group. His enthusiasm for all research topics was always contagious and inspiring for me. Furthermore, he encouraged me during my long writing break and showed understanding and patience at the same time.

In no inferior way, I thank Prof. Dr. Tessa Lühmann. Under her tutelage I felt comfortable working independently, knowing I can rely on her comprehensive scientific knowledge and inexhaustible support at any time. I thank her for being both my mentor and a friend during this journey.

Special thanks to Marcus Gutmann, a seemingly polymath, who supported me in countless tasks. Unfortunately, his foosball skills do not match his scientific abilities.

Thank you to all my other fellow Ph.D. colleagues who have made the lab the workplace that I have enjoyed so much. Cecilia Amstalden, Alexandra Braun, Eva Gator, Gabriel Jones, Sebastian Puhl, Marika Rosenberger, Isabel Schultz, and Vera Werner – every one of you made this time a wonderful experience that I will always remember fondly.

In addition, I would like to thank Dr. Sacha Zügner for all the meaningful as well as nonsensical conversations. It was a pleasure to be your practical student education sidekick. Also special thanks to Christine Schneider who had to handle all my applications for extension among other organizational matters.

Thanks to my family and friends for their encouragement during this work.

I would also like to thank my parents-in-law Sieglinde and Hans-Peter for welcoming me so warmly into their family.

Finally, I want to thank my wife Julia for her support and patience especially while I was writing this thesis. I am grateful to be able to share both joy and burden with you.

13 Documentation of Authorship

This section contains a list of the individual contribution of each author to the publication reprinted in this thesis.

P1	**(A1) G. Wandrey, (A2) J. Wurzel, (A3) K. Hoffmann, (A4) T. Ladner, (A5) J. Büchs, (A6) L. Meinel and (A7) T. Lühmann**, Probing unnatural amino acid integration into enhanced green fluorescent protein by genetic code expansion with a high-throughput screening platform. Journal of Biological Engineering, 2016, 10:11.

Assignment	**A1**	**A2**	**A3**	**A4**	**A5**	**A6**	**A7**	**∑ in %**
Subcloning		5						*5*
Protein expression, purification		6						*6*
Protein characterization (SDS-PAGE, mass spectrometry, fluorescence spectrometry, western blotting)		6						*6*
ELISA measurements		8						*8*
Cultivation experiments	6		5					*11*
RSM development	5			4.5				*9.5*
Online monitoring	10.5							*10.5*
Manuscript writing	9	6			2.5	2.5	9	*29*
Correction of the manuscript	3.5	2		1	2.5	2.5	3.5	*15*
Total	34	33	5	5.5	5	5	12.5	*100*